# NACA

# RESEARCH MEMORANDUM

## EFFECTS OF LEADING-EDGE DEVICES AND TRAILING-EDGE FLAPS ON LONGITUDINAL CHARACTERISTICS OF TWO 47.7° SWEPTBACK WINGS OF ASPECT RATIOS 5.1 AND 6.0 AT A REYNOLDS NUMBER OF $6.0 \times 10^6$



By Reino J. Salmi

Langley Aeronautical Laboratory
Langley Air Force Base, Va.



NATIONAL ADVISORY COMMITTEE
FOR AERONAUTICS

WASHINGTON

August 30, 1950

NATIONAL ADVISORY COMMITTEE FOR AERONAUTICS

RESEARCH MEMORANDUM

# EFFECTS OF LEADING-EDGE DEVICES AND TRAILING-EDGE FLAPS ON LONGITUDINAL CHARACTERISTICS OF TWO 47.7° SWEPTBACK WINGS OF ASPECT RATIOS 5.1 AND 6.0 AT A REYNOLDS NUMBER OF $6.0 \times 10^6$

By Reino J. Salmi

## SUMMARY

An investigation was conducted in the Langley 19-foot pressure tunnel to determine the effects of leading-edge stall-control devices and trailing-edge flaps on the longitudinal stability characteristics of a 47.7° sweptback wing for which aspect ratios of 5.1 and 6.0 could be obtained by interchangeable wing tips. In addition to tests of various spans of the leading-edge devices and trailing-edge flaps, the effects of wing fences, roughness, and a fuselage were determined. Most of the data were obtained at a Reynolds number of about $6.0 \times 10^6$ (Mach number of 0.14).

The results showed that large improvements in the static longitudinal stability of the wings could be obtained by the use of leading-edge flaps. The greatest improvement was obtained with leading-edge flaps of half-span or less in combination with the shortest-span trailing-edge flaps. A drooped nose also improved the stability, but in most cases it was less effective than the leading-edge flap. Increasing the span of the trailing-edge flaps beyond 0.400 semispan affected the stability adversely; the destabilizing effect was greater for the double slotted flaps than the split flaps. The effects of the leading-edge devices and trailing-edge flaps on the stability characteristics were essentially the same for both the aspect ratio 5.1 and 6.0 wings. The highest values of the maximum lift coefficient obtained on combinations which exhibited only very small unstable variations in the pitching moment were 1.48 for the combination of 0.400 semispan double slotted flaps and 0.475 semispan leading-edge flaps on the aspect ratio 5.1 wing and 1.53 for the combination of 0.359 semispan double slotted flaps and 0.527 semispan leading-edge flaps on the aspect ratio 6.0 wing.

## INTRODUCTION

In order to increase the range of highly sweptback-wing aircraft, it becomes desirable to use wings of large aspect ratio. Reference 1 points out, however, that highly swept wings of large aspect ratio have inherently poor longitudinal stability characteristics and, therefore, the problem of instability in the high angle-of-attack range must be considered. However, the possibility of eliminating the longitudinal instability of sweptback wings by means of leading-edge devices has been shown by previous investigations, such as references 2 and 3. Furthermore, the low effectiveness of ordinary split trailing-edge flaps on highly swept wings indicates the desirability of investigating other types of flaps.

With these considerations in mind, an investigation was conducted in the Langley 19-foot pressure tunnel to determine the effectiveness of leading-edge devices and double slotted trailing-edge flaps on two wings of 47.7° of sweepback and aspect ratios of 5.1 and 6.0 with NACA 64-210 airfoil sections normal to the 0.286-chord line. Most of the data were obtained at a Reynolds number of approximately $6.0 \times 10^6$ (Mach number of 0.14). The longitudinal characteristics of the plain wings have been previously reported in reference 4. The results of a similar investigation on a 47.5° sweptback wing of aspect ratio 3.4 are reported in reference 5.

## SYMBOLS

The moments are referred to an assumed center of gravity which is located at the quarter-chord point of the mean aerodynamic chord projected on the plane of symmetry. The symbols are defined as follows:

| | |
|---|---|
| $C_L$ | lift coefficient (Lift/qS) |
| $C_D$ | drag coefficient (Drag/qS) |
| $C_m$ | pitching-moment coefficient (pitching moment/qS$\bar{c}$) |
| S | wing area |
| $\bar{c}$ | mean aerodynamic chord |
| c | wing chord |
| c' | wing chord normal to 0.286-chord line |

| | |
|---|---|
| $q$ | dynamic pressure $(\rho V^2/2)$ |
| $V$ | velocity |
| $\rho$ | mass density of air |
| $R$ | Reynolds number $(\rho V\bar{c}/\mu)$ |
| $M$ | Mach number $(V/a)$ |
| $\mu$ | coefficient of viscosity of air |
| $a$ | speed of sound |
| $L/D$ | lift-drag ratio |
| $s$ | distance |
| $\alpha$ | angle of attack of root chord line |
| $\delta_n$ | drooped-nose deflection angle |
| $A$ | aspect ratio |

Subscripts:

| | |
|---|---|
| max | maximum |
| v | vertical |
| g | glide path |
| h | horizontal |

## DESCRIPTION OF MODEL

The geometric characteristics of the models are shown in figure 1. The wings were constructed from an all-steel unswept-wing model used in the investigation of reference 6. The sweepback angle of the leading edge was $47.7^\circ$, and interchangeable aluminum wing tips gave aspect ratios of 5.1 and 6.0 with corresponding taper ratios of 0.383 and 0.313. The wings had NACA 64-210 airfoil sections normal to the 0.286-chord line. The aspect ratio 5.1 and 6.0 wings had $1.32^\circ$ and $1.72^\circ$ of washout about the 0.286-chord line. The dihedral angle was zero for both aspect ratios.

The leading-edge flaps had a constant chord of 3.05 inches measured normal to the leading edge and were deflected down 45° from the wing-chord plane, measured normal to the leading edge. The drooped leading edge was hinged on the wing lower surface at the 16-percent chord line. Droop deflections of 20° and 30° about the hinge line could be maintained. The various spans of drooped-nose and leading-edge flaps tested are shown in figures 2(a) and 2(b).

The trailing-edge split flaps were made of $\frac{1}{16}$-inch duralumin and were deflected 60° about the hinge line. The flap chord was equal to 20 percent of the wing chord perpendicular to 0.286-chord line (fig. 2(c)). The double slotted flaps were made of duralumin and steel and were deflected 50°, measured in a plane normal to the 0.286-chord line (fig. 2(d)). The double slotted flap chord was equal to 25 percent of the wing chord perpendicular to 0.286-chord line, and the flap vane had a chord of 7.5 percent of the wing chord. Various spans of split and double slotted flaps were provided, as shown in figure 2. A small part of the double slotted flaps at the center section was omitted because of construction difficulties.

Several types of fences were used on the model as shown in figures 2(e) and 2(f). The fences which were used in combination with the leading-edge devices were located at a wing station 5 percent of the semispan outboard of the inboard end of the device.

The fuselage was circular in cross section and had a fineness ratio of 11.0. An incidence of 2° was maintained between the fuselage center line and wing root chord line.

## TESTS

The tests were made in the Langley 19-foot pressure tunnel with the air compressed to a pressure of approximately 33 pounds per square inch. Figure 3 shows the model mounted in the tunnel.

The lift, drag, and pitching moment were measured through an angle-of-attack range from -4° through maximum lift. The stall progression was determined from observations of wool tufts attached to the upper surface of the wing. The roughness tests were made using standard roughness as described in reference 7. Most of the tests were made at a Reynolds number of $6.0 \times 10^6$ with a corresponding Mach number of 0.14, and a few tests were made at a Reynolds number of $3.0 \times 10^6$ with a corresponding Mach number of 0.07.

## CORRECTIONS TO DATA

The data presented herein have been corrected for air-stream misalinement, support tare and interference effects, and for jet-boundary effects.

The jet-boundary corrections for the angle of attack and drag coefficient were obtained by a method based on reference 8. Corrections to the pitching moment due to the tunnel-induced distortion of the wing loading were also determined. The corrections are as follows:

| | A = 5.1 | A = 6.0 |
|---|---|---|
| $\Delta\alpha$ | $0.905C_L$ | $0.980C_L$ |
| $\Delta C_D$ | $0.0139C_L^2$ | $0.0152C_L^2$ |
| $\Delta C_m$ | $0.004C_L$ | $0.008C_L$ |

All corrections were added to the data.

## RESULTS AND DISCUSSION

The discussion is concerned mainly with the results obtained with the aspect ratio 5.1 wing, inasmuch as most of the data were obtained with the aspect ratio 5.1 wing (table I) and since the results obtained with the aspect ratio 6.0 wing were very similar.

### Static Longitudinal Stability Characteristics

The use of moderate-span leading-edge devices resulted in a marked improvement in stability although varying degrees of instability generally occurred at moderate lift coefficients. (See fig. 4.) At the maximum lift coefficient the pitching moment would break either stable or unstable, depending on the configuration.

The unstable variations which occurred at moderately high lift coefficients may, however, be considerably reduced on a complete airplane configuration by the effects of a horizontal tail (for example, references 3, 9, and 10). In addition, it was shown that an increase in the stability was obtained at the maximum lift coefficient when the tail was located in the optimum position, which in most cases was below the wing-chord plane extended.

Effects of leading-edge and trailing-edge flap span on stability.- A general summary of the effects of variations in the leading-edge and

trailing-edge flap span on the stability characteristics is presented in figure 5. Stability is dependent on both the span of the leading-edge flaps and the trailing-edge flaps. The range of spans is limited for both the leading-edge and trailing-edge flaps for which the unstable aerodynamic-center shift prior to the maximum lift is less than $0.15\bar{c}$. Reference to an aerodynamic-center shift of less than $0.15\bar{c}$ is not intended as a criterion for judging the stability but was arbitrarily chosen to aid in the comparison of the various flap configurations.

Figure 6 shows that, with the trailing-edge flaps neutral, the greatest reduction in the forward movement of the aerodynamic center throughout the lift range was obtained with the leading-edge flaps ranging in span from $0.375b/2$ to $0.475b/2$. For leading-edge flap spans of $0.525b/2$ or greater, the pitching-moment curves exhibited unstable breaks near the maximum lift coefficient.

The effectiveness of the shorter-span leading-edge flaps was considerably increased when the shortest-span trailing-edge flaps were deflected. (See figs. 4(b), 7, 8, and 9.) The most favorable pitching-moment characteristics were obtained with the $0.400b/2$ double slotted flaps and $0.375b/2$ leading-edge flaps, in which case the amount of forward movement of the aerodynamic center was small and a stable moment break was obtained at the maximum lift. For leading-edge flap spans of 0.525 or greater, unstable moment breaks were obtained at the maximum lift for the $0.400b/2$ and $0.516b/2$ double slotted flaps; whereas with the $0.626b/2$ double slotted flaps, the pitching moment became unstable at the maximum lift coefficient regardless of the leading-edge flap span.

The $0.400b/2$ split flaps were also more effective in reducing the forward movement of the aerodynamic center with the shorter spans of leading-edge flaps and increased the range of leading-edge flap spans to $0.575b/2$ for which stable moment breaks were obtained at the maximum lift. The pitching-moment break at the maximum lift was also stable for the $0.618b/2$ split flaps in combination with the $0.375b/2$ and $0.475b/2$ leading-edge flaps. (Figs. 4(a), 10, 11, and 12.)

The effects of the leading-edge and trailing-edge flaps on the stability characteristics were not appreciably affected by increasing the aspect ratio from 5.1 to 6.0, except that the unstable variations that occurred in the moderately high lift-coefficient range were generally larger for the aspect ratio 6.0 wing (figs. 13 to 19). For the majority of the combinations that exhibited only small unstable variations, a severe vibration at the wing tips was encountered.

Flow observations.- A visual survey, by means of a tuft attached to a wooden probe, of the flow over the wing with the leading-edge and

trailing-edge flaps deflected showed that a vortex originated at the apex of the wing at a moderately high angle of attack and followed the leading edge to a point just inboard of the inboard end of the leading-edge flap, where it turned into the stream direction and trailed off the wing. Increasing the angle of attack caused the vortex to turn into the stream at a wing station farther inboard and eventually to sweep back from the apex at an angle considerably greater than the leading-edge sweep angle. As the angle of attack was increased, the vortex also gradually increased in size and finally dissipated into the free stream near the apex. Reference 4 points out that the vortex flow also developed on the wings with the flaps neutral. The stall studies based on the behavior of the surface tufts (figs. 20 and 21) do not adequately describe the flow over the wing but may be indicative of the nature of the flow near the boundary layer. It was observed that the inboard boundary of the stalled area, as indicated by the surface tufts, generally coincided with the location at which the vortex core turned into the stream direction. The need for pressure-distribution measurements is evident if the effects of the various flow phenomena as indicated by the tuft studies and probe surveys are to be clearly understood.

The longer spans of the leading-edge flaps permitted unstable breaks in the pitching moment near the maximum lift due to stalling at a wing station near the midspan of the flaps although, in some cases, the instability was delayed to higher lift coefficients.

When stalling begins, the adverse effects on the stability due to an increase in the trailing-edge flap span may result from the loss of the additional lift due to the flaps, which is extended farther outboard. Inasmuch as the stall pattern is little affected by the type of trailing-edge flap used, it may be expected that increases in the span of the double slotted flaps will have greater adverse effects on the stability than similar increases in the split-flap span.

Effect of drooped nose on stability.- The drooped nose was generally less effective than the leading-edge flap in improving the stability because of its inability to prevent separation over the tip sections (figs. 22 to 28). This is illustrated in figure 20 which shows the stall progressions of the wing with 0.516b/2 double slotted flaps in combination with the 0.475b/2 leading-edge flaps and 0.475b/2 drooped nose. Figure 20 shows that in both cases the separation began near the inboard end of the leading-edge device; but with the drooped nose, the stall would spread toward the tips when the angle of attack was increased, whereas the leading-edge flaps prevented the outboard panel from stalling. Figures 25 and 26 show that, in general, no large differences in the stability characteristics were obtained between the 20° and 30° drooped-nose deflection

angles. As in the case of the leading-edge flaps, the most favorable pitching-moment characteristics with the drooped nose were obtained with the 0.400b/2 trailing-edge flaps deflected (figs. 4(c), 4(d), and 26).

Effect of fences on stability.- The fences did not produce a stable moment curve for any of the positions tested on the plain wing, although the amount of forward movement of the aerodynamic center was greatly reduced. Figure 29 shows that the greatest reduction in the forward shift of the aerodynamic center was obtained with the complete fence at the 0.60b/2 station. Removing the rear 75 percent of the fence on the upper surface did not decrease its effectiveness appreciably.

Tuft studies of the wing with a complete fence showed that the separation would originate near the leading edge on the inboard side of the fence, whereas the plain wing stalled first at the tips. At a higher angle of attack, the wing with the fence also stalled at the tip; but the stalled area inboard of the fence also spread farther inboard, thus counteracting some of the instability due to the tip stall.

The use of fences with combinations of leading-edge devices and trailing-edge flaps usually resulted in a slight improvement in the pitching-moment characteristics as shown in figures 4(c), 4(d), and 30.

Effects of Reynolds number, roughness, and fuselage interference.- The effects of leading-edge roughness and Reynolds number variation were investigated for a stable combination consisting of 0.400b/2 double slotted flaps and 0.375b/2 leading-edge flaps (fig. 31). A reduction in the Reynolds number from $6.0 \times 10^6$ to $3.0 \times 10^6$ caused a gradual decrease in stability with increasing lift coefficient up to moderately high lift coefficients, beyond which a gradual increase in stability occurred up to the maximum lift. Figure 31 also shows that the addition of standard roughness along the wing leading edge and leading-edge flap resulted in a similar destabilizing effect up to moderately high lift coefficients, with an increase in stability existing to the maximum lift.

In order to determine the effects of localized roughness along the leading edge, some tests were made on a combination with 0.618b/2 split flaps and 0.475b/2 leading-edge flaps with roughness placed on the wing leading edge inboard of the leading-edge flap, on the leading-edge flap only, and on both the wing and leading-edge flap. With roughness on the inboard part of the wing only, the stability at high lift coefficients was improved (fig. 32). This improvement suggests the use of a leading-edge device to induce separation at the wing root in order to obtain more favorable moment characteristics. Roughness on the

leading-edge flap only had a negligible effect on the pitching-moment characteristics as compared with the smooth condition, indicating that the surface condition of the leading-edge flap does not greatly influence its effectiveness. The stability in the high-lift range was slightly improved when roughness was applied to both the wing and flap.

The fuselage had no appreciable effect on the shape of the pitching-moment curves at the stall for any of the configurations tested (fig. 33). The fuselage caused a small forward shift in the aerodynamic center for all the combinations tested.

## Lift Characteristics

Effect of leading-edge and trailing-edge flaps on maximum lift.- The maximum lift coefficient of the plain wing was increased from 1.16 (fig. 6) to 1.22 by the 0.618b/2 split flaps (fig. 12) and to 1.43 by the 0.626b/2 double slotted flaps (fig. 9). The relatively small increments in maximum lift are to be expected, however, because of the large sweep angle.

The leading-edge flaps also increased the maximum lift coefficient, and a maximum value of about 1.36 was obtained with the 0.525b/2 leading-edge flap (fig. 6). Figure 34 shows that, for leading-edge flaps of about 0.275b/2 or less, no apparent increase in the maximum lift was obtained. In general, the variation of the maximum lift coefficient with leading-edge flap span was relatively independent of the trailing-edge-flap configuration. From figure 22 it can be seen that the drooped nose also increased the maximum lift coefficient, a value of about 1.38 being obtained with the 0.475b/2 drooped nose deflected 20°. The highest values of $C_{L_{max}}$ obtained with combinations for which the unstable variations were less than $0.15\bar{c}$ were 1.48 for the combination of 0.400b/2 double slotted flaps and 0.475b/2 leading-edge flaps (fig. 7), and 1.43 for the combination of 0.500b/2 split flaps and 0.475b/2 leading-edge flaps (fig. 11). The highest value of $C_{L_{max}}$ measured was about 1.70 for the combination of 0.626b/2 double slotted flaps and 0.475b/2 leading-edge flaps on the aspect ratio 5.1 wing.

Increasing the aspect ratio from 5.1 to 6.0 resulted in slightly higher values of the maximum lift coefficient for the configurations with a stable moment break at $C_{L_{max}}$. Figure 14 shows that a maximum lift coefficient of about 1.53 was obtained for the aspect ratio 6.0 wing with 0.359b/2 double slotted flaps and 0.526b/2 leading-edge flaps.

Flap effectiveness at zero angle of attack.- In reference 2, a method of estimating the flap effectiveness of a sweptback wing at

zero angle of attack was presented. The formula used, which was revised from reference 11, is believed to represent the first-order effects of sweepback and is as follows:

$$\Delta C_L = J \Delta c_l C_{L_{\alpha_\Lambda}} \cos \Lambda$$

where

$J$ factor depending on aspect ratio, taper ratio, and flap span (reference 11)

$\Delta c_l$ two-dimensional lift increment

$C_{L_{\alpha_\Lambda}}$ calculated lift-curve slope of swept wing

$\Lambda$ angle of sweep of quarter-chord line

Figure 35 shows that the experimental values of $\Delta C_L$ were slightly greater than the calculated values for the split flaps and considerably greater for the double slotted flaps. The reason for this is not readily apparent; as pointed out in reference 2, the effects of sweepback on the variation with flap span of the lift increment due to flap deflection appears to be dependent on the type of flap considered. The effectiveness of the double slotted flaps in providing large lift increments at low angles of attack may be a major advantage in avoiding extreme nose-up attitudes in the high-lift range.

Effects of Reynolds number, roughness, and fuselage.- The effects of low Reynolds number and wing roughness were determined for a combination consisting of 0.400b/2 double slotted flaps and 0.375b/2 leading-edge flaps (fig. 31). Reducing the Reynolds number from $6.0 \times 10^6$ to $3.0 \times 10^6$ reduced the maximum lift coefficient about 0.05. Standard roughness reduced the maximum lift coefficient about 0.02. Locating roughness at various positions along the leading edge of the combination with 0.618b/2 split flaps and 0.475b/2 leading-edge flaps (fig. 32) had a relatively small effect on the lift characteristics. The fuselage increased the lift-curve slope slightly, but its effects on $C_{L_{max}}$ were small (fig. 33).

## Lift-Drag Ratios

The effects of the leading-edge and trailing-edge flaps on the drag can be conveniently evaluated from considerations of the lift-drag ratios. Inasmuch as the leading-edge devices delay the separation

at the tips, it may be expected that the lift-drag ratios in the moderately high-lift range would be increased considerably by the leading-edge devices. Figure 36 shows that both the leading-edge flaps and drooped nose increased the lift-drag ratio of the plain wing only slightly for lift coefficients above approximately 0.8. The maximum L/D of the plain wing was reduced considerably by the leading-edge flaps, whereas the drooped nose caused only a slight decrease in the maximum lift-drag ratio. As also shown in figure 36, an increase in the leading-edge flap span caused an increase in the L/D in the high-lift range but reduced the maximum value and the values at low lifts.

The effects of the trailing-edge flaps on the lift-drag ratios are presented in figure 37. The superposed grid showing the gliding speed and vertical velocity may be of help in ascertaining the significance of the changes in L/D caused by the flaps. As shown in figure 37, the maximum values of L/D were reduced when the trailing-edge flap span was increased, but the values of L/D were increased in the high-lift range. This effect was evident for the split flaps and the double slotted flaps. From considerations of the gliding speed and vertical velocity, it becomes evident that the increases in L/D at the high lift coefficients are of greater significance than the reduction of the maximum values of L/D in the moderate lift range because lower gliding speeds can be maintained for a given sinking speed.

Calculations of the power-off landing-flare characteristics were made by the method of reference 12 and are presented in figure 38 for various combinations of leading-edge and trailing-edge flaps. It can be seen that superior landing-flare characteristics were obtained for the configurations with the trailing-edge flaps neutral. With the double slotted and split flaps in combination with the 0.475b/2 leading-edge flaps, sinking speeds of 23 feet per second were obtained at the start of the flare but heights of 56 and 53 feet were required, respectively. When only the 0.475b/2 leading-edge flaps were used, a sinking speed of 16.2 feet per second was obtained at the start of the flare and an altitude of 32 feet was required. The only advantage of the trailing-edge flaps was in the lower forward speeds obtained at touchdown. These calculations are, however, for power-off landings and the combinations with the highest values of $C_{L_{max}}$ are of prime importance for power-on landings.

## CONCLUSIONS

The following concluding remarks are based on the tests of two 47.7° sweptback wings of aspect ratios 5.1 and 6.0:

1. Large improvements in the static longitudinal stability characteristics were obtained by the use of leading-edge flaps with the trailing-edge flaps both deflected and neutral. The best stability characteristics were obtained with leading-edge flaps of half-span or less in combination with the 0.4 semispan trailing-edge flaps.

2. The drooped nose also improved the stability, but in most cases was less effective than the leading-edge flaps.

3. Increasing the span of the trailing-edge flaps affected the stability adversely. The destabilizing effect was greater for the double slotted flaps than for the split flaps.

4. The use of wing fences alone did not provide stability, but the fences increased slightly the effectiveness of the leading-edge devices.

5. The effects of the leading-edge and trailing-edge flaps on the stability characteristics were essentially the same for the aspect ratio 5.1 and 6.0 wings.

6. The highest values of the maximum lift coefficient obtained with combinations that exhibited only very small unstable variations were: 1.48 (0.400 semispan double slotted flaps and 0.475 semispan leading-edge flaps on the aspect ratio 5.1 wing), 1.43 (0.500 semispan split flaps and 0.475 semispan leading-edge flaps on the aspect ratio 5.1 wing), and 1.53 (0.359 semispan double slotted flaps and 0.527 semispan leading-edge flaps on the aspect ratio 6.0 wing).

Langley Aeronautical Laboratory
National Advisory Committee for Aeronautics
Langley Air Force Base, Va.

## REFERENCES

1. Shortal, Joseph A., and Maggin, Bernard: Effect of Sweepback and Aspect Ratio on Longitudinal Stability Characteristics of Wings at Low Speeds. NACA TN 1093, 1946.

2. Koven, William, and Graham, Robert R.: Wind-Tunnel Investigation of High-Lift and Stall-Control Devices on a 37° Sweptback Wing of Aspect Ratio 6 at High Reynolds Numbers. NACA RM L8D29, 1948.

3. Foster, Gerald V., and Fitzpatrick, James E.: Longitudinal-Stability Investigation of High-Lift and Stall-Control Devices on a 52° Sweptback Wing with and without Fuselage and Horizontal Tail at a Reynolds Number of $6.8 \times 10^6$. NACA RM L8I08, 1948.

4. Salmi, Reino J., and Carros, Robert J.: Longitudinal Characteristics of Two 47.7° Sweptback Wings with Aspect Ratios of 5.1 and 6.0 at Reynolds Numbers up to $10 \times 10^6$. NACA RM L50A04, 1950.

5. Pasamanick, Jerome, and Sellers, Thomas B.: Low-Speed Investigation of Leading-Edge and Trailing-Edge Flaps on a 47.5° Sweptback Wing of Aspect Ratio 3.4 at a Reynolds Number of $4.4 \times 10^6$. NACA RM L50E02, 1950.

6. Sivells, James C., and Spooner, Stanley H.: Investigation in the Langley 19-Foot Pressure Tunnel of Two Wings of NACA 65-210 and 64-210 Airfoil Sections with Various Type Flaps. NACA Rep. 942, 1949.

7. Abbott, Ira H., Von Doenhoff, Albert E., and Stivers, Louis S., Jr.: Summary of Airfoil Data. NACA Rep. 824, 1945.

8. Eisenstadt, Bertram J.: Boundary-Induced Upwash for Yawed and Swept-Back Wings in Closed Circular Wind Tunnels. NACA TN 1265, 1947.

9. Foster, Gerald V., and Griner, Roland F.: A Study of Several Factors Affecting the Stability Contributed by a Horizontal Tail at Various Vertical Positions on a Sweptback-Wing Airplane Model. NACA RM L9H19, 1949.

10. Spooner, Stanley H., and Martina, Albert P.: Longitudinal Stability Characteristics of a 42° Sweptback Wing and Tail Combination at a Reynolds Number of $6.8 \times 10^6$. NACA RM L8E12, 1948.

11. Pearson, Henry A., and Anderson, Raymond F.: Calculation of the Aerodynamic Characteristics of Tapered Wings with Partial-Span Flaps. NACA Rep. 665, 1939.

12. Lovell, J. Calvin, and Lipson, Stanley: An Analysis of the Effect of Lift-Drag Ratio and Stalling Speed on Landing-Flare Characteristics. NACA TN 1930, 1949.

TABLE I.- INDEX TO FIGURES

| | Figure number | |
|---|---|---|
| | A = 5.1 | A = 6.0 |
| Summary of pitching-moment characteristics | 4 and 5 | |
| Effects of leading-edge flaps on plain wing | 6 | 13 |
| Effects of leading-edge flaps with double slotted flaps deflected | 7 to 9 | 14 to 16 |
| Effects of leading-edge flaps with split flaps deflected | 10 to 12 | 17 to 19 |
| Stall studies | 20 and 21 | |
| Effects of drooped nose on plain wing | 22 | |
| Effects of drooped nose with split flaps deflected | 23 to 25 | |
| Effects of drooped nose with double slotted flaps deflected | 26 to 28 | |
| Effects of wing fences | 29 and 30 | 30 |
| Effects of wing roughness and Reynolds number | 31 and 32 | |
| Effects of fuselage | 33 | 33 |
| Effects of leading-edge flap span on $C_{L_{max}}$ | 34 | |
| Trailing-edge-flap effectiveness at zero angle of attack | 35 | |
| Lift-drag ratios of various combinations | 36 and 37 | |
| Landing-flare characteristics | 38 | |

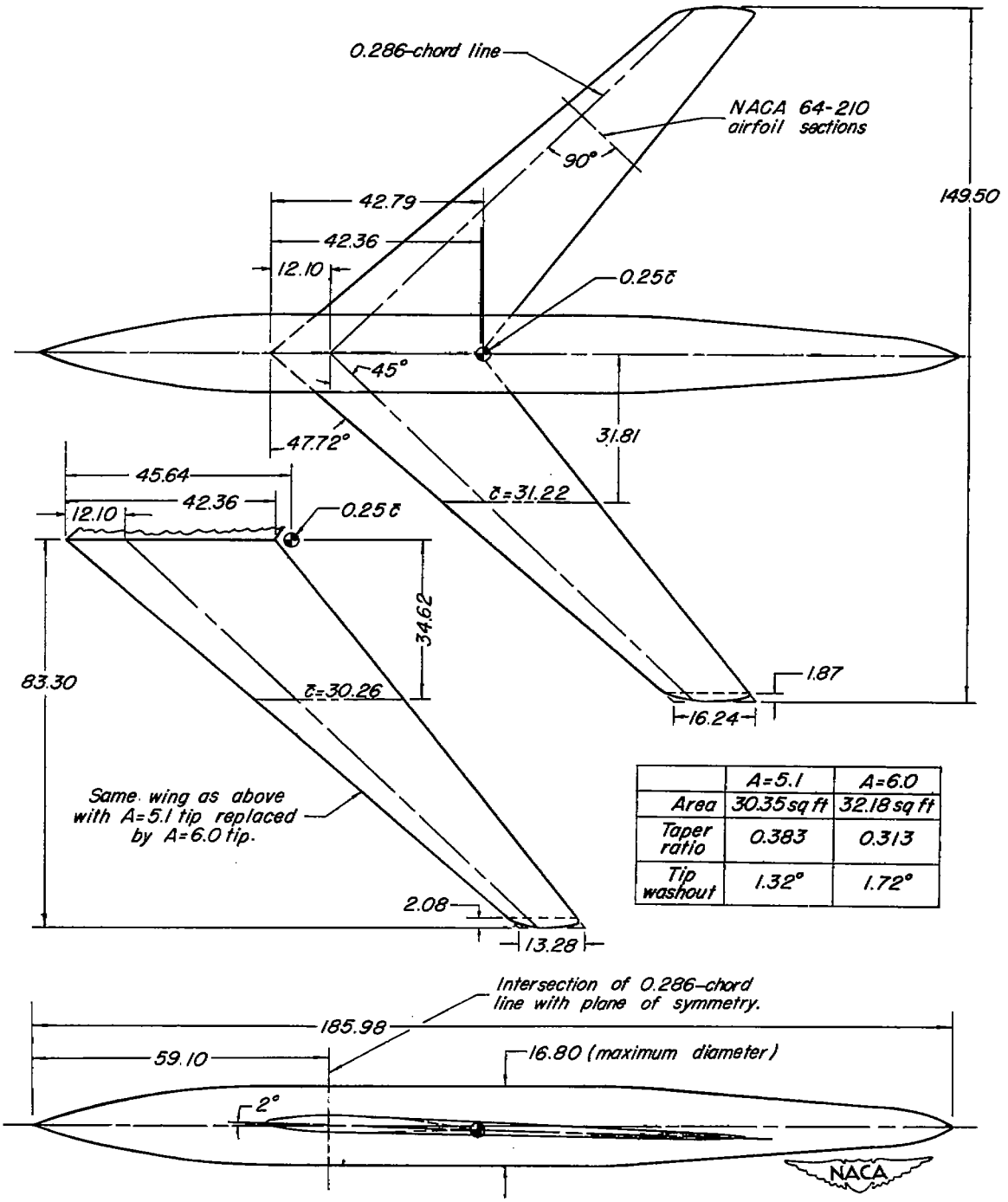


| | A=5.1 | A=6.0 |
|---|---|---|
| Area | 30.35 sq ft | 32.18 sq ft |
| Taper ratio | 0.383 | 0.313 |
| Tip washout | 1.32° | 1.72° |

Figure 1.- Geometry of the 47.7° sweptback wings of aspect ratios 5.1 and 6.0. All dimensions are in inches.

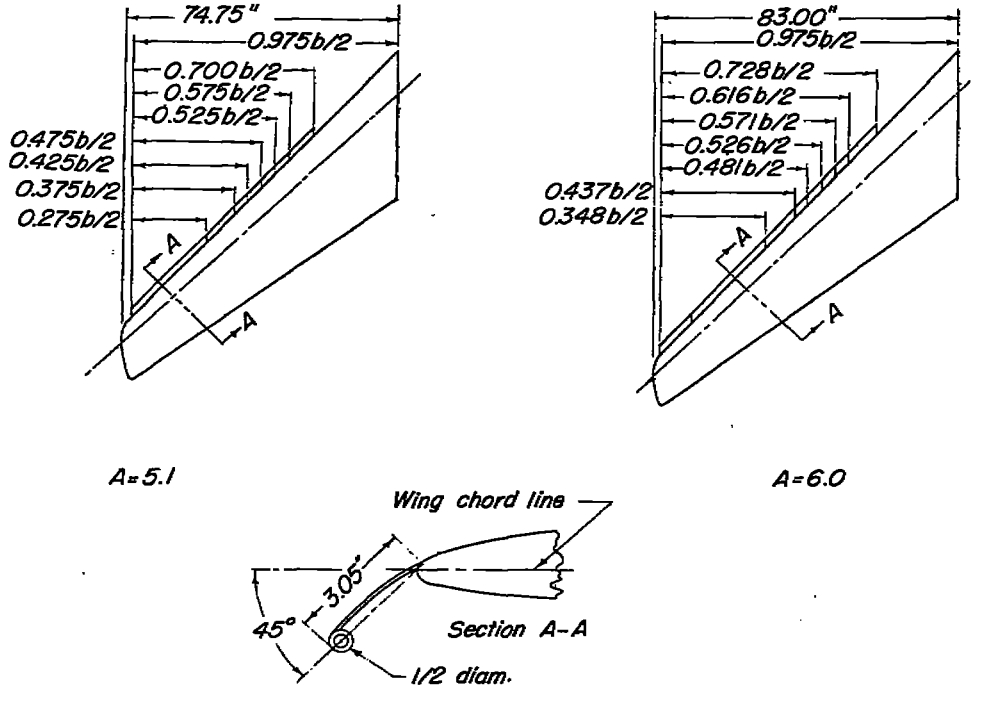


(a) Leading-edge flap.

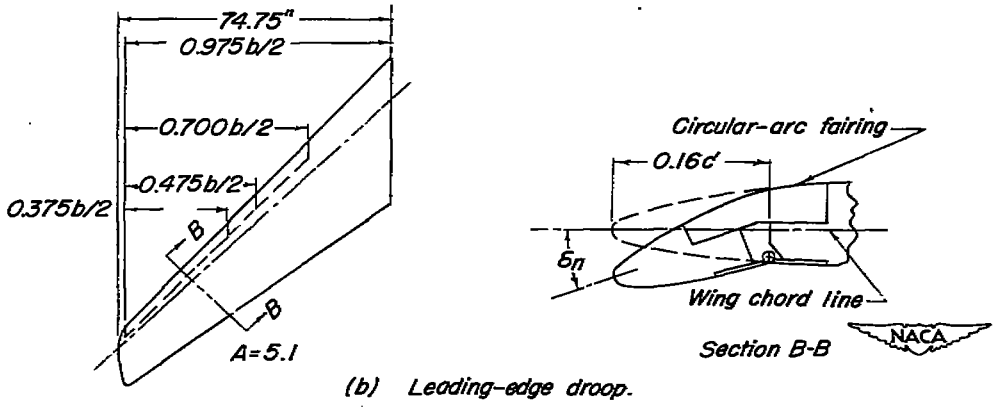


(b) Leading-edge droop.

Figure 2.- Details of leading-edge devices, trailing-edge flaps, and fences used on the 47.7° sweptback wings of aspect ratios 5.1 and 6.0.

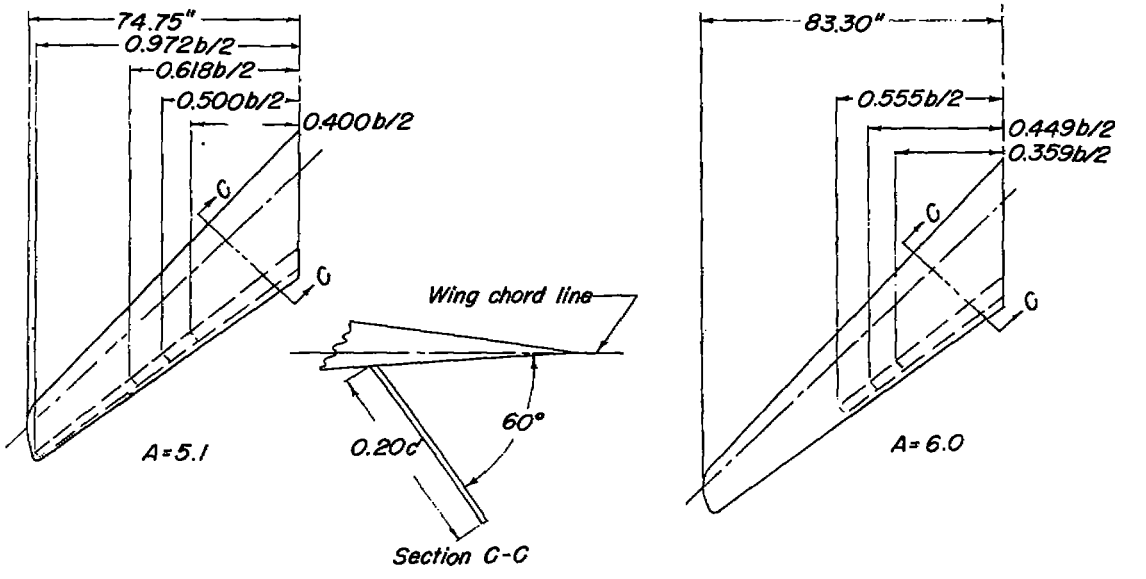


(c) Split flaps.

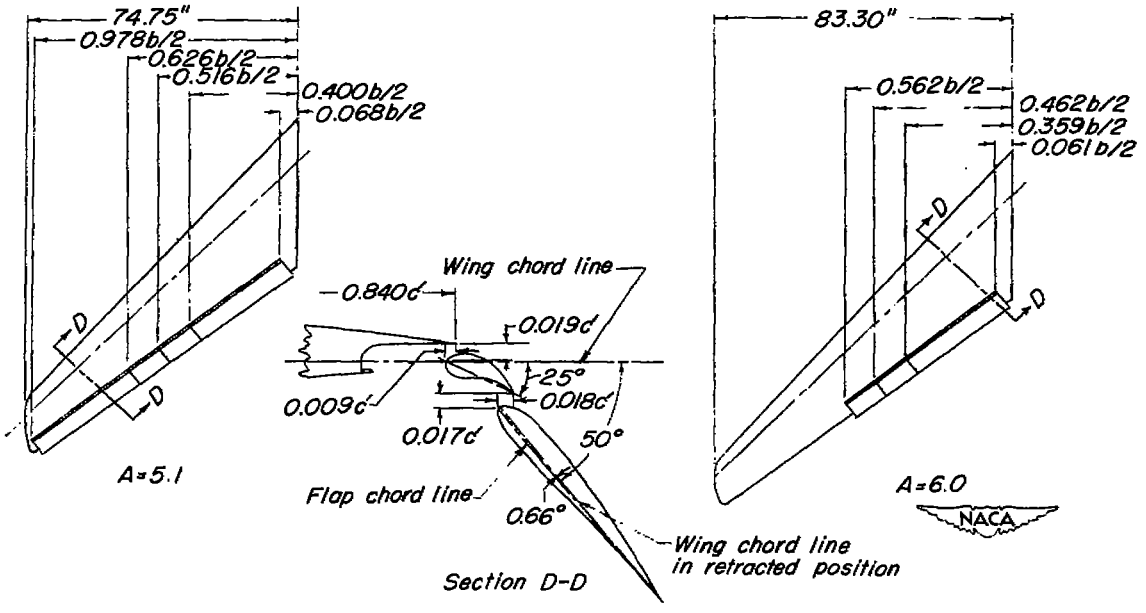


(d) Double-slotted flaps.

Figure 2.- Continued.

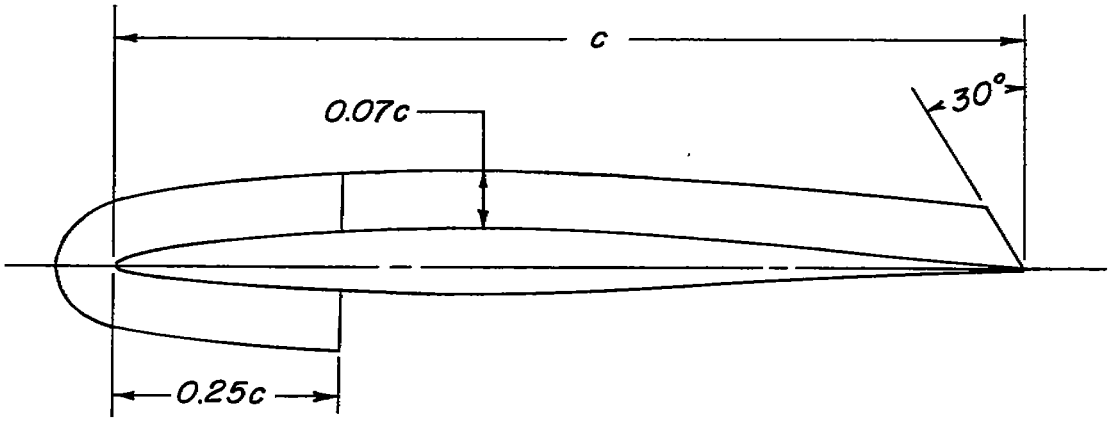


*(e) Type of fence tested on plain wing.*

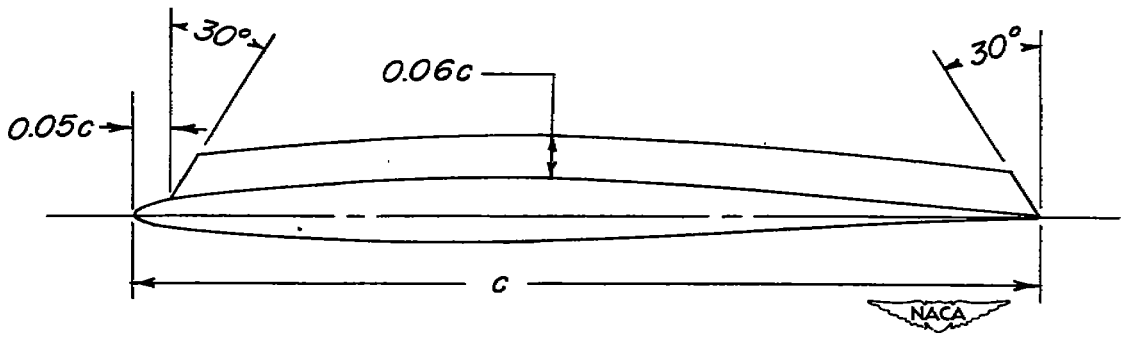


*(f) Type of fence used with leading-edge devices.*

Figure 2.- Concluded.


(a) Aspect ratio 5.1 wing with double slotted flaps and leading-edge flaps.

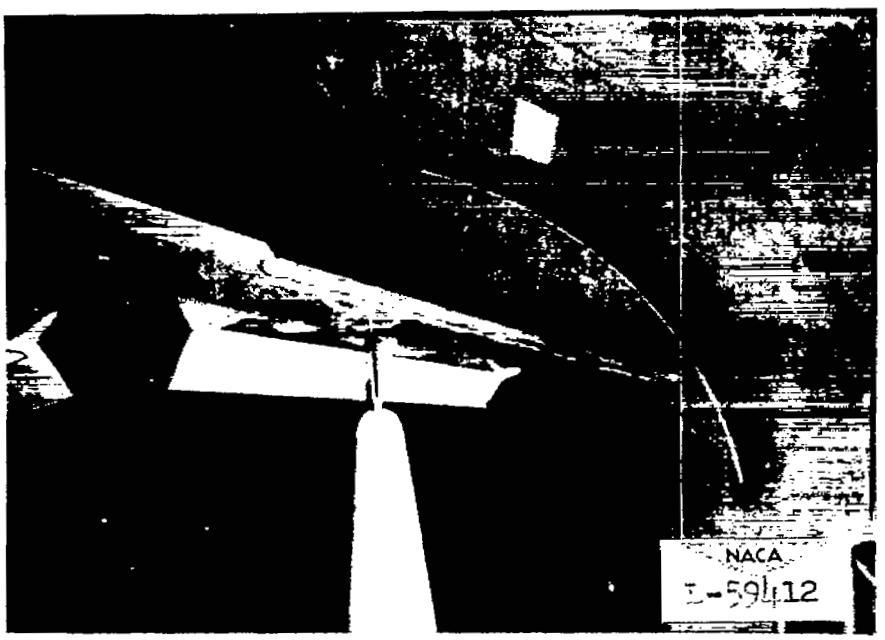


(b) Close-up showing drooped nose.

Figure 3.- The 47.7° sweptback wing mounted in the Langley 19-foot tunnel.

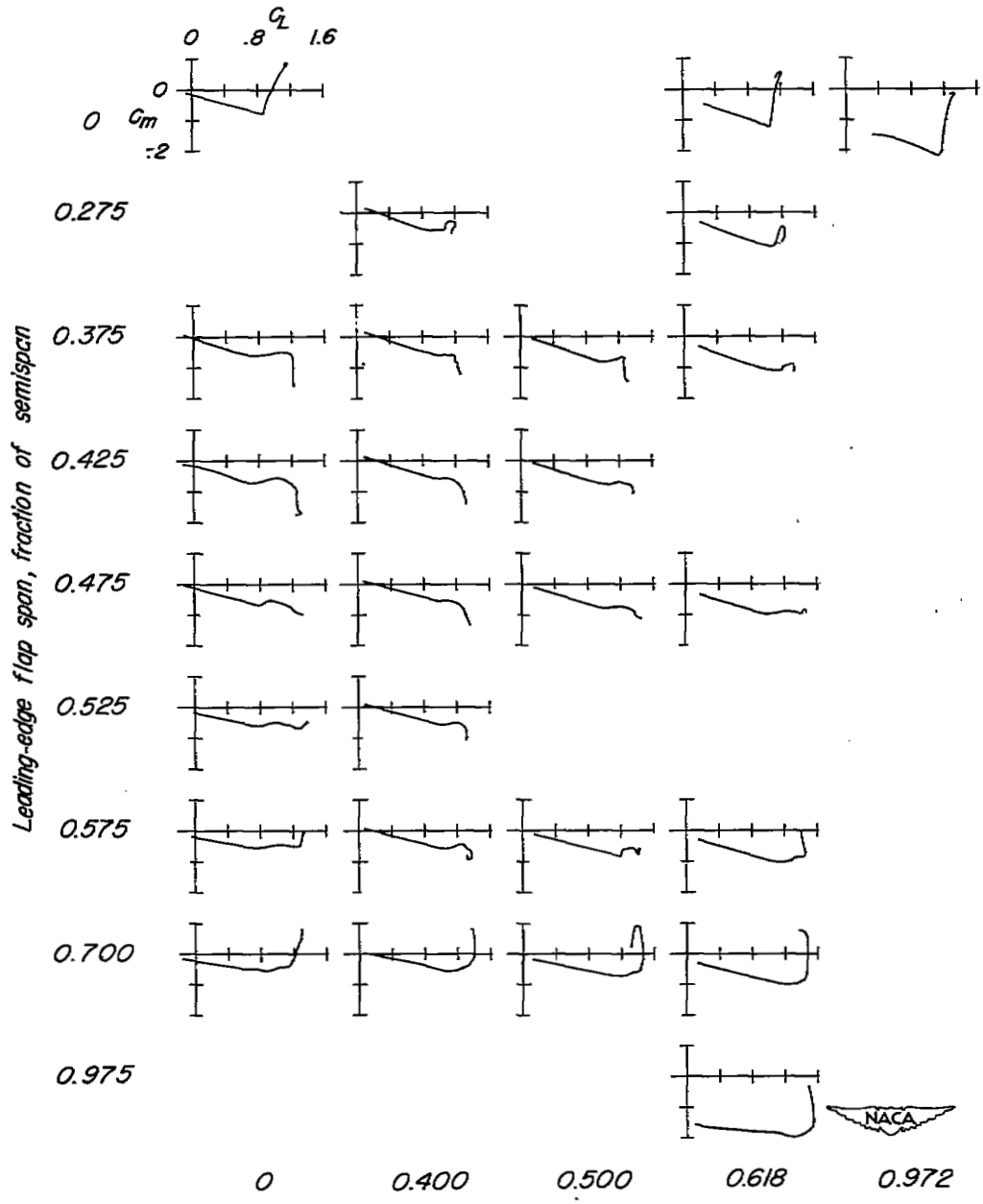


(a) Split flaps and leading-edge flaps.

Figure 4.- Summary of pitching-moment characteristics of the 47.7° swept-back wing of aspect ratio 5.1 with various combinations of leading-edge devices and trailing-edge flaps. $R \approx 6.0 \times 10^6$.

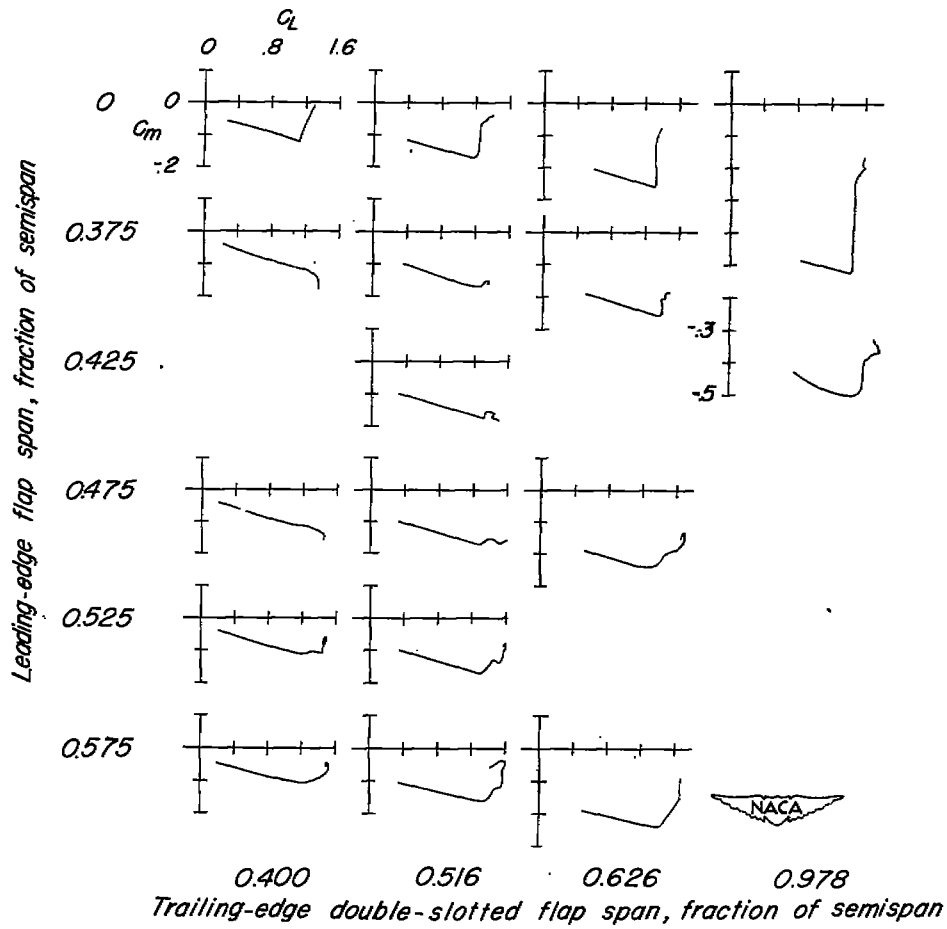


(b) Double slotted flaps and leading-edge flaps.

Figure 4.- Continued.

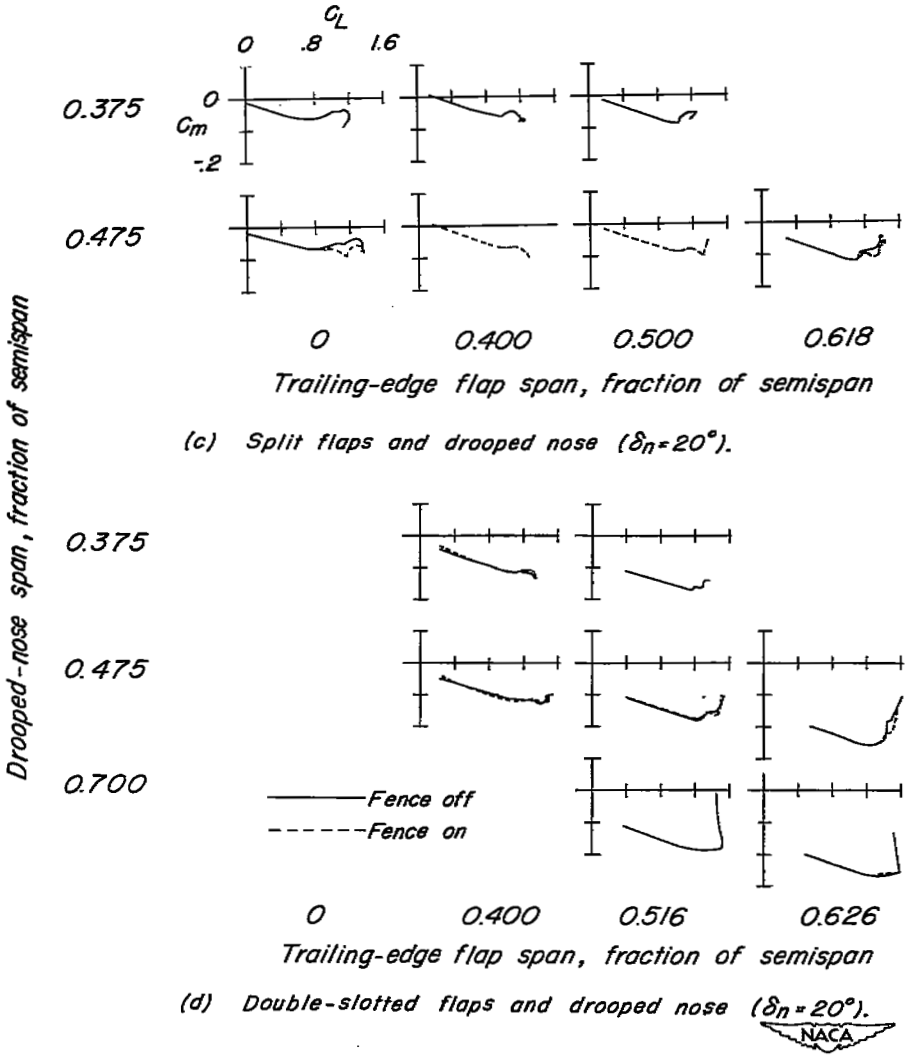


(c) Split flaps and drooped nose ($\delta_n = 20°$).

(d) Double-slotted flaps and drooped nose ($\delta_n = 20°$).

Figure 4.- Concluded.

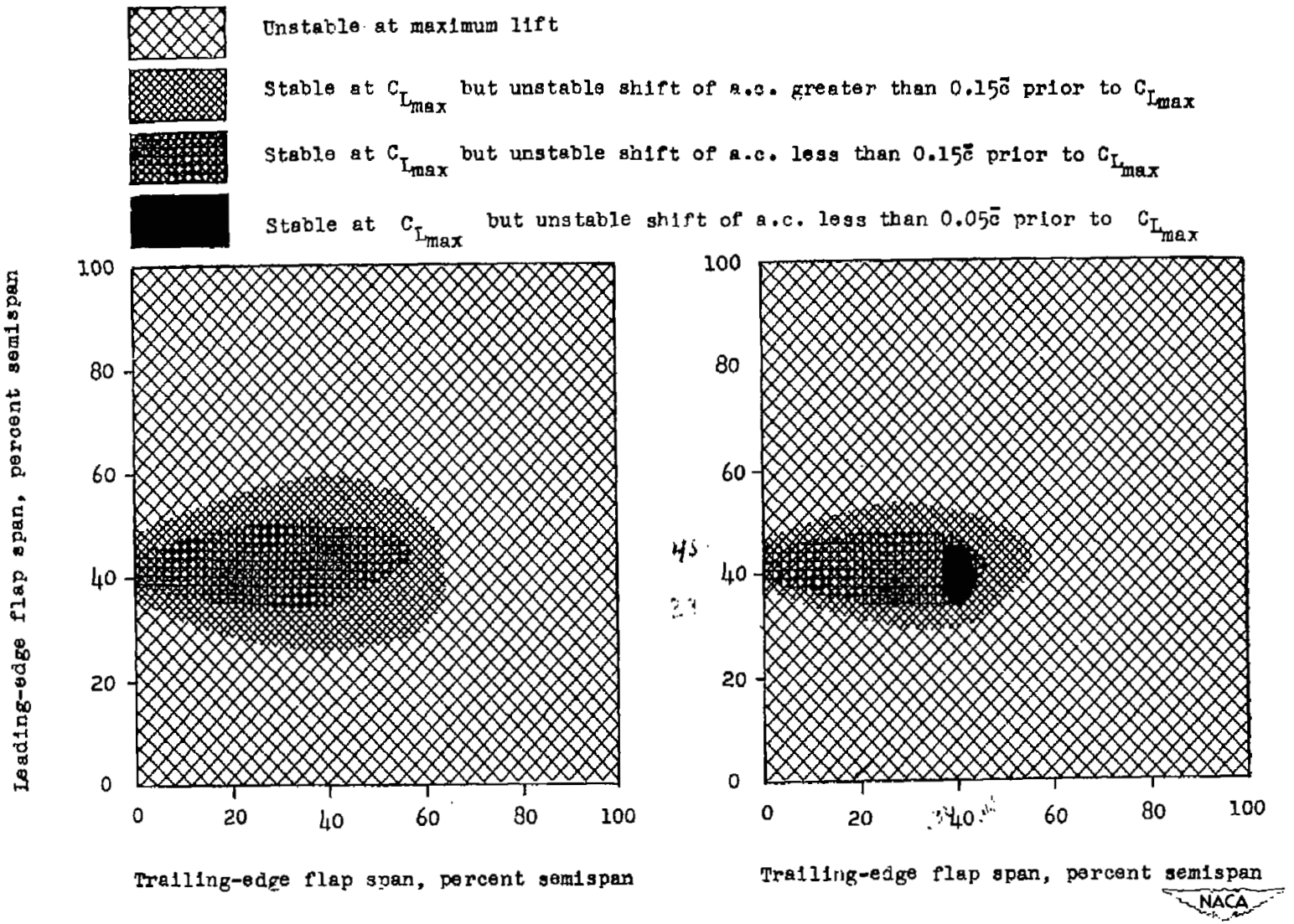


(a) Split flaps.

(b) Double slotted flaps.

Figure 5.- General summary of the effects of leading-edge and trailing-edge flap span on longitudinal stability characteristics of a $47.7^{\circ}$ sweptback wing of aspect ratio 5.1.

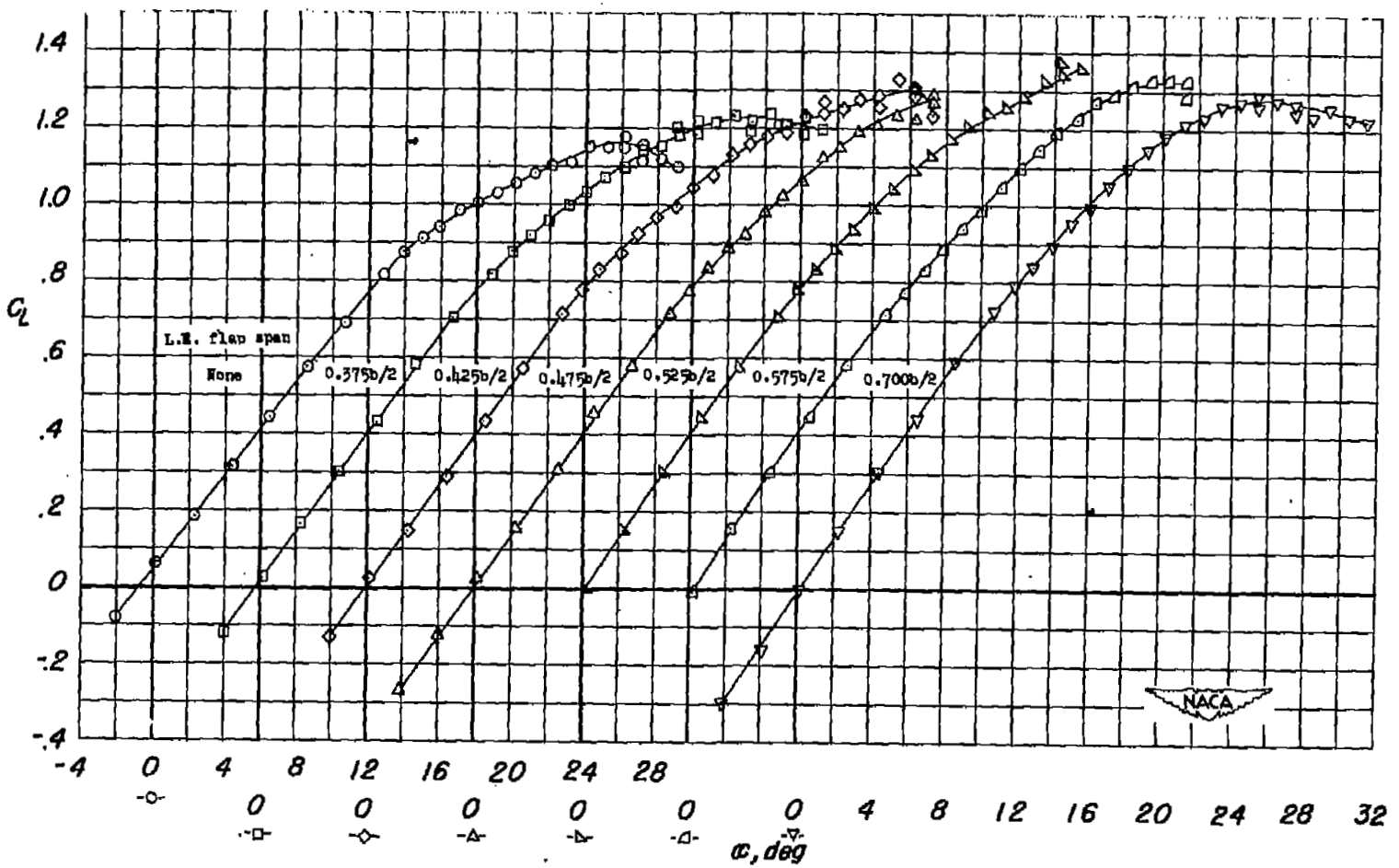


(a) $C_L$ against α.

Figure 6.- Effects of leading-edge flaps of various spans on the aerodynamic characteristics of a 47.7° sweptback wing of aspect ratio 5.1.
$R = 6.0 \times 10^6$.

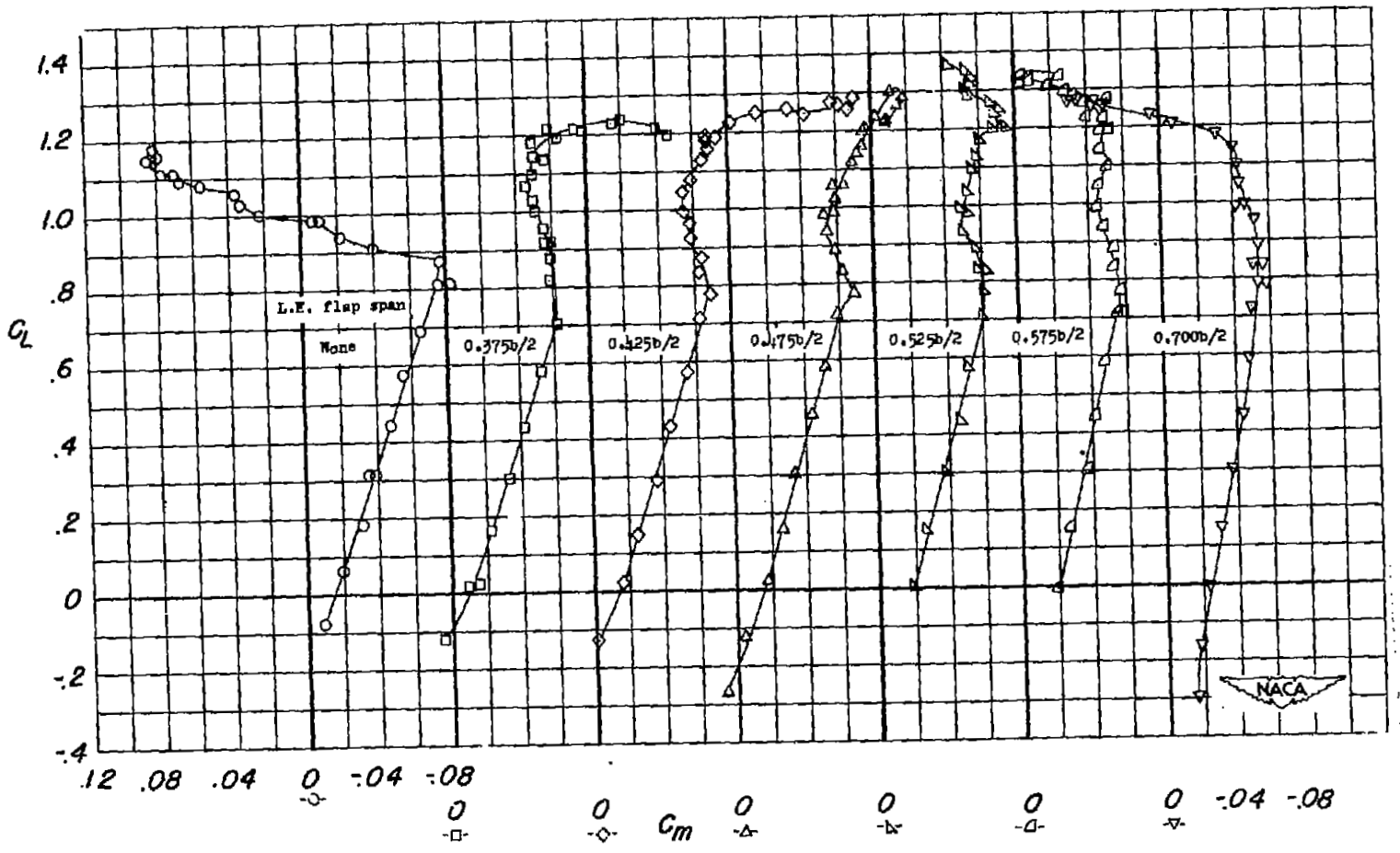


(b) $C_L$ against $C_m$.

Figure 6.- Continued.

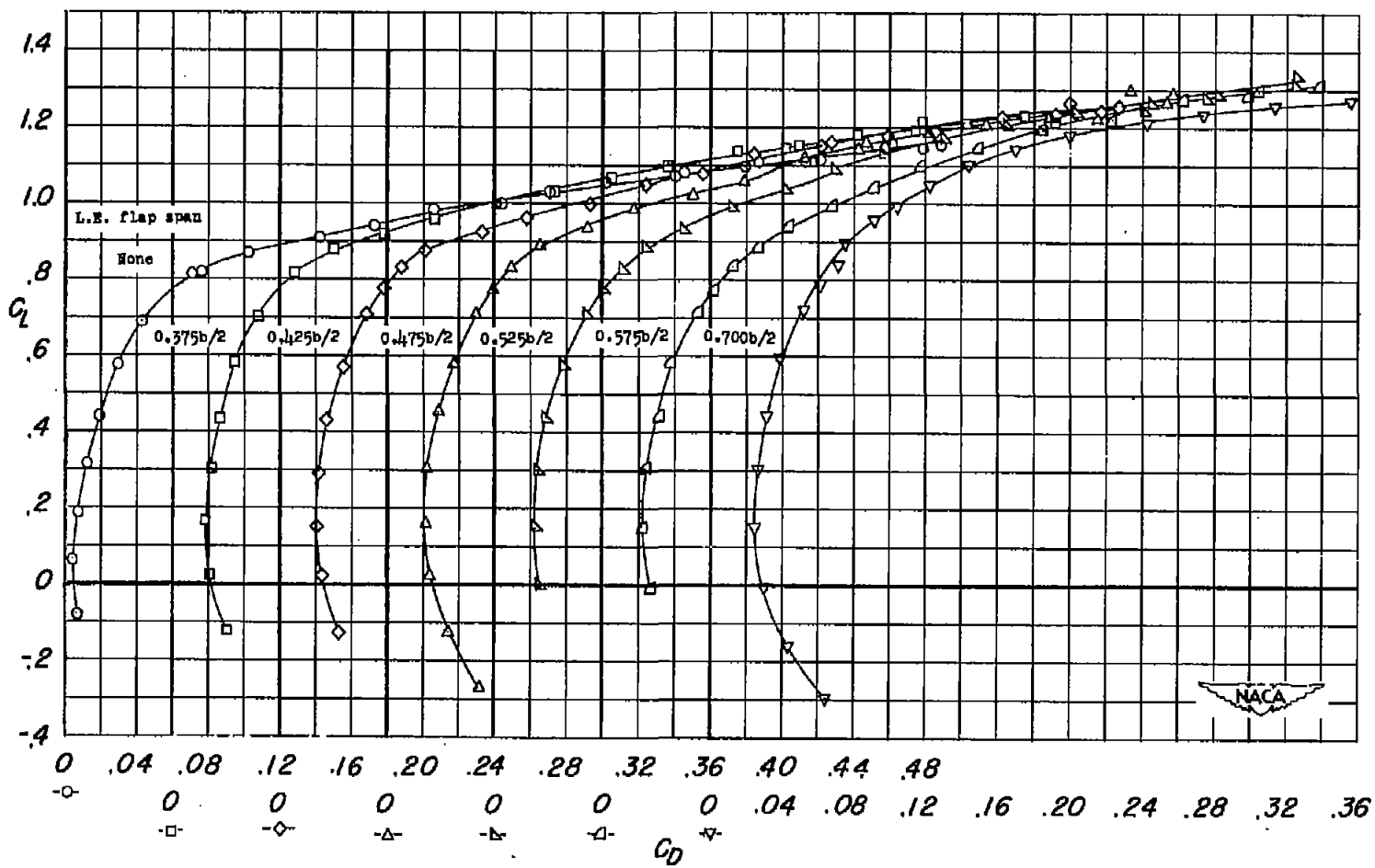


(c) $C_L$ against $C_D$.

Figure 6.- Concluded.

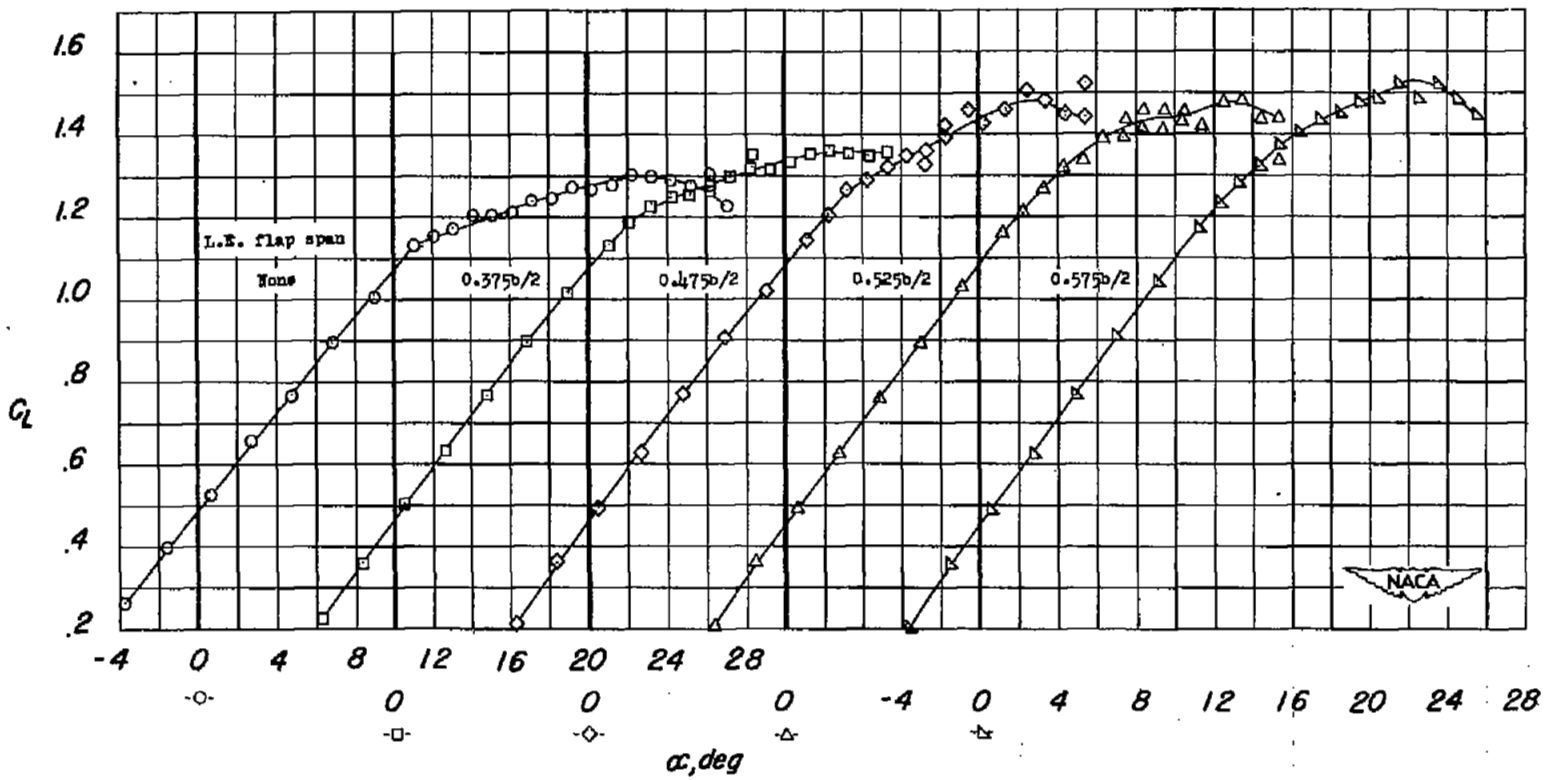


(a) $C_L$ against $\alpha$.

Figure 7.- Effects of leading-edge flaps of various spans on the aerodynamic characteristics of a 47.7° sweptback wing of aspect ratio 5.1 with 0.400b/2 trailing-edge double slotted flaps. $R = 6.0 \times 10^6$.

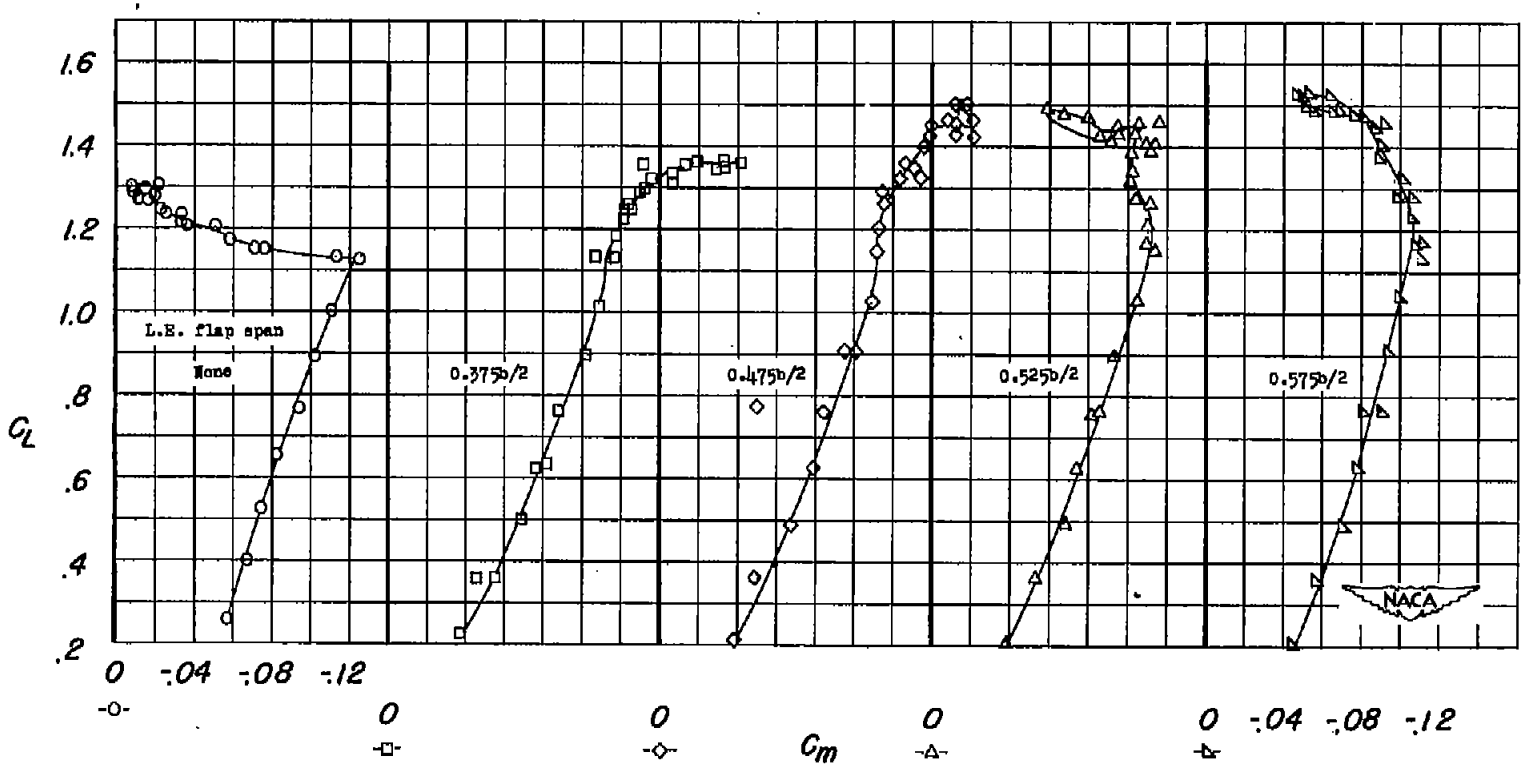


(b) $C_L$ against $C_m$.

Figure 7.- Continued.

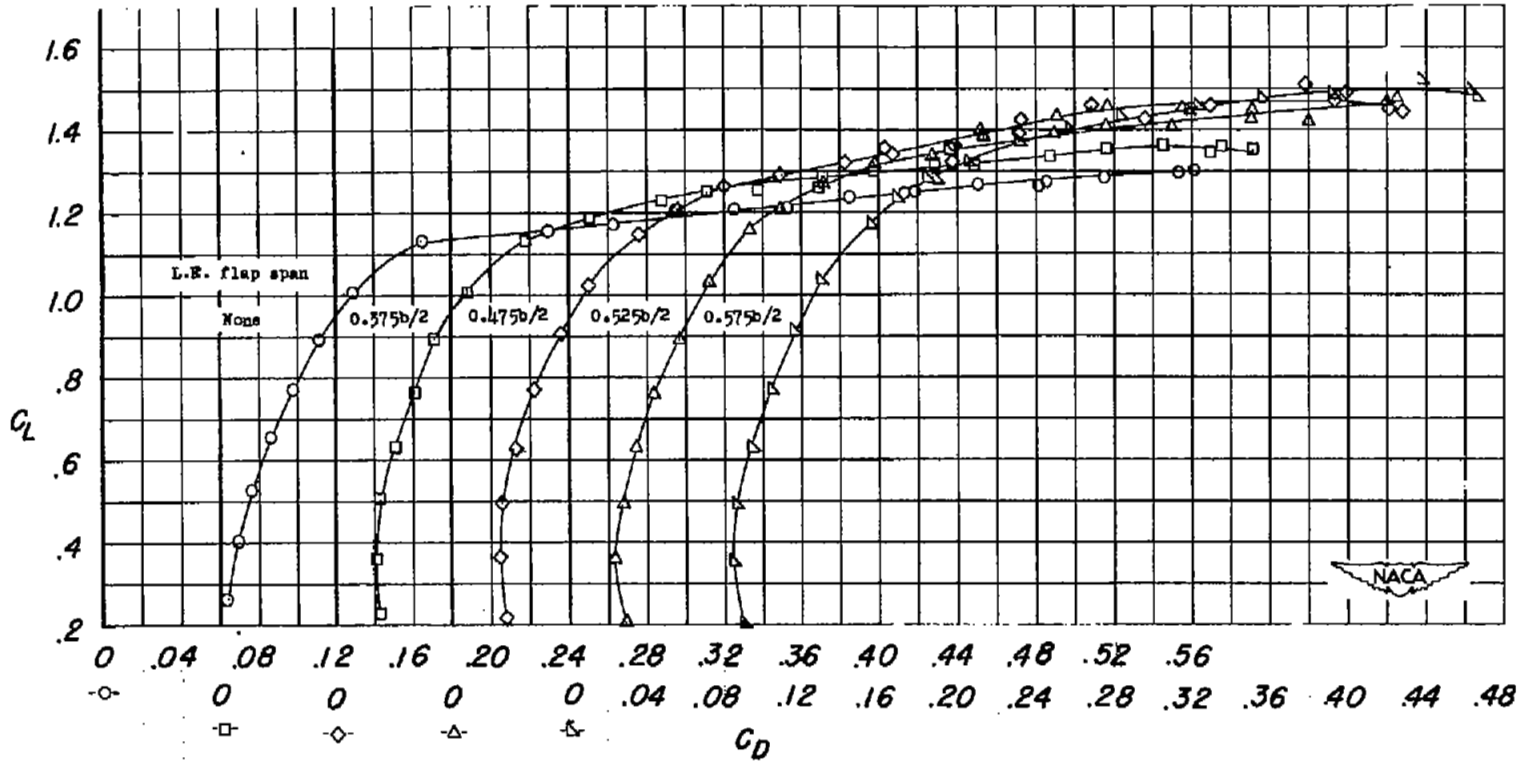


(c) $C_L$ against $C_D$.

Figure 7.- Concluded.

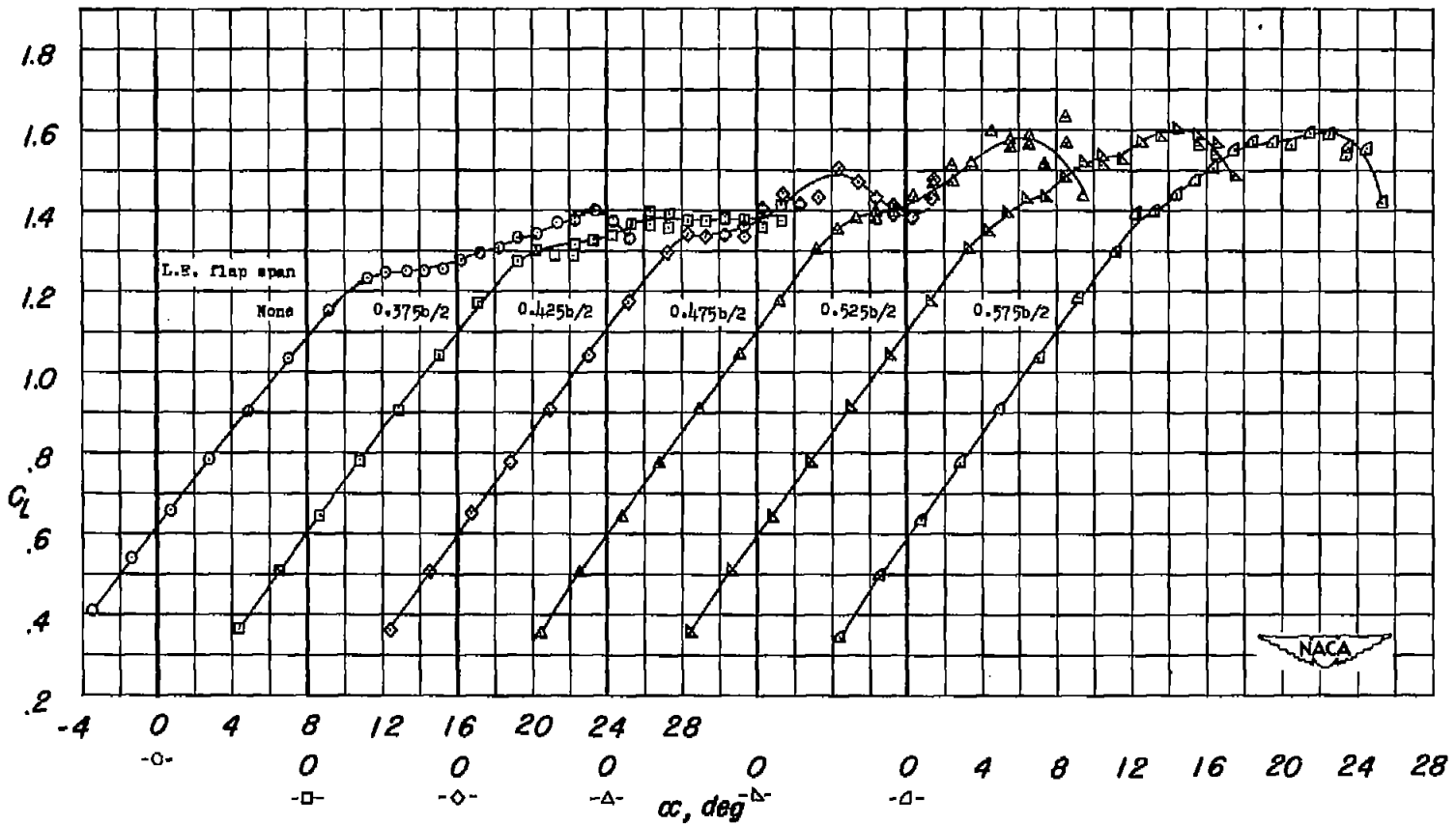


(a) $C_L$ against $\alpha$.

Figure 8.- Effects of leading-edge flaps of various spans on the aerodynamic characteristics of a 47.7° sweptback wing of aspect ratio 5.1 with 0.516b/2 trailing-edge double slotted flaps. $R = 6.0 \times 10^6$.

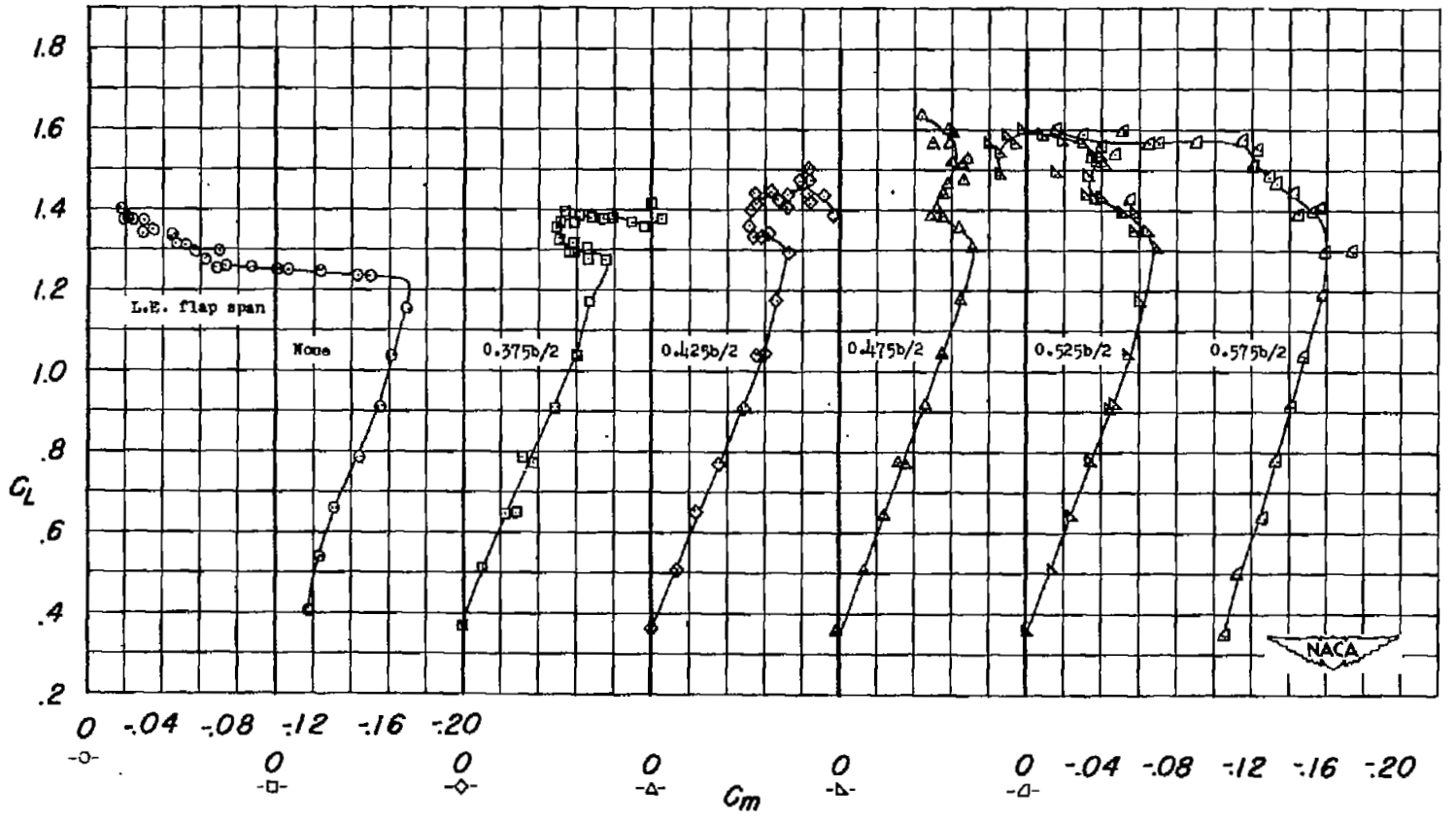


(b) $C_L$ against $C_m$.

Figure 8.- Continued.

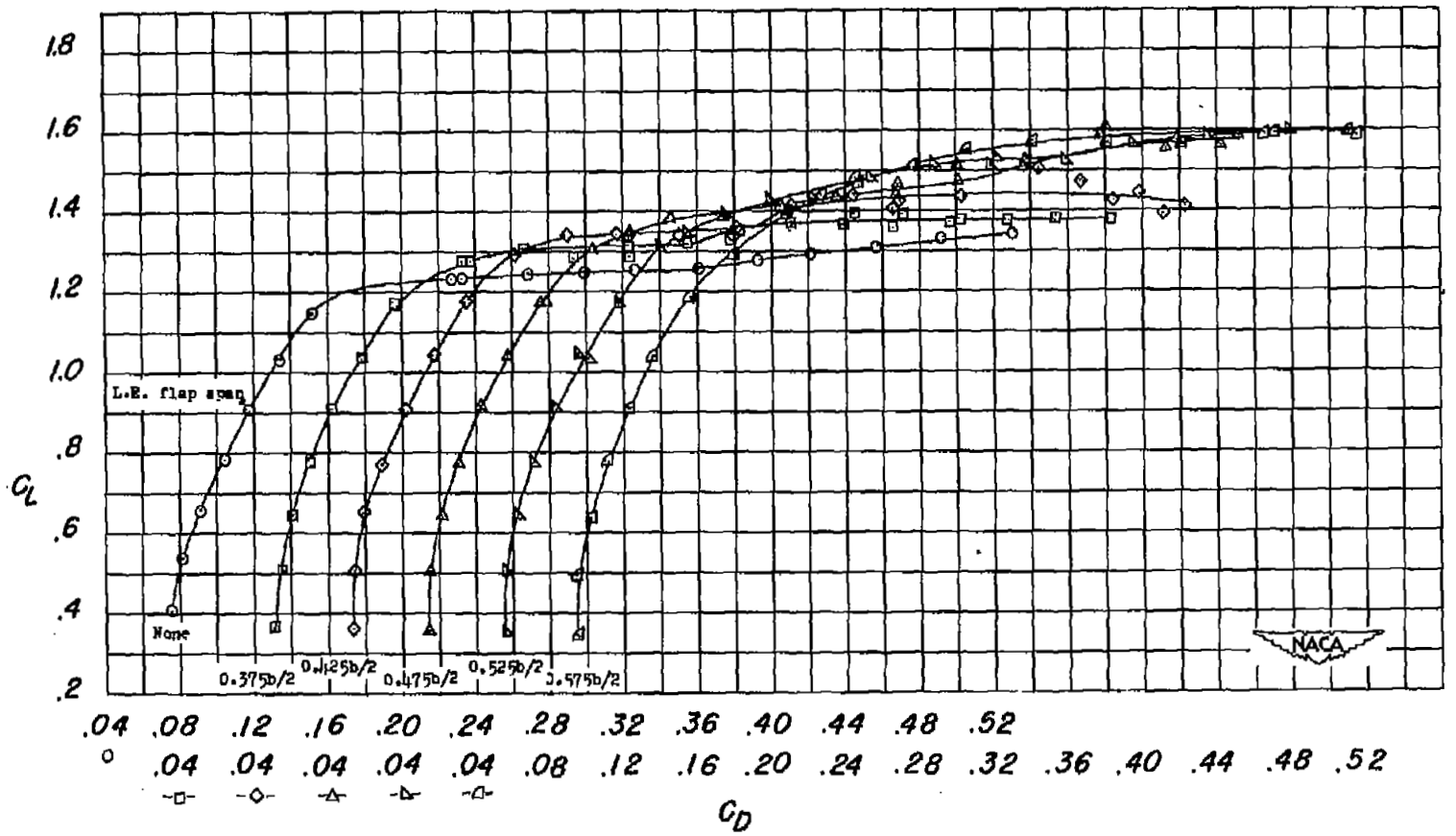


(c) $C_L$ against $C_D$.

Figure 8.- Concluded.

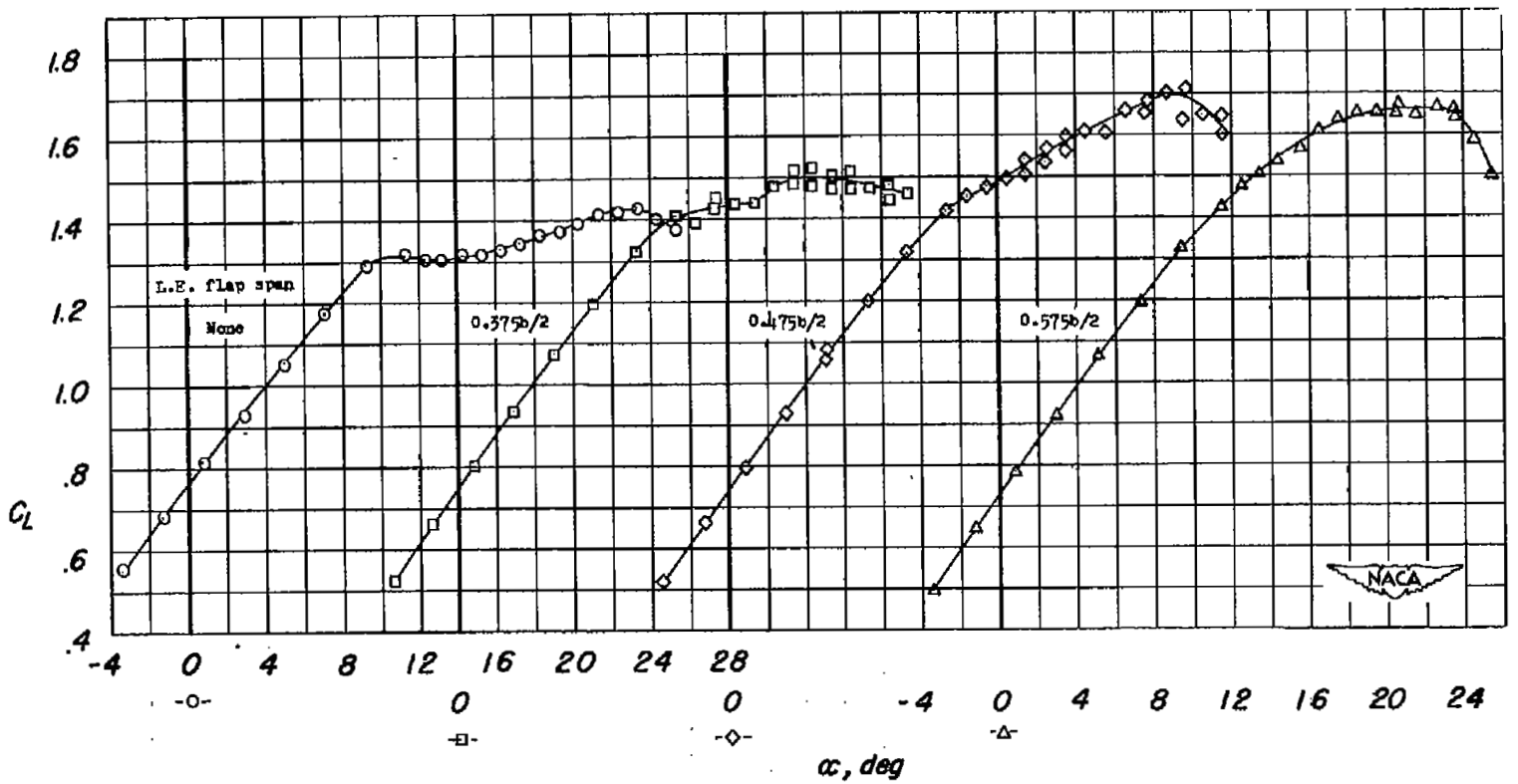


(a) $C_L$ against $\alpha$.

Figure 9.- Effects of leading-edge flaps of various spans on the aerodynamic characteristics of a 47.7° sweptback wing of aspect ratio 5.1 with 0.626b/2 trailing-edge double slotted flaps. $R = 6.0 \times 10^6$.

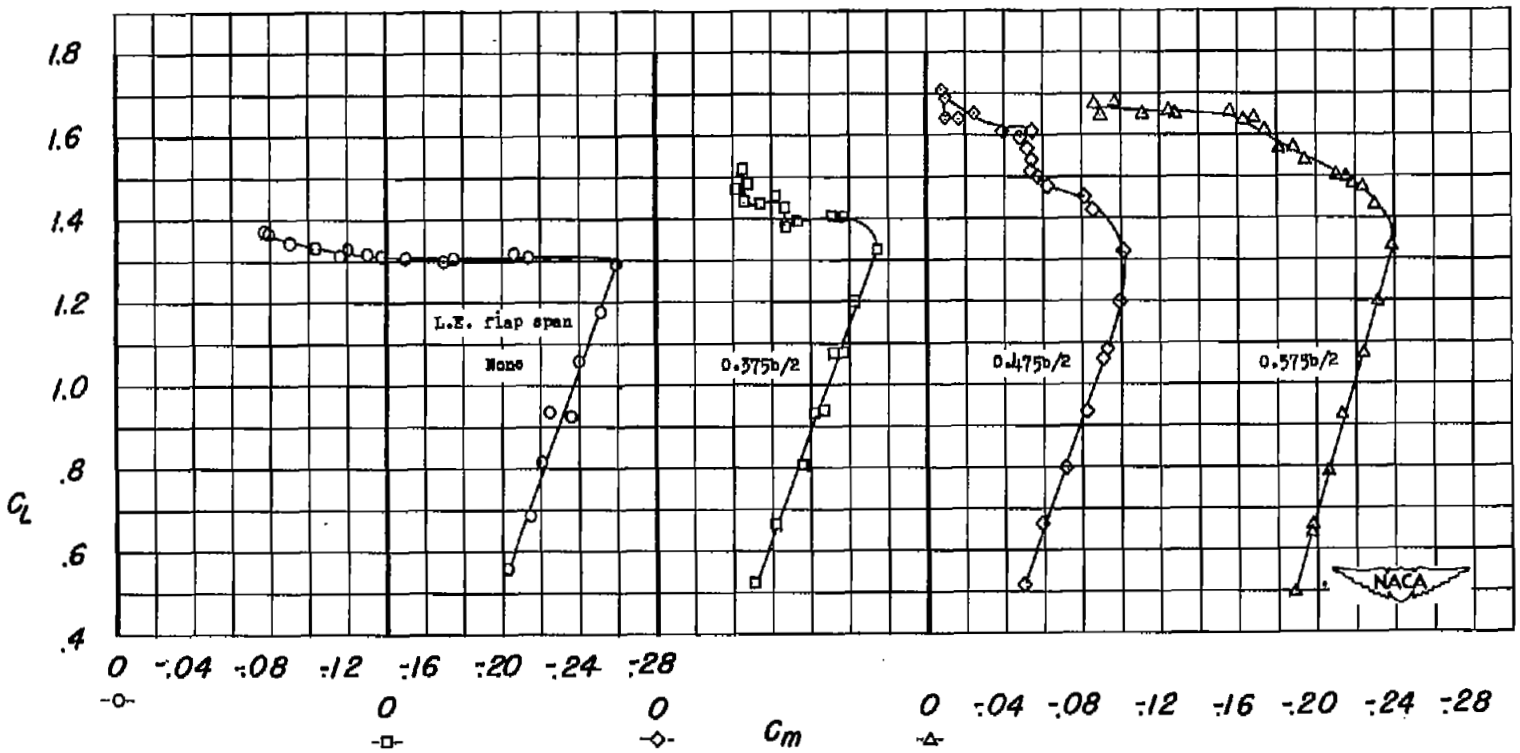


(b) $C_L$ against $C_m$.

Figure 9.- Continued.

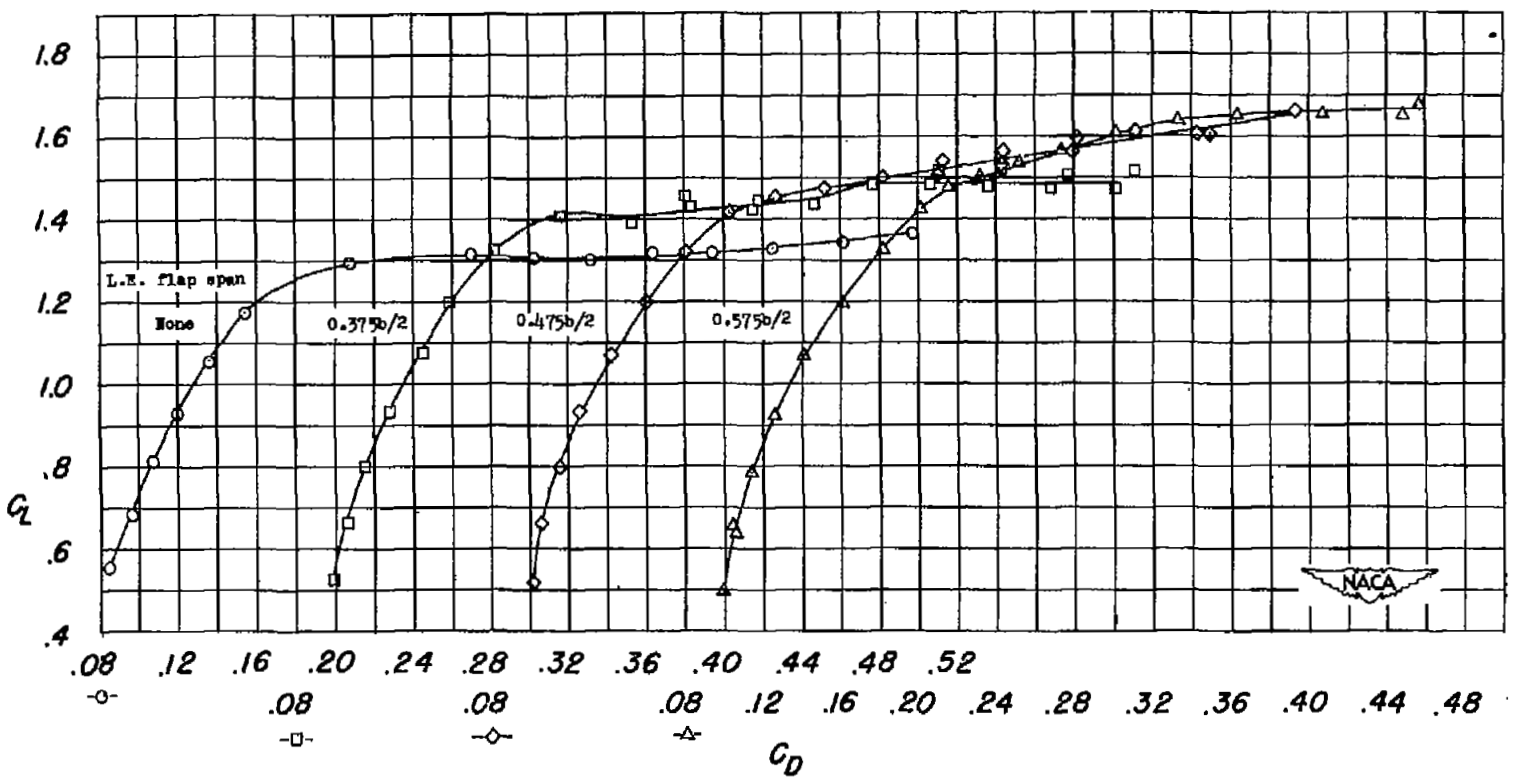


(c) $C_L$ against $C_D$.

Figure 9.- Concluded.

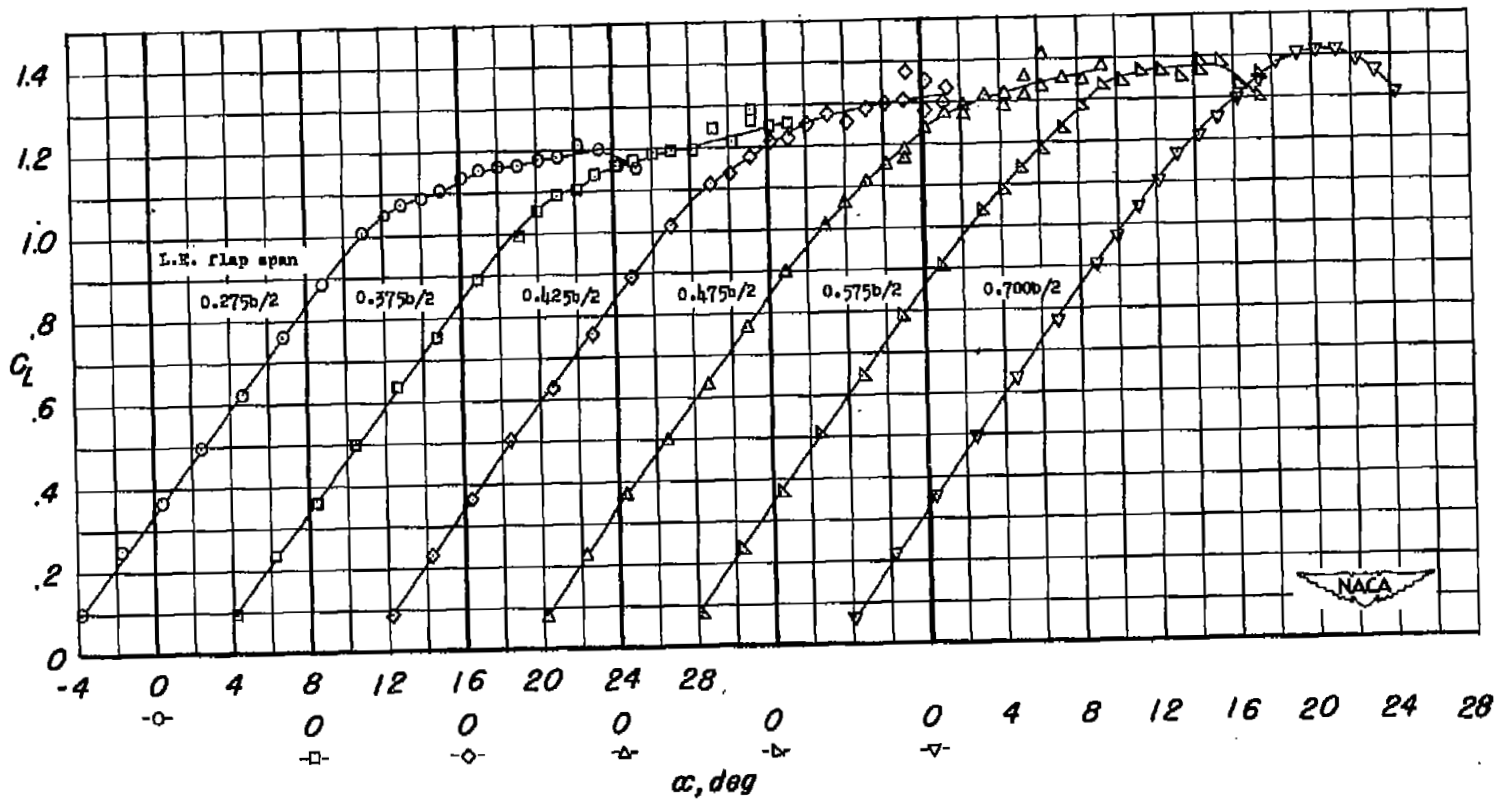


(a) $C_L$ against α.

Figure 10.- Effects of leading-edge flaps of various spans on the aerodynamic characteristics of a 47.7° sweptback wing of aspect ratio 5.1 with 0.400b/2 trailing-edge split flaps. $R = 6.0 \times 10^6$.

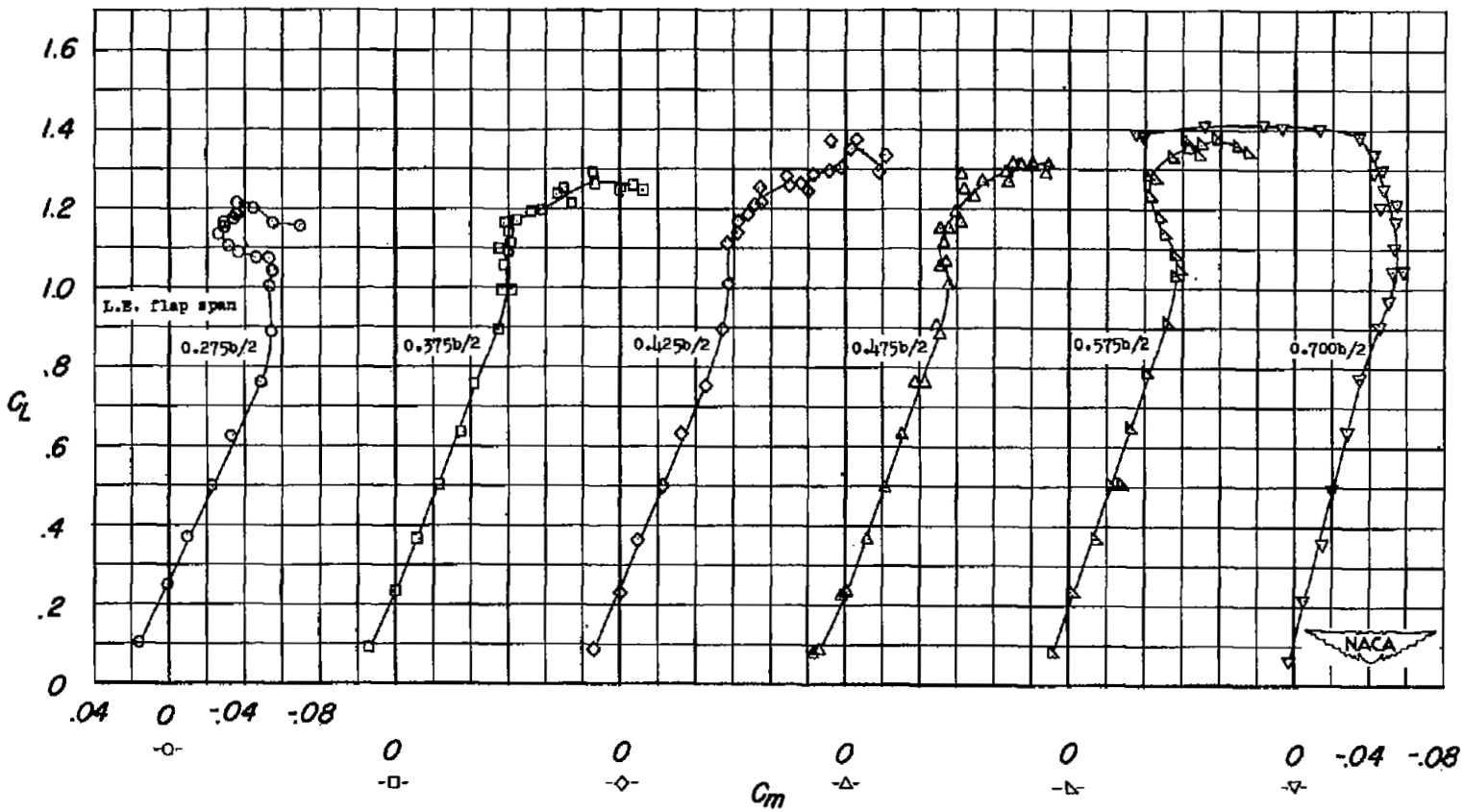


(b) $C_L$ against $C_m$.

Figure 10.- Continued.

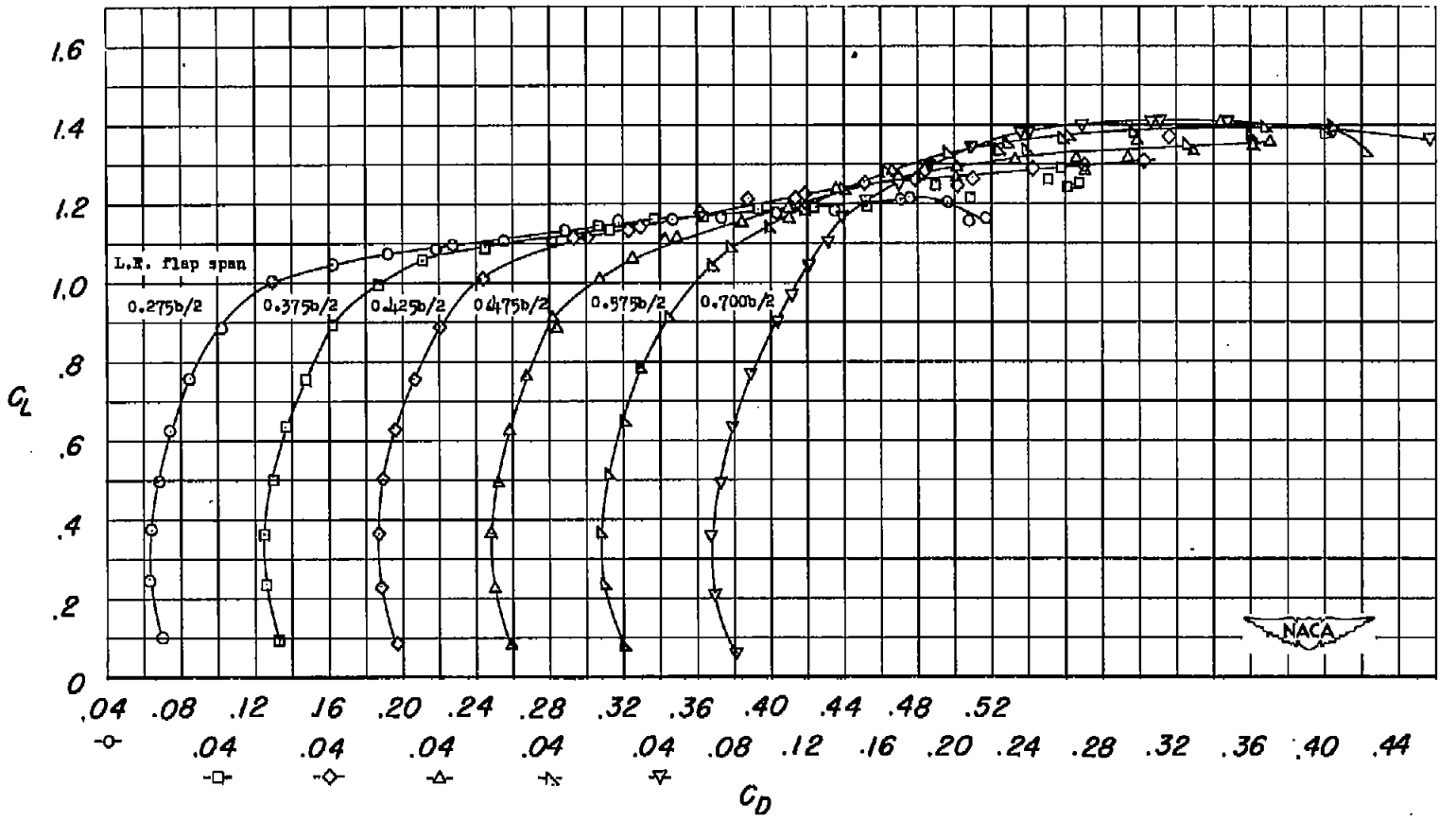


(c) $C_L$ against $C_D$.

Figure 10.- Concluded.

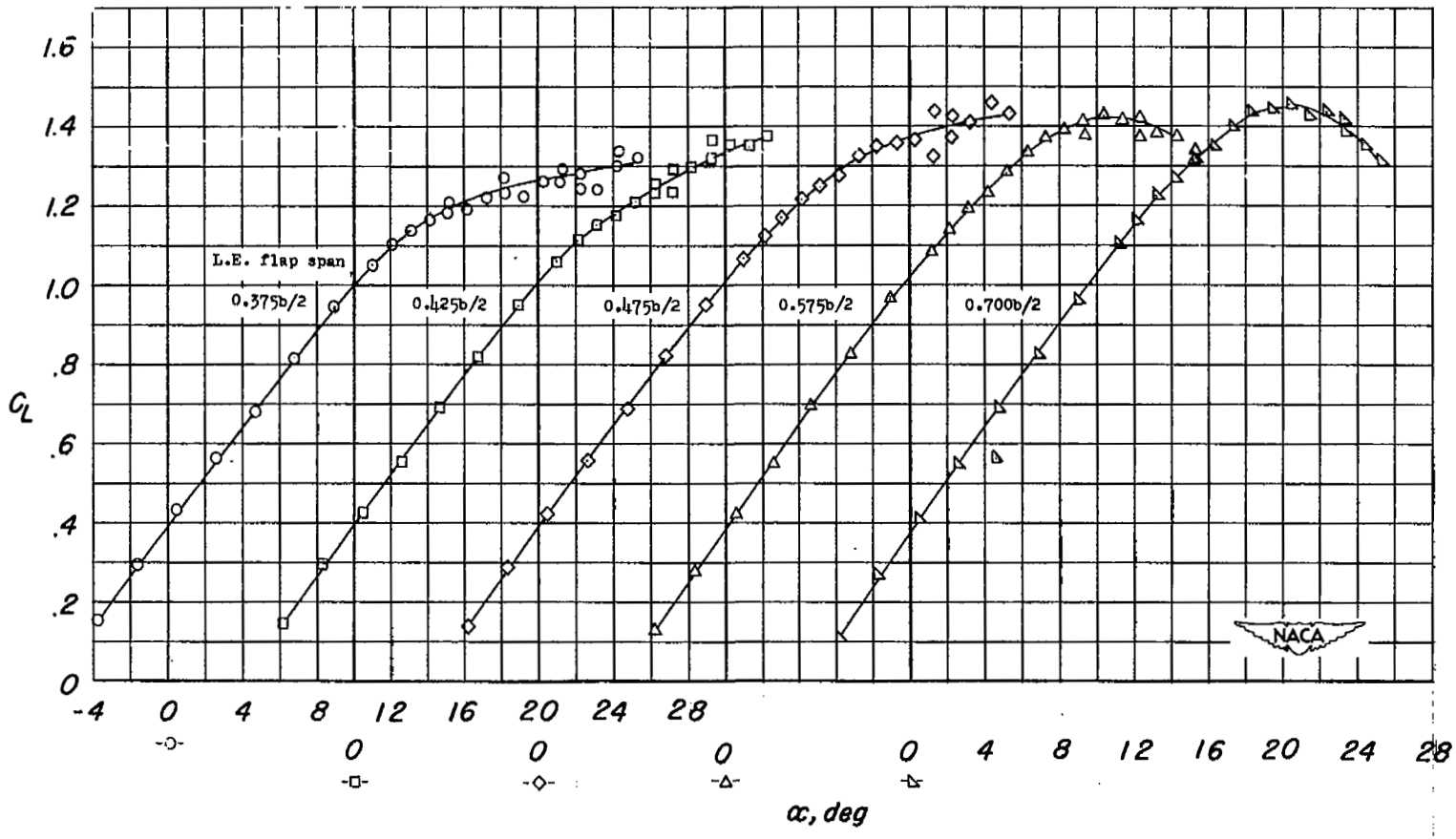


(a) $C_L$ against α.

Figure 11.- Effects of leading-edge flaps of various spans on the aerodynamic characteristics of a 47.7° wing of aspect ratio 5.1 with 0.500b/2 trailing-edge split flaps. $R = 6.0 \times 10^6$.

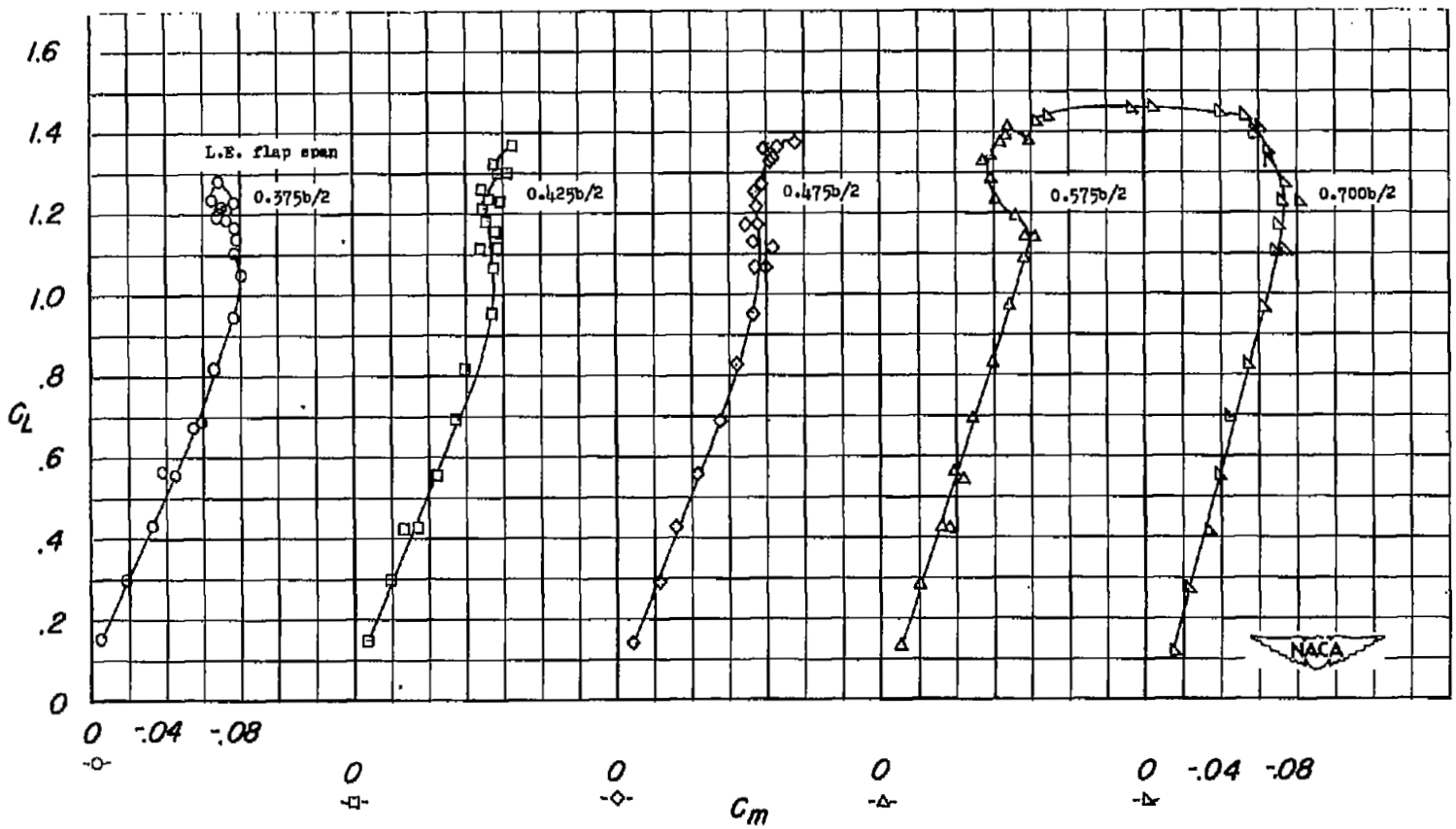


(b) $C_L$ against $C_m$.

Figure 11.- Continued.

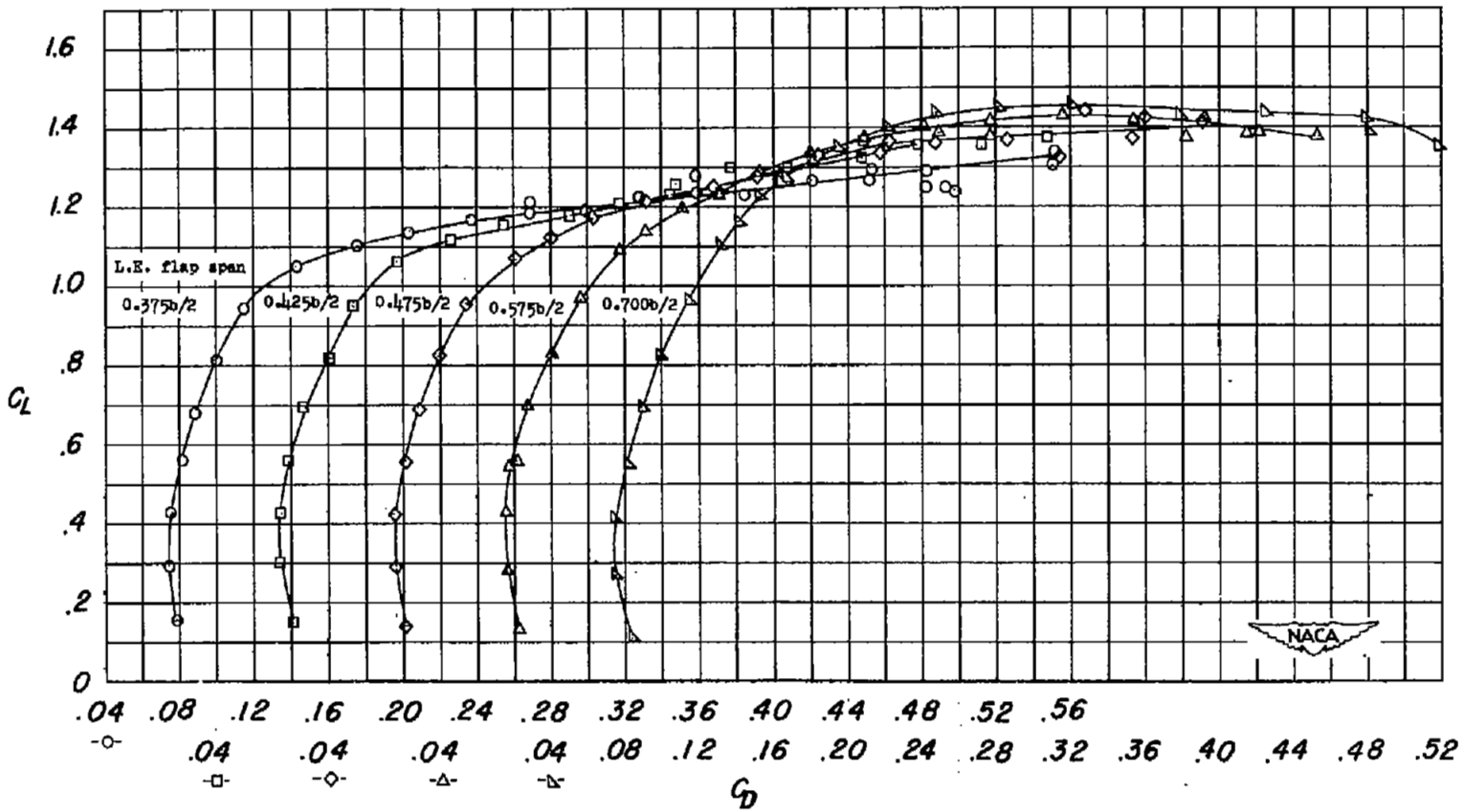


(c) $C_L$ against $C_D$.

Figure 11.- Concluded.

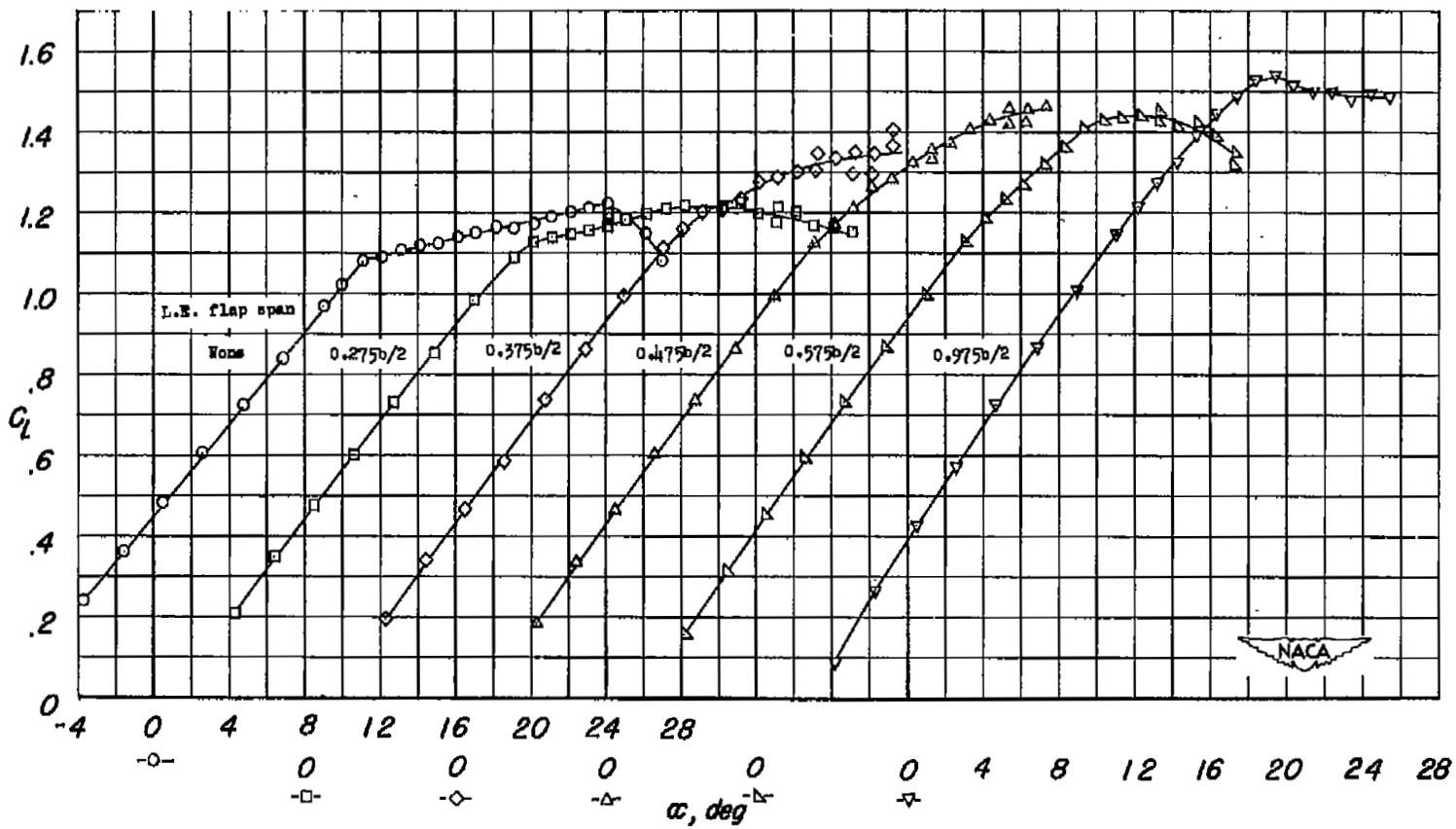


(a) $C_L$ against $\alpha$.

Figure 12.- Effects of leading-edge flaps of various spans on the aerodynamic characteristics of a 47.7° sweptback wing of aspect ratio 5.1 with 0.618b/2 trailing-edge split flaps deflected. $R = 6.0 \times 10^6$.

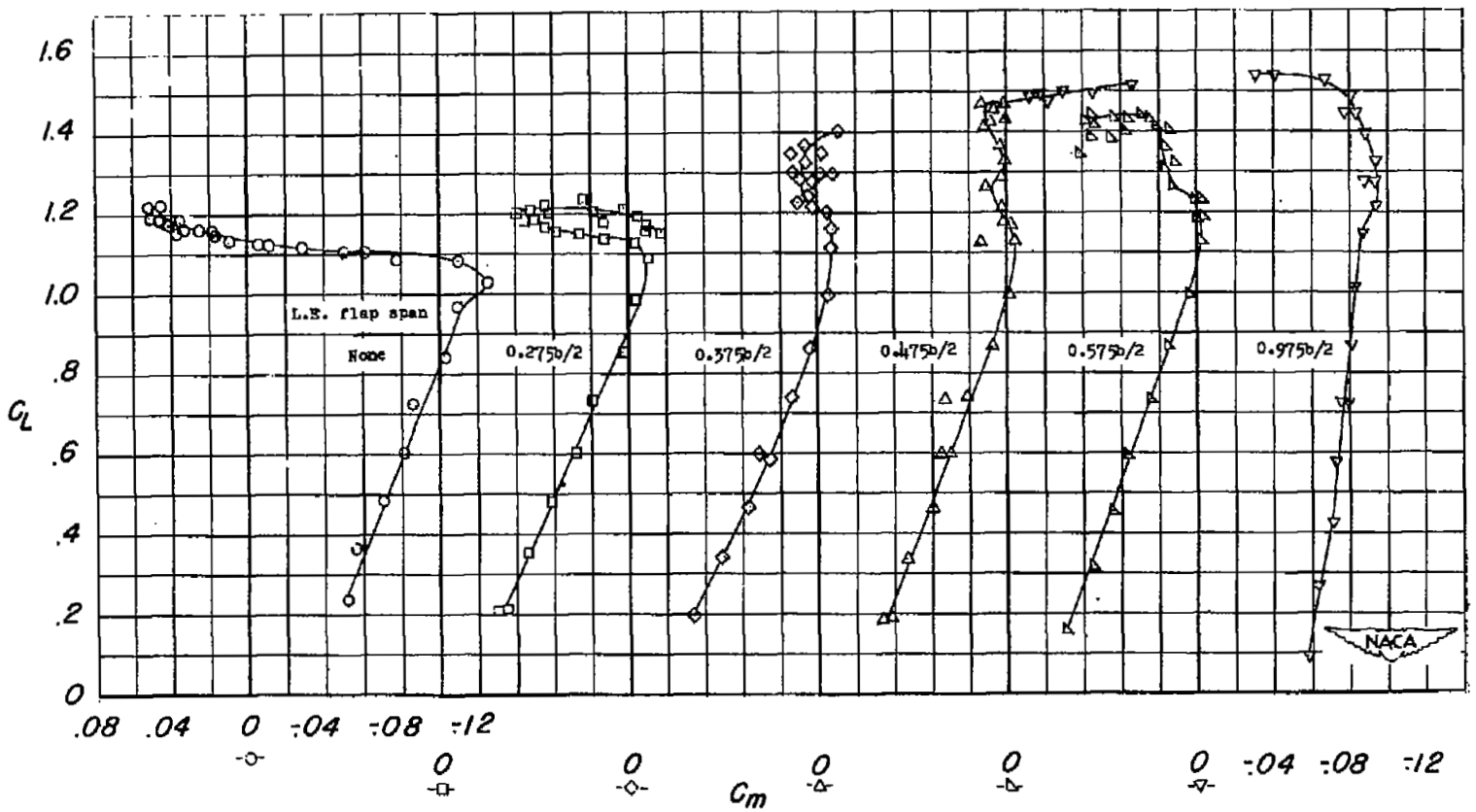


(b) $C_L$ against $C_m$.

Figure 12.- Continued.

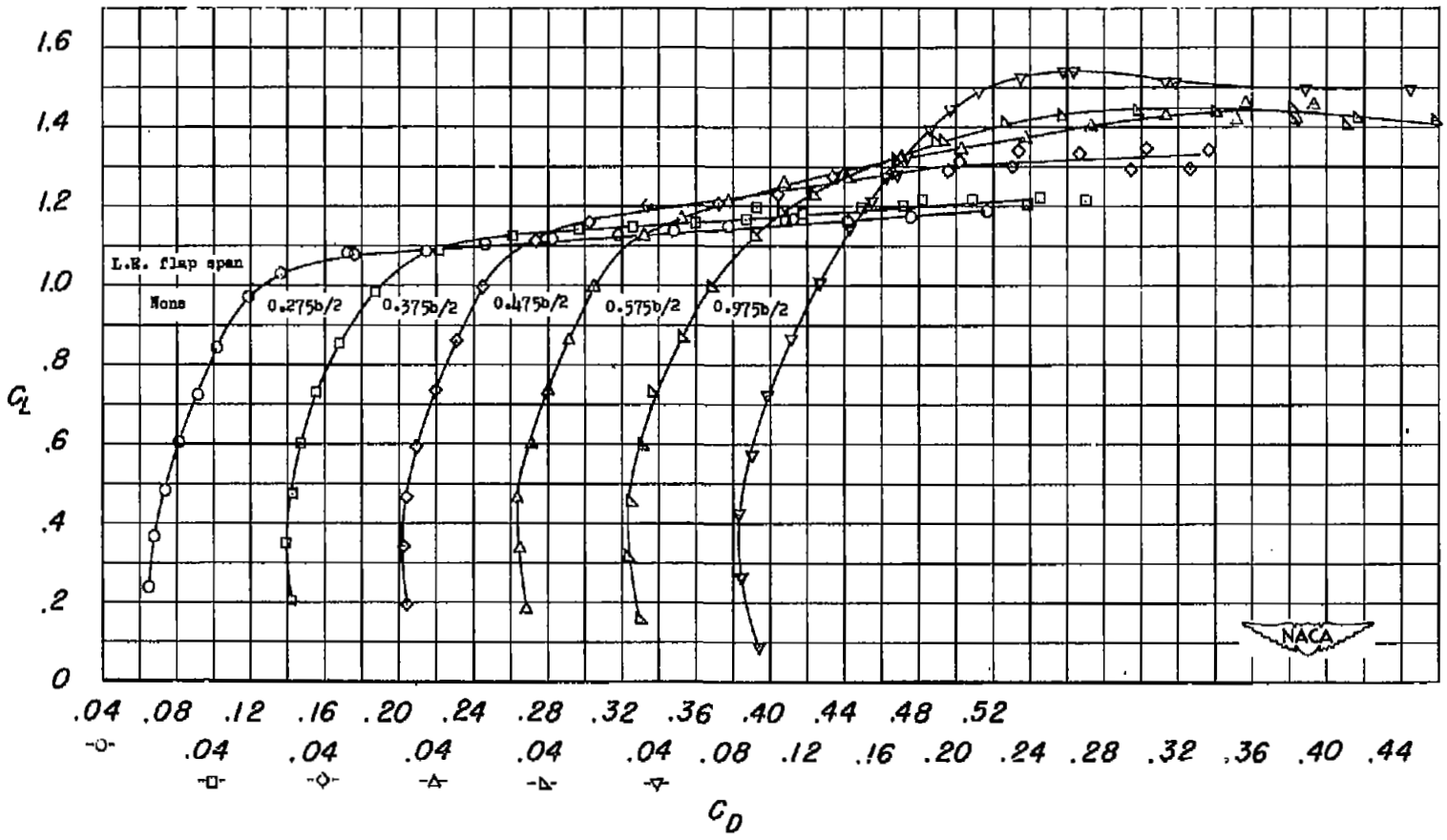


(c) $C_L$ against $C_D$.

Figure 12.- Concluded.

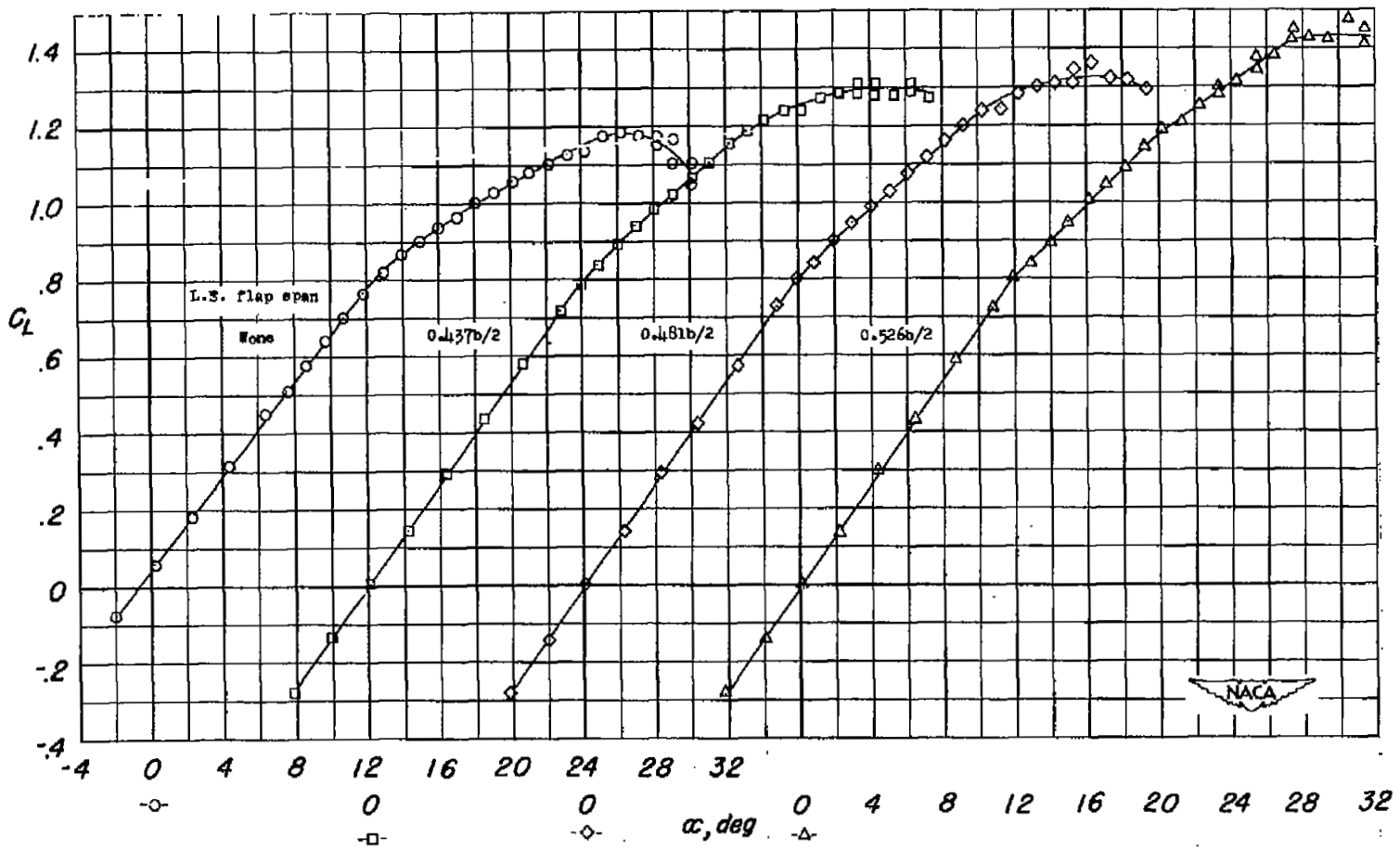


(a) $C_L$ against α.

Figure 13.- Effects of leading-edge flaps of various spans on the aerodynamic characteristics of a 47.7° sweptback wing of aspect ratio 6.0. $R = 6.0 \times 10^6$.

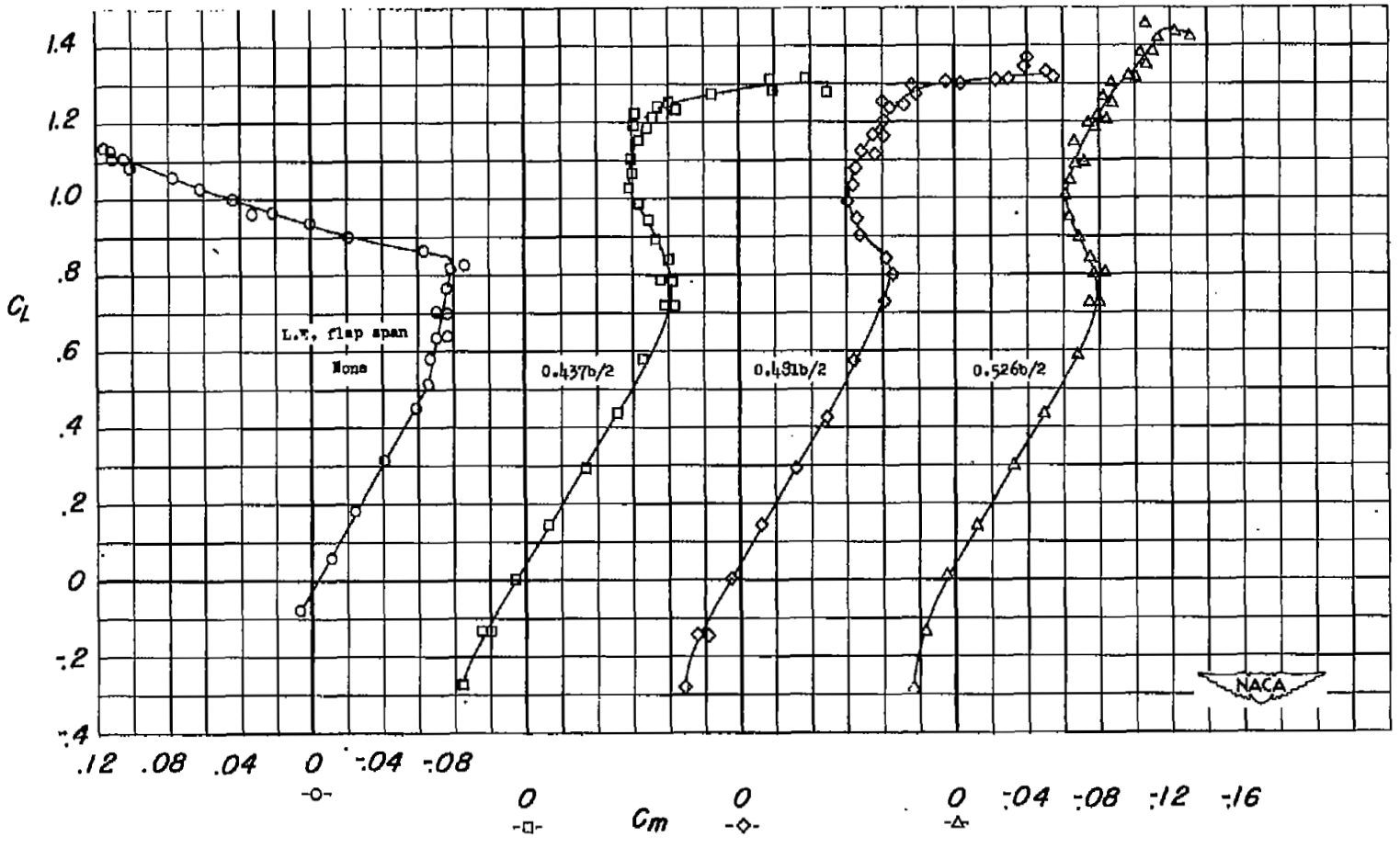


(b) $C_L$ against $C_m$.

Figure 13.- Continued.

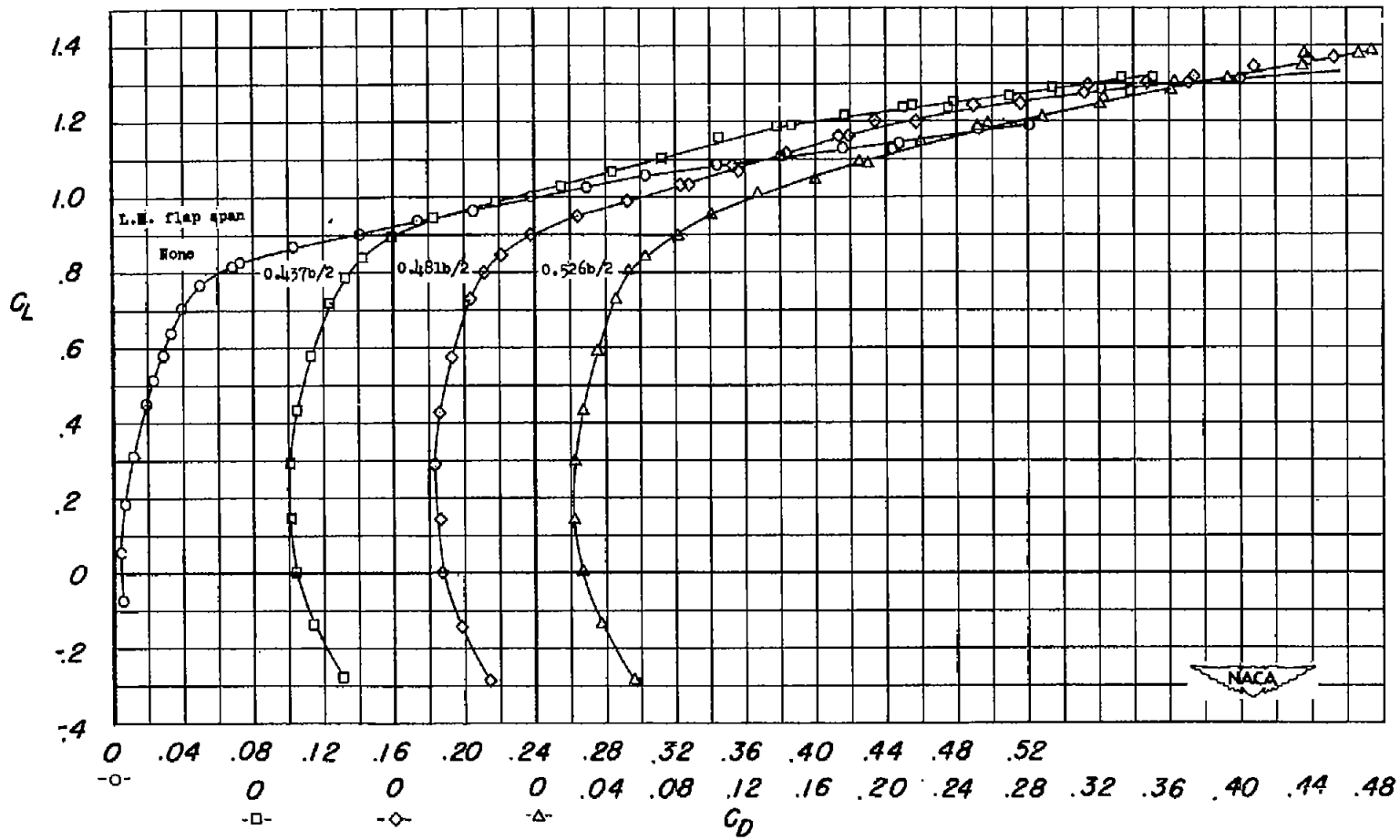


(c) $C_L$ against $C_D$.

Figure 13.- Concluded.

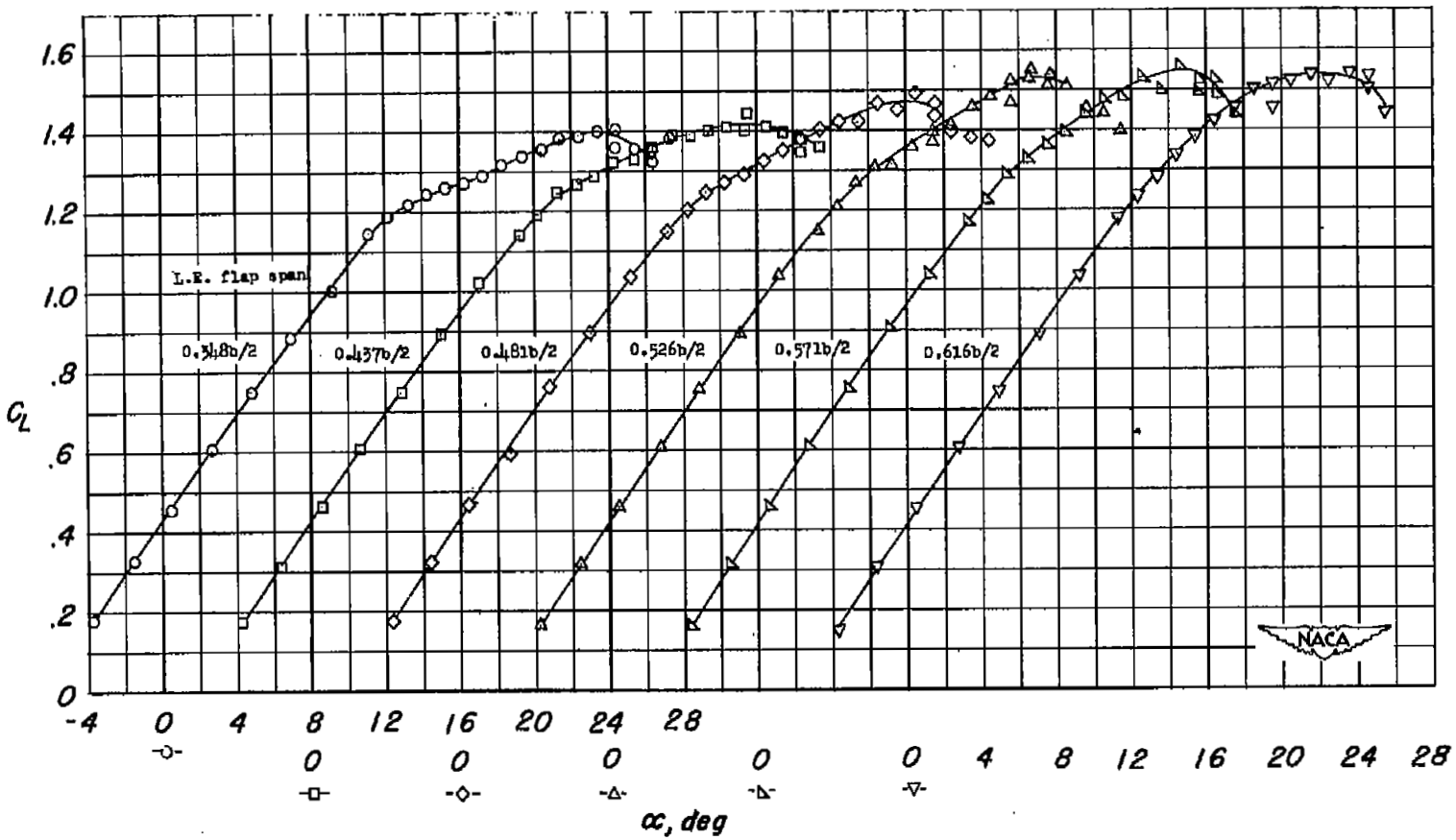


(a) $C_L$ against $\alpha$.

Figure 14.- Effects of leading-edge flaps of various spans on the aerodynamic characteristics of a 47.7° sweptback wing of aspect ratio 6.0 with 0.359b/2 trailing-edge double slotted flaps. $R = 6.0 \times 10^6$.

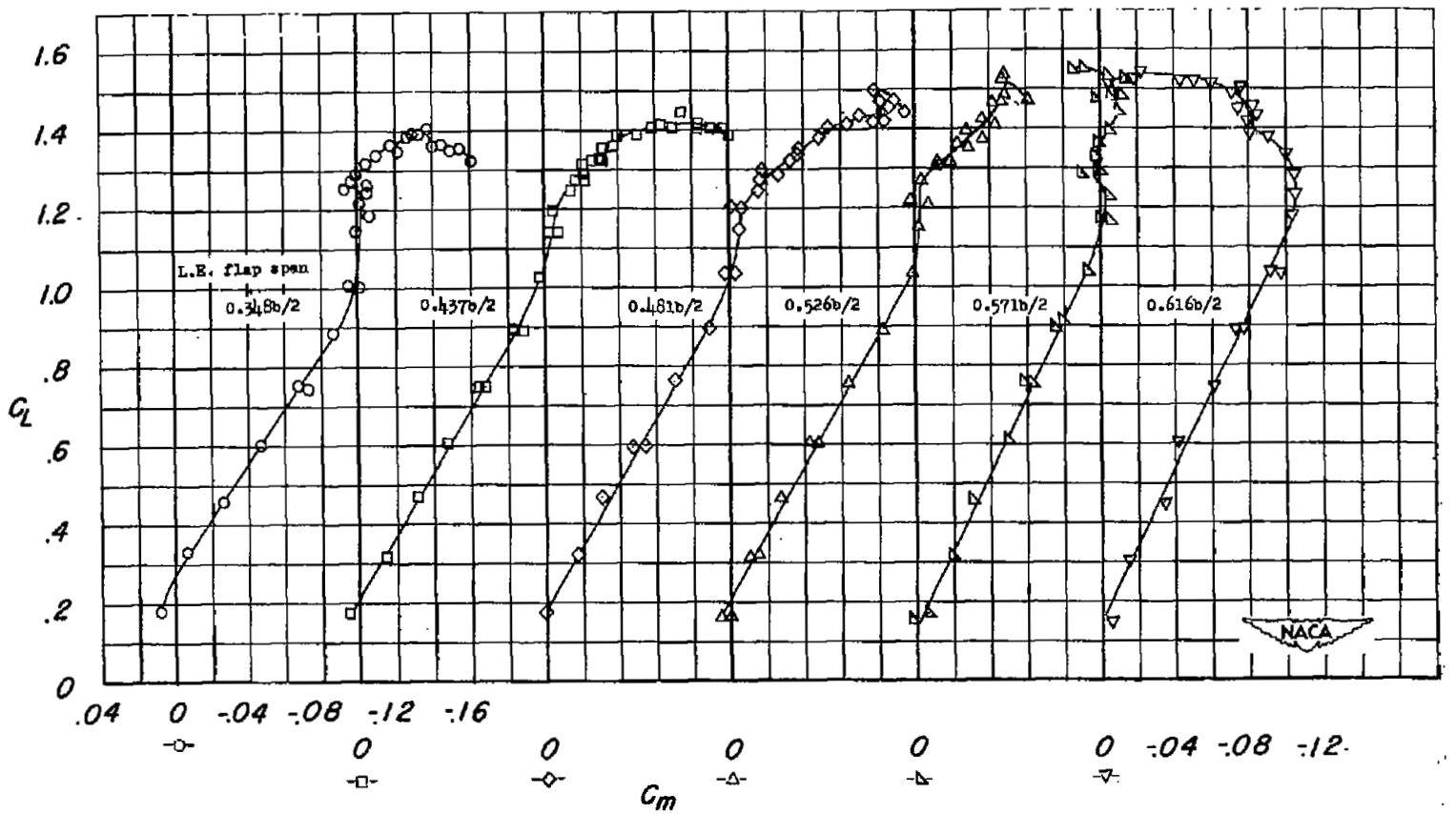


(b) $C_L$ against $C_m$.

Figure 14.- Continued.

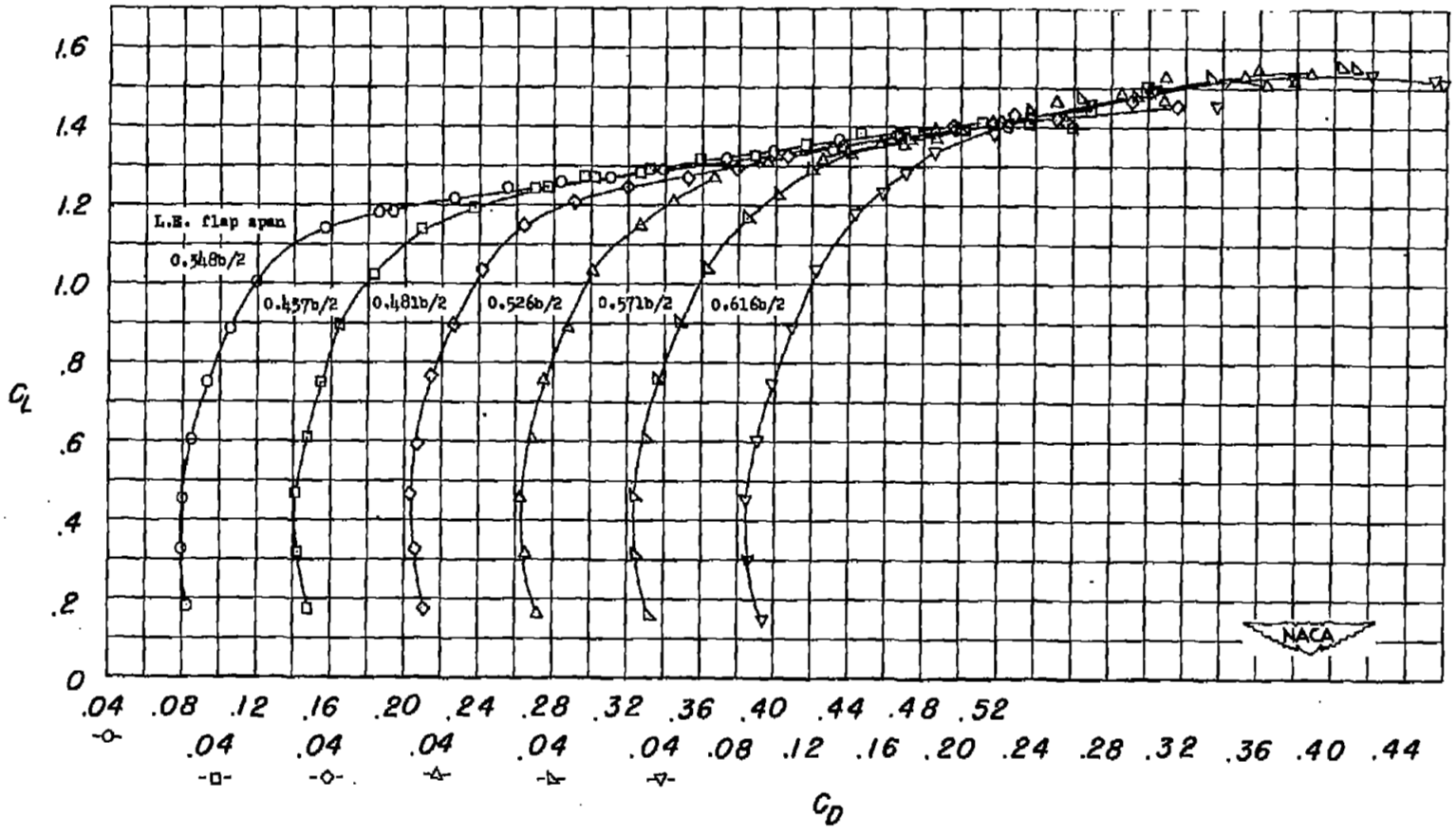


(c) $C_L$ against $C_D$.

Figure 14.- Concluded.

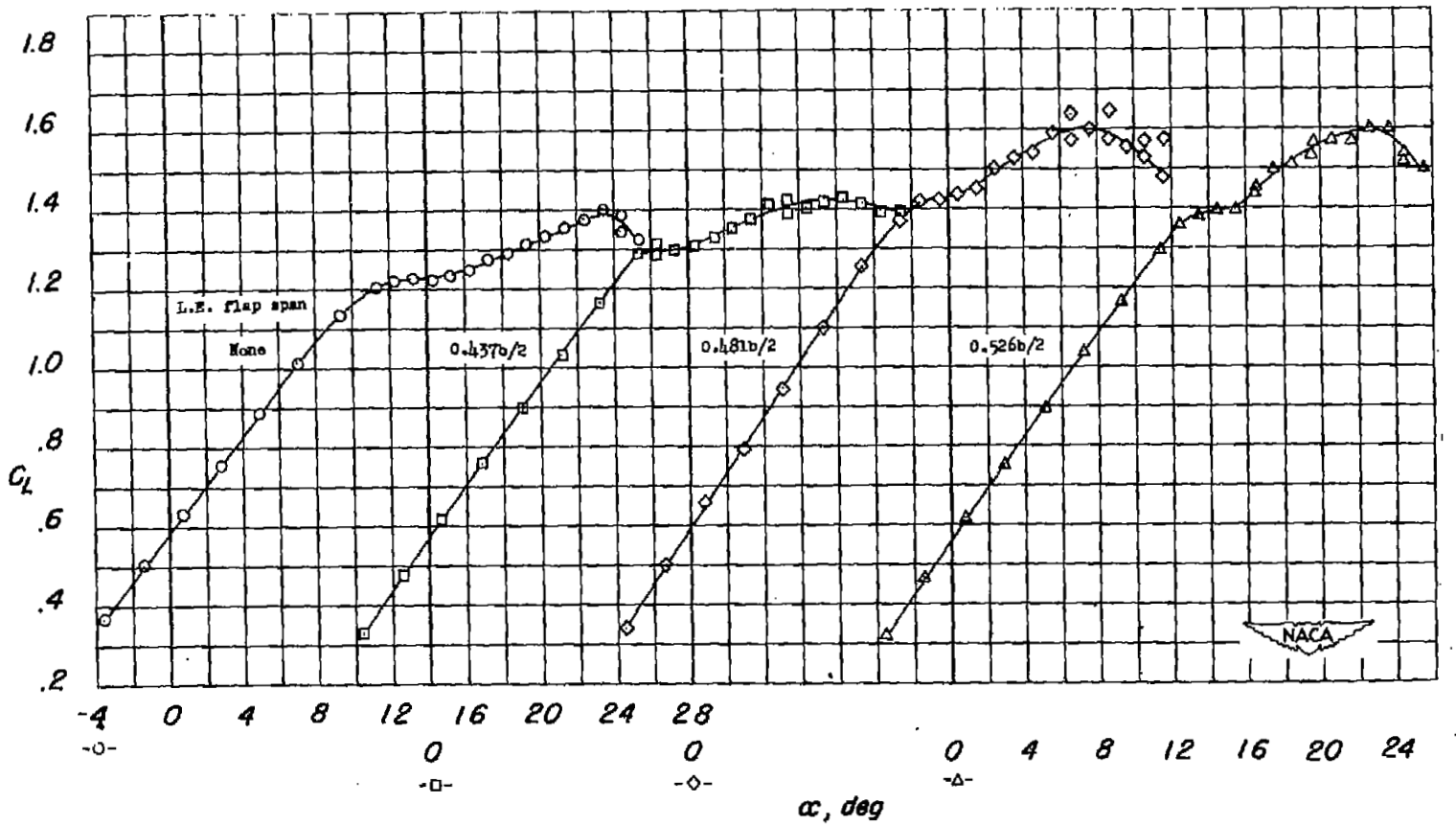


(a) $C_L$ against $\alpha$.

Figure 15.- Effects of leading-edge flaps of various spans on the aerodynamic characteristics of a 47.7° sweptback wing of aspect ratio 6.0 with 0.462b/2 trailing-edge double slotted flaps. $R = 6.0 \times 10^6$.

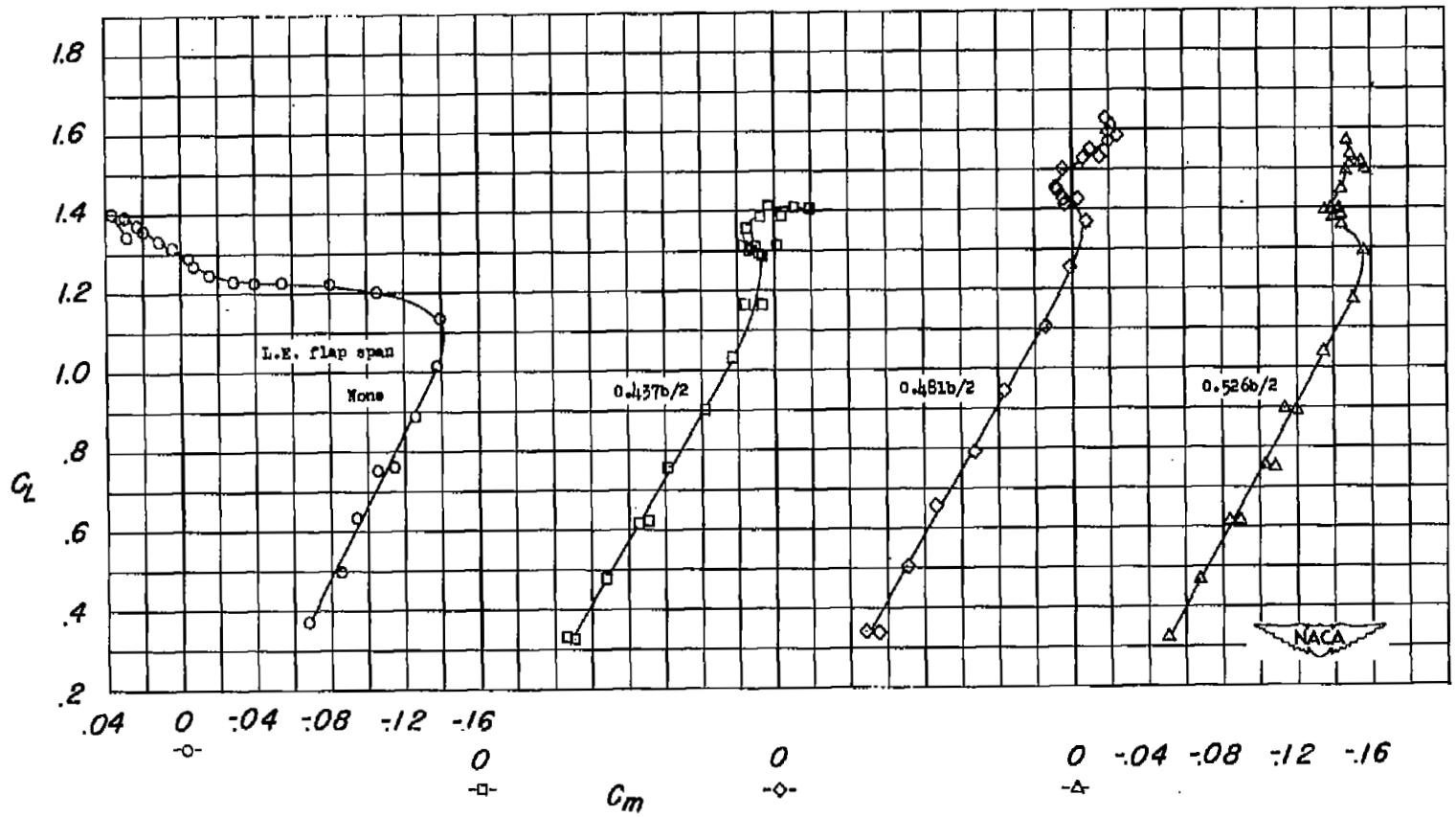


(b) $C_L$ against $C_m$.

Figure 15.- Continued.

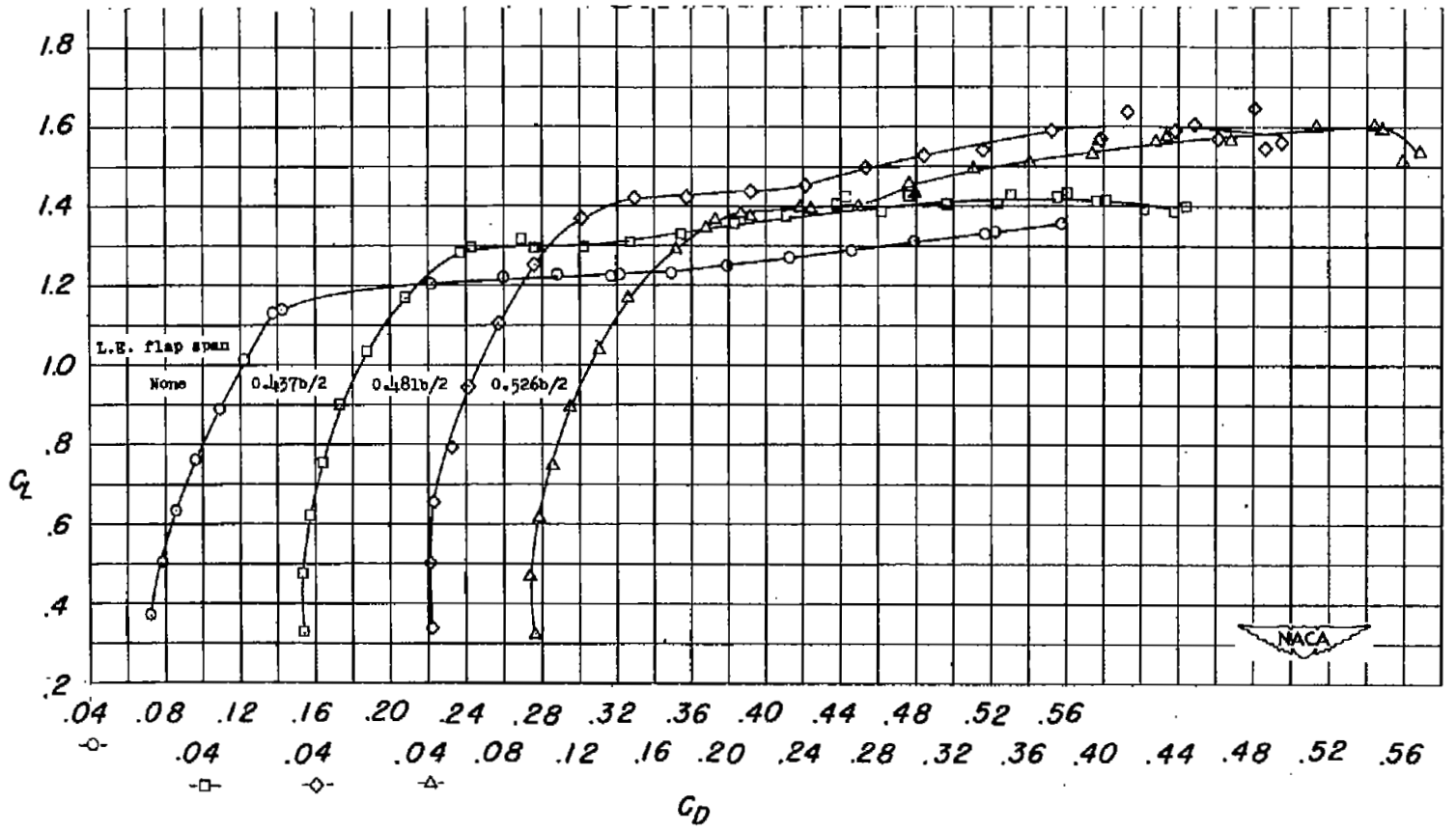


(c) $C_L$ against $C_D$.

Figure 15.- Concluded.

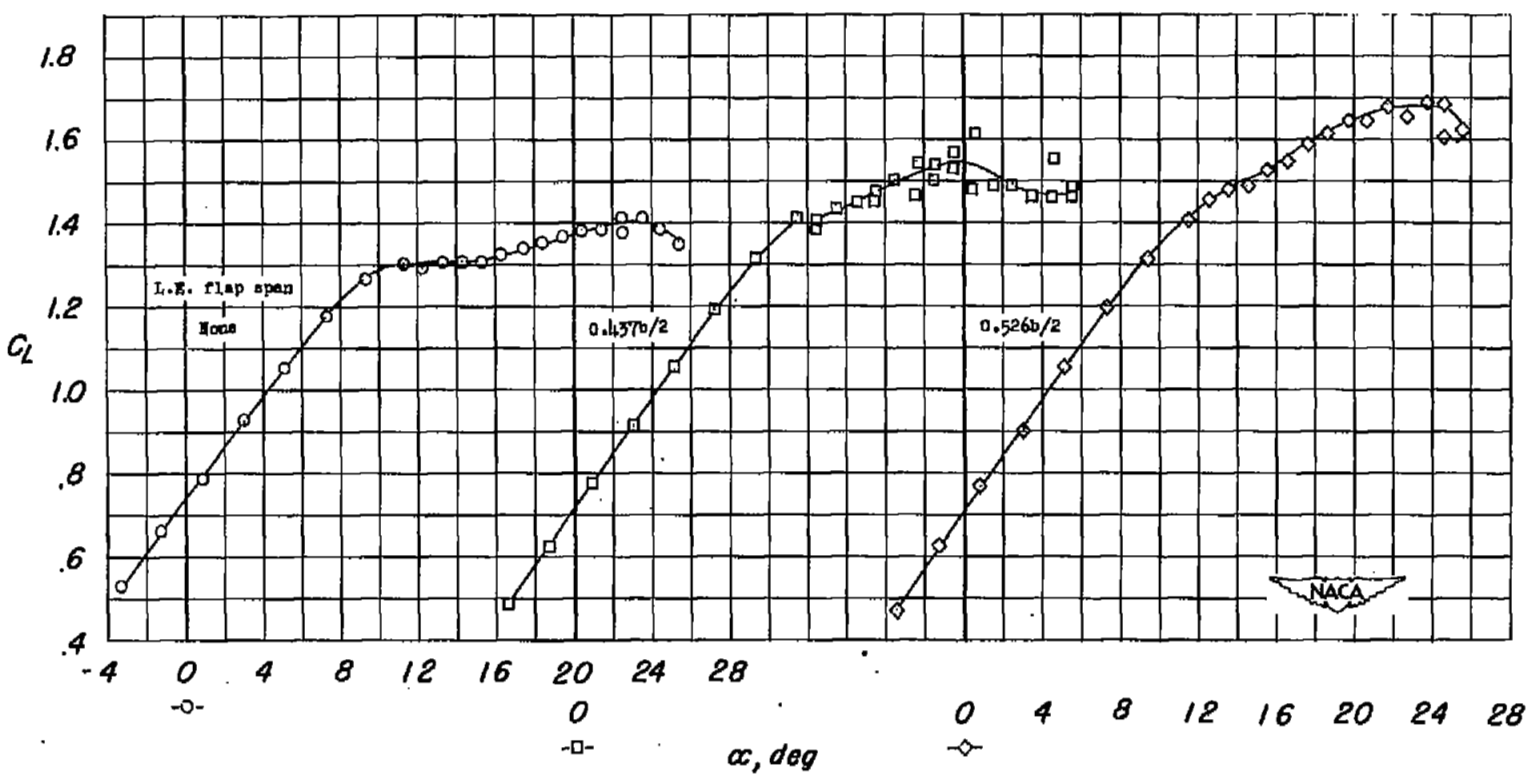


(a) $C_L$ against $\alpha$.

Figure 16.- Effects of leading-edge flaps of various spans on the aerodynamic characteristics of a 47.7° sweptback wing of aspect ratio 6.0 with 0.562b/2 trailing-edge double slotted flaps. $R = 6.0 \times 10^6$.

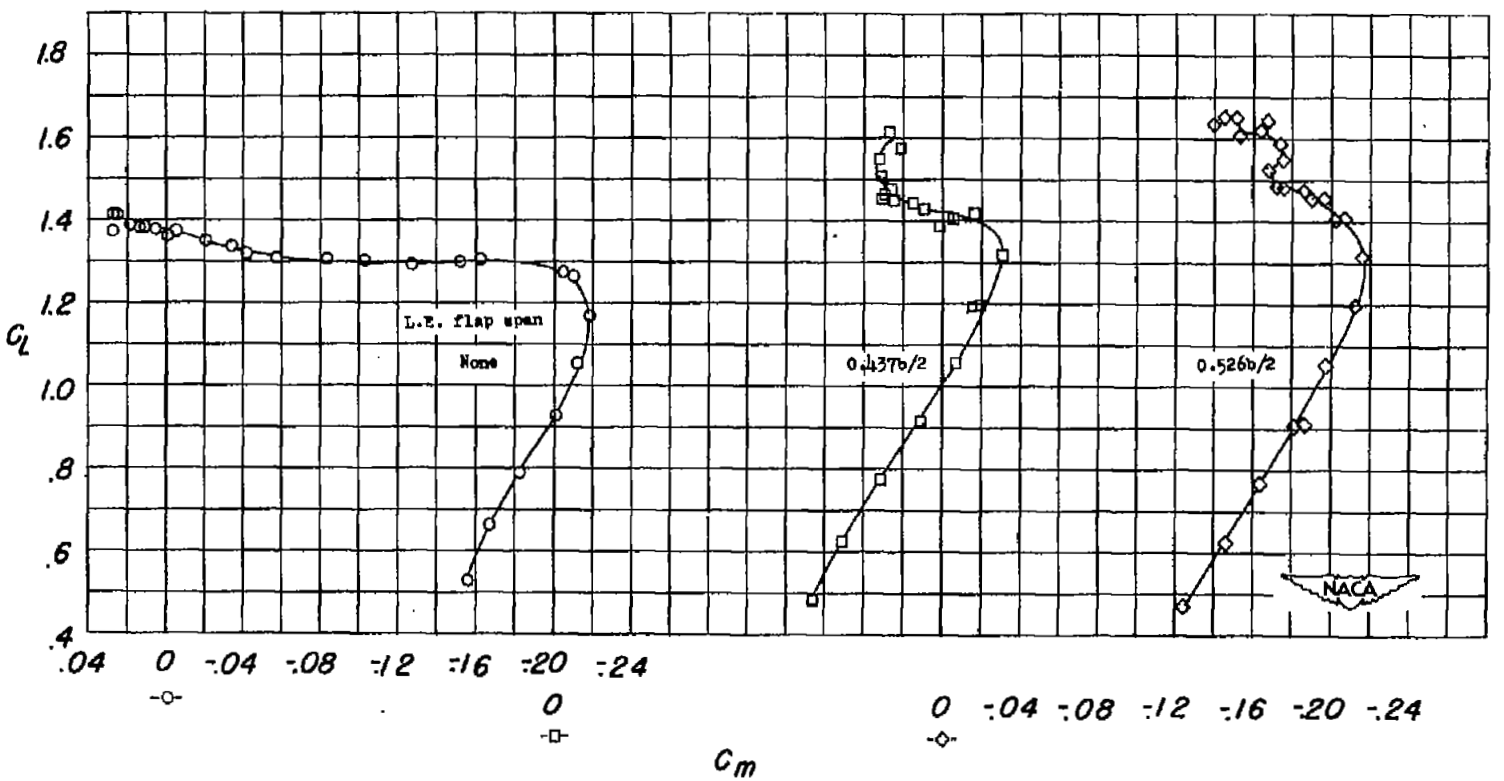


(b) $C_L$ against $C_m$.

Figure 16.- Continued.

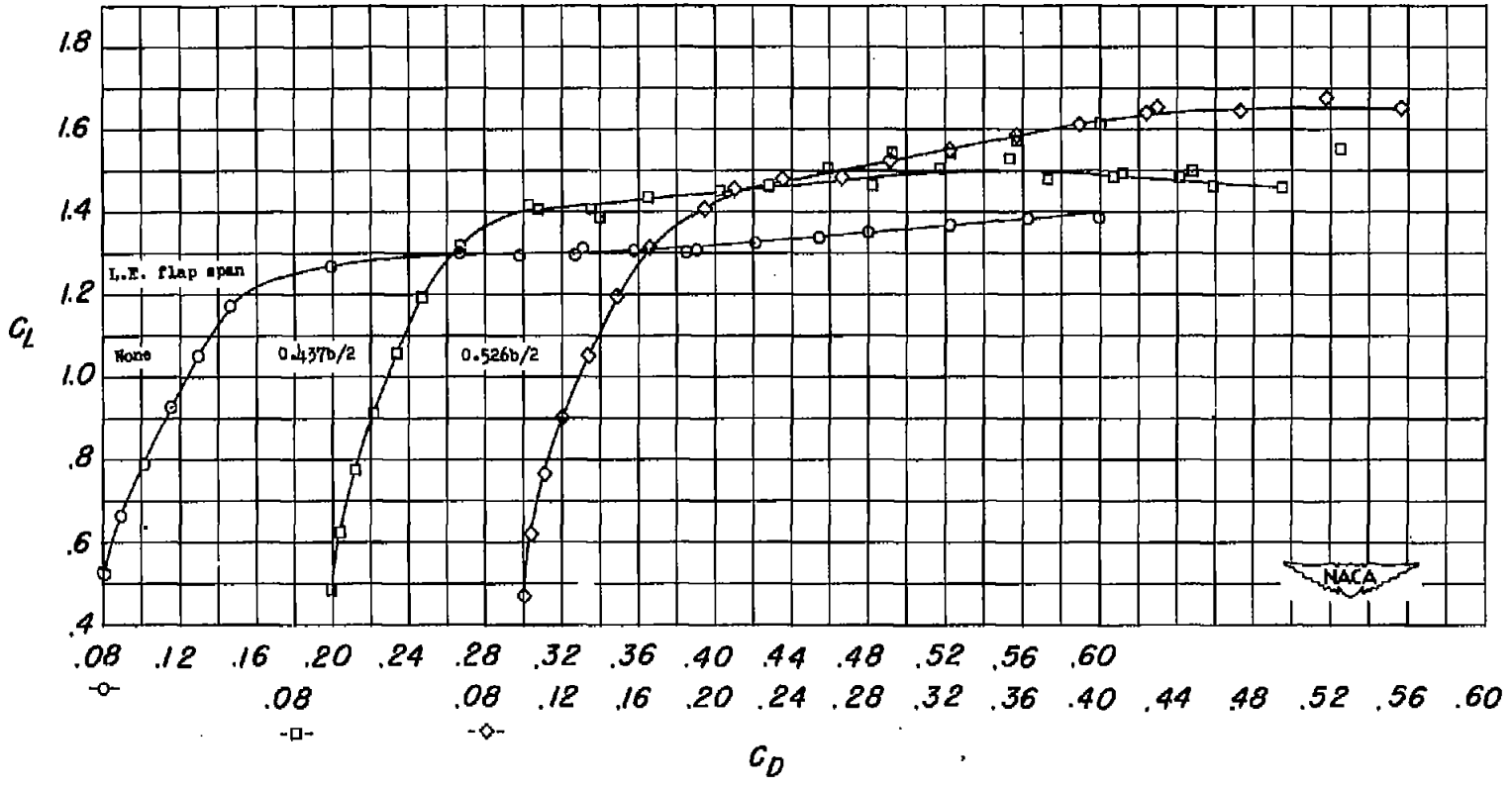


(c) $C_L$ against $C_D$.

Figure 16.- Concluded.

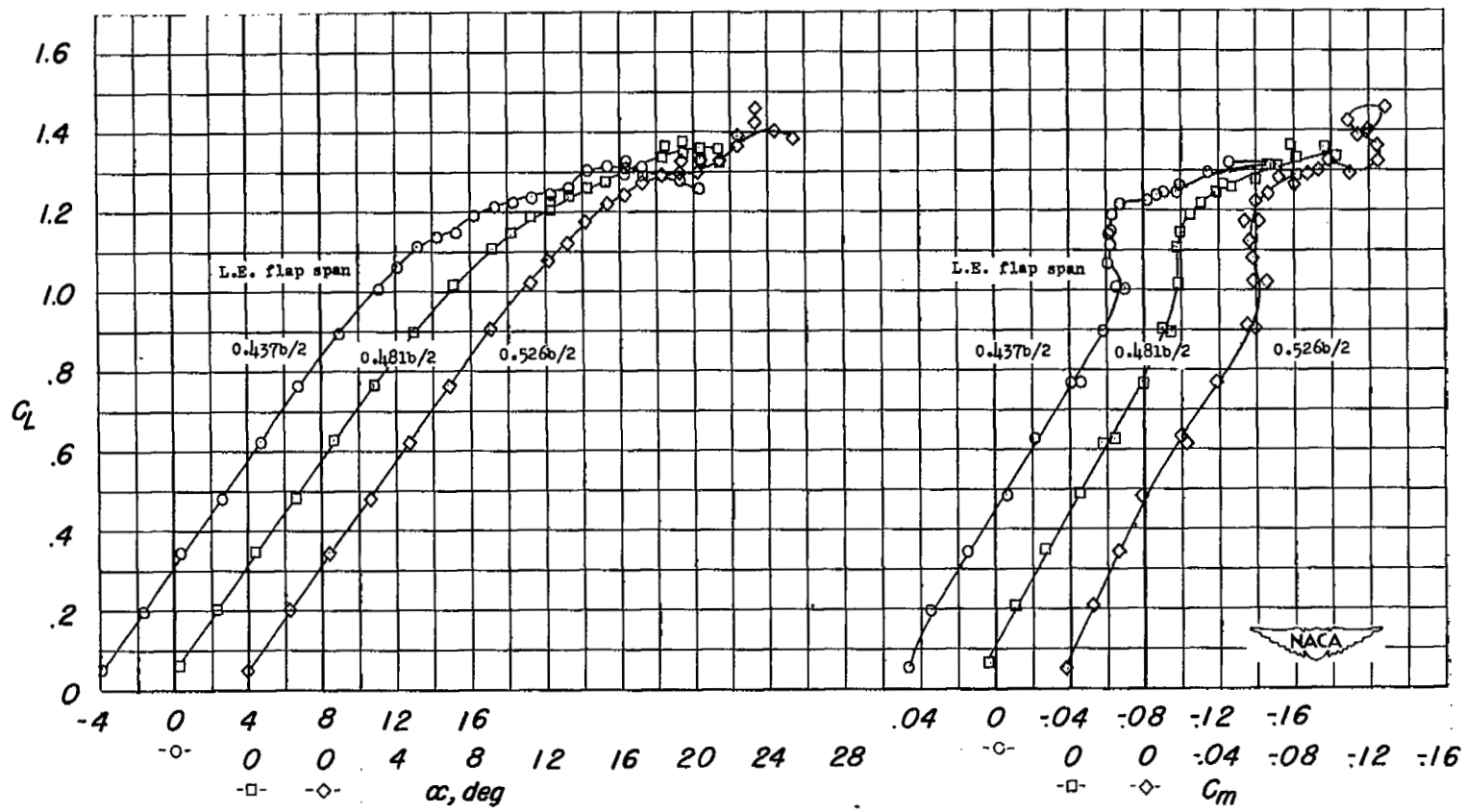


(a) $C_L$ against $\alpha$ and $C_m$.

Figure 17.- Effects of leading-edge flaps of various spans on the aerodynamic characteristics of a 47.7° sweptback wing of aspect ratio 6.0 with 0.359b/2 trailing-edge split flaps. $R = 6.0 \times 10^6$.

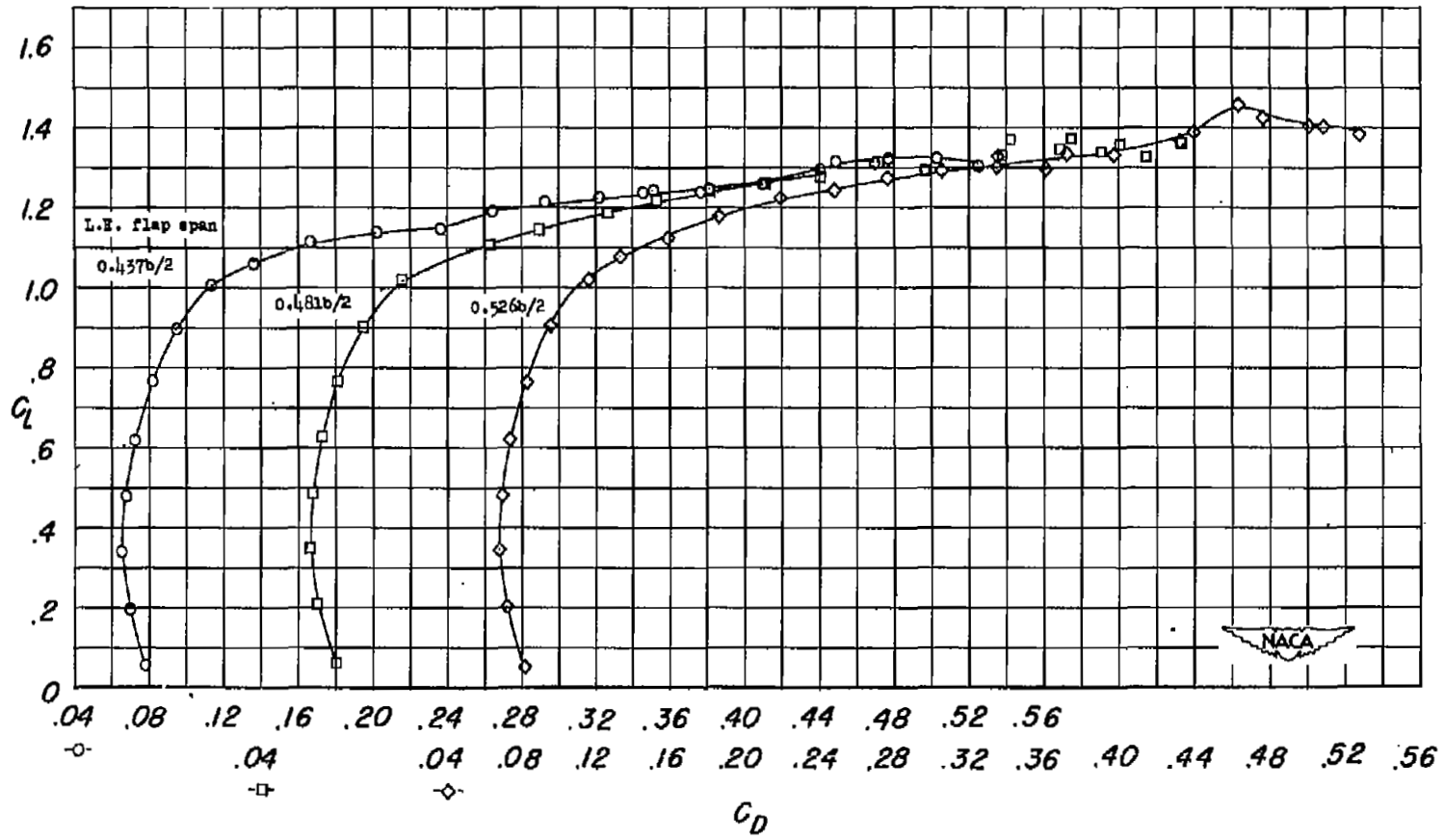


(b) $C_L$ against $C_D$.

Figure 17.- Concluded.

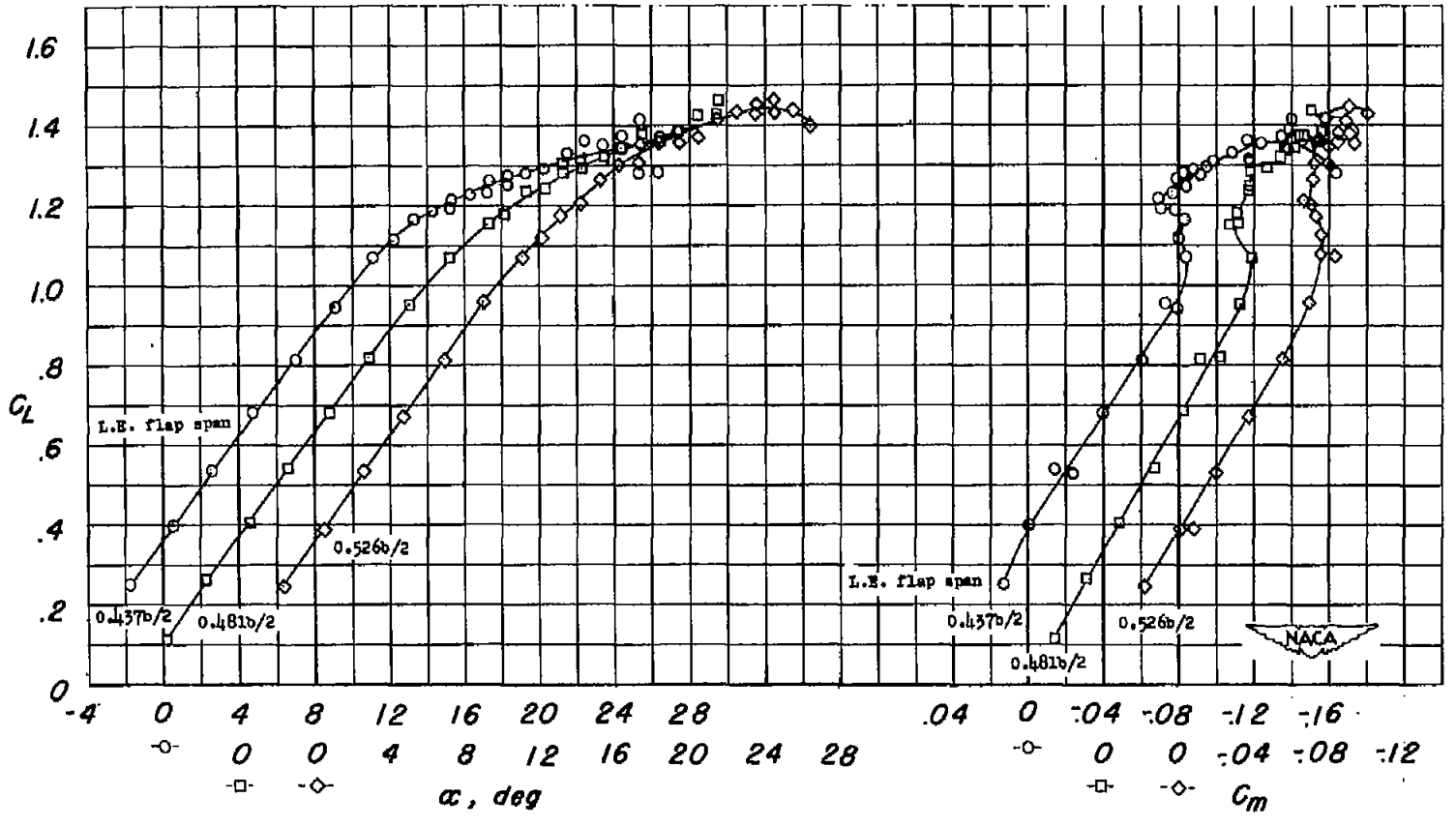


(a) $C_L$ against $\alpha$ and $C_m$.

Figure 18.- Effects of leading-edge flaps of various spans on the aerodynamic characteristics of a 47.7° sweptback wing of aspect ratio 6.0 with 0.449b/2 trailing-edge split flaps. $R = 6.0 \times 10^6$.

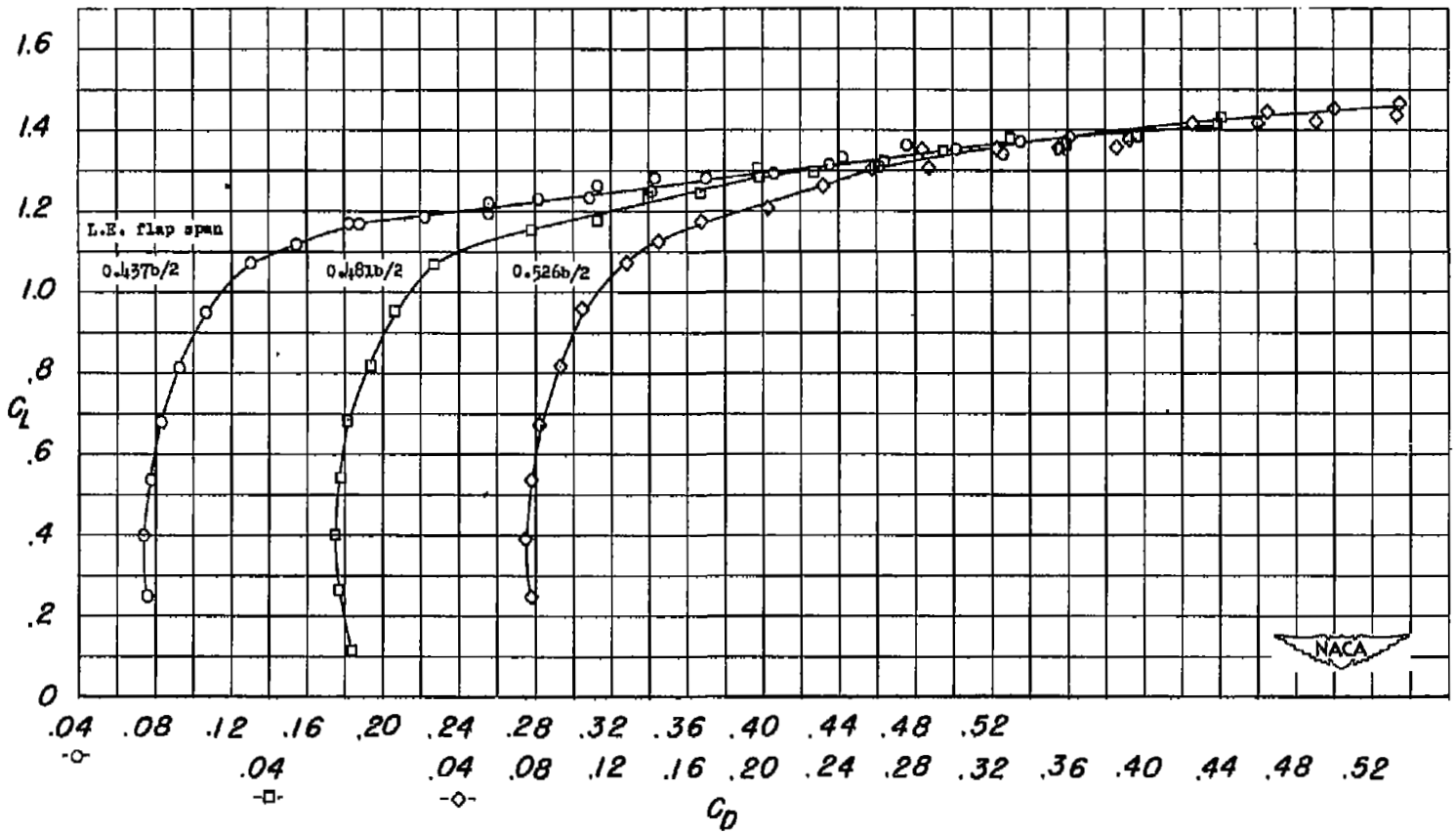


(b) $C_L$ against $C_D$.

Figure 18.- Concluded.

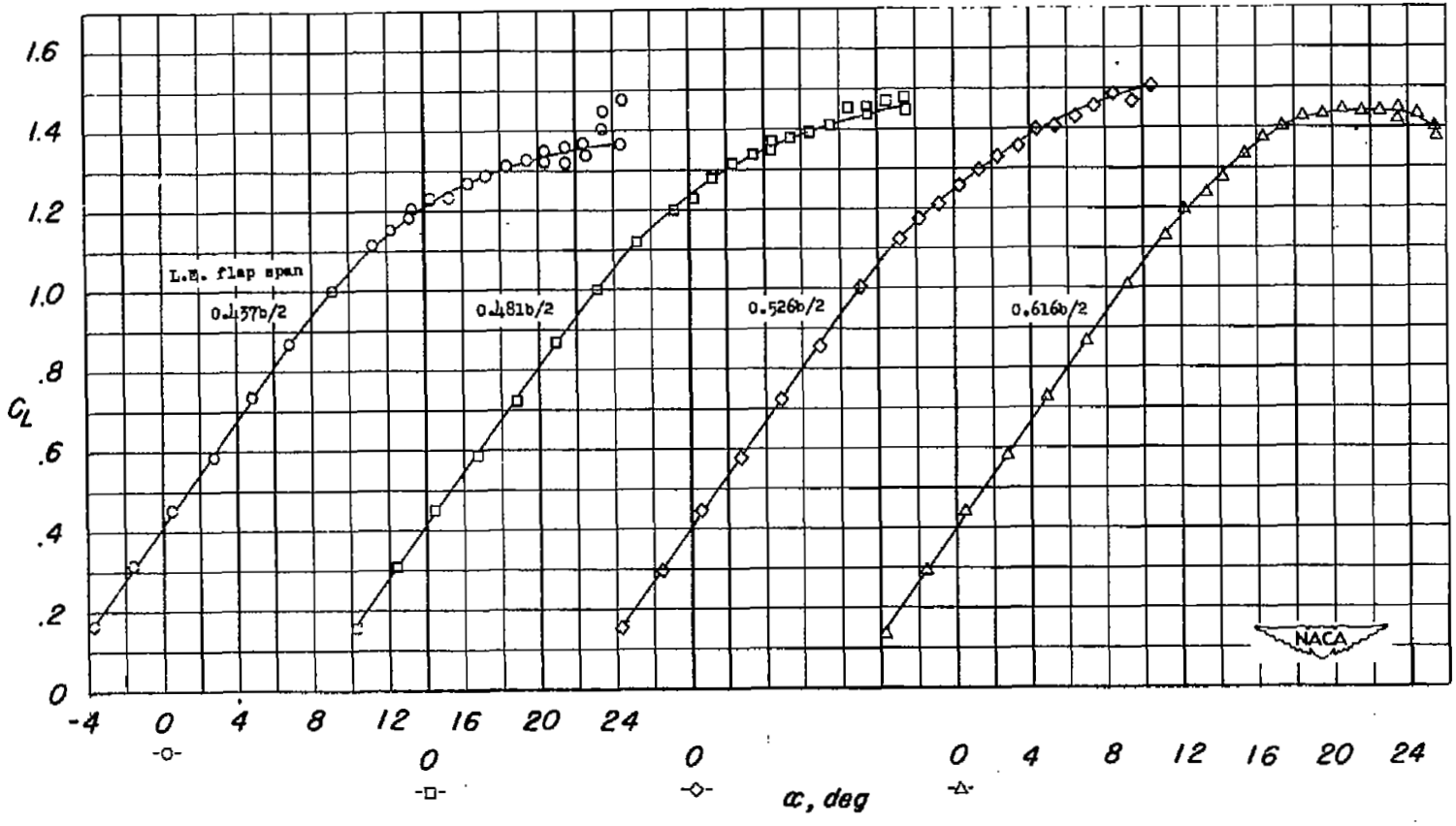


(a) $C_L$ against $\alpha$.

Figure 19.- Effects of leading-edge flaps of various spans on the aerodynamic characteristics of a 47.7° sweptback wing of aspect ratio 6.0 with 0.555b/2 trailing-edge split flaps. $R = 6.0 \times 10^6$.

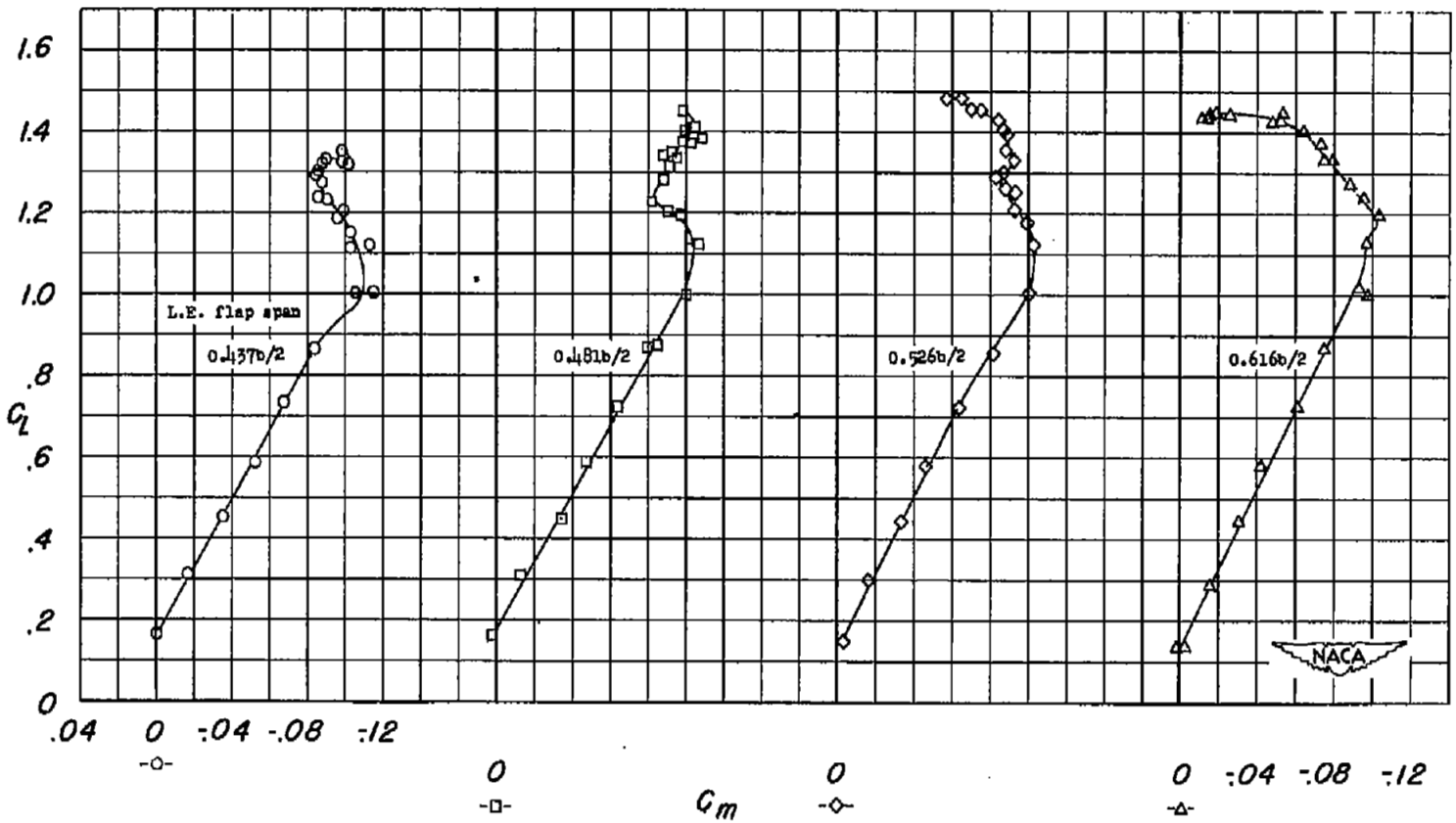


(b) $C_L$ against $C_m$.

Figure 19.- Continued.

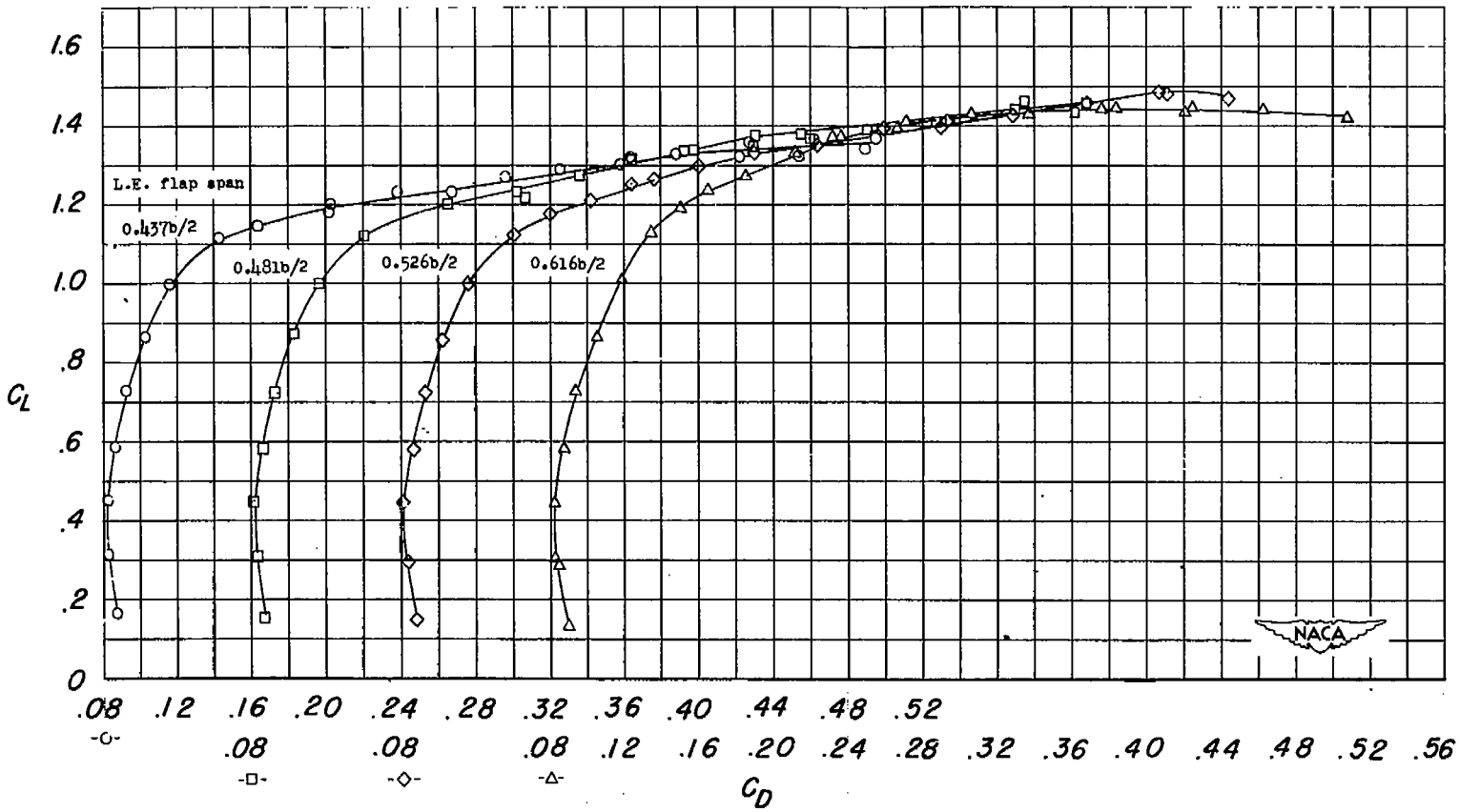


(c) $C_L$ against $C_D$.

Figure 19.- Concluded.

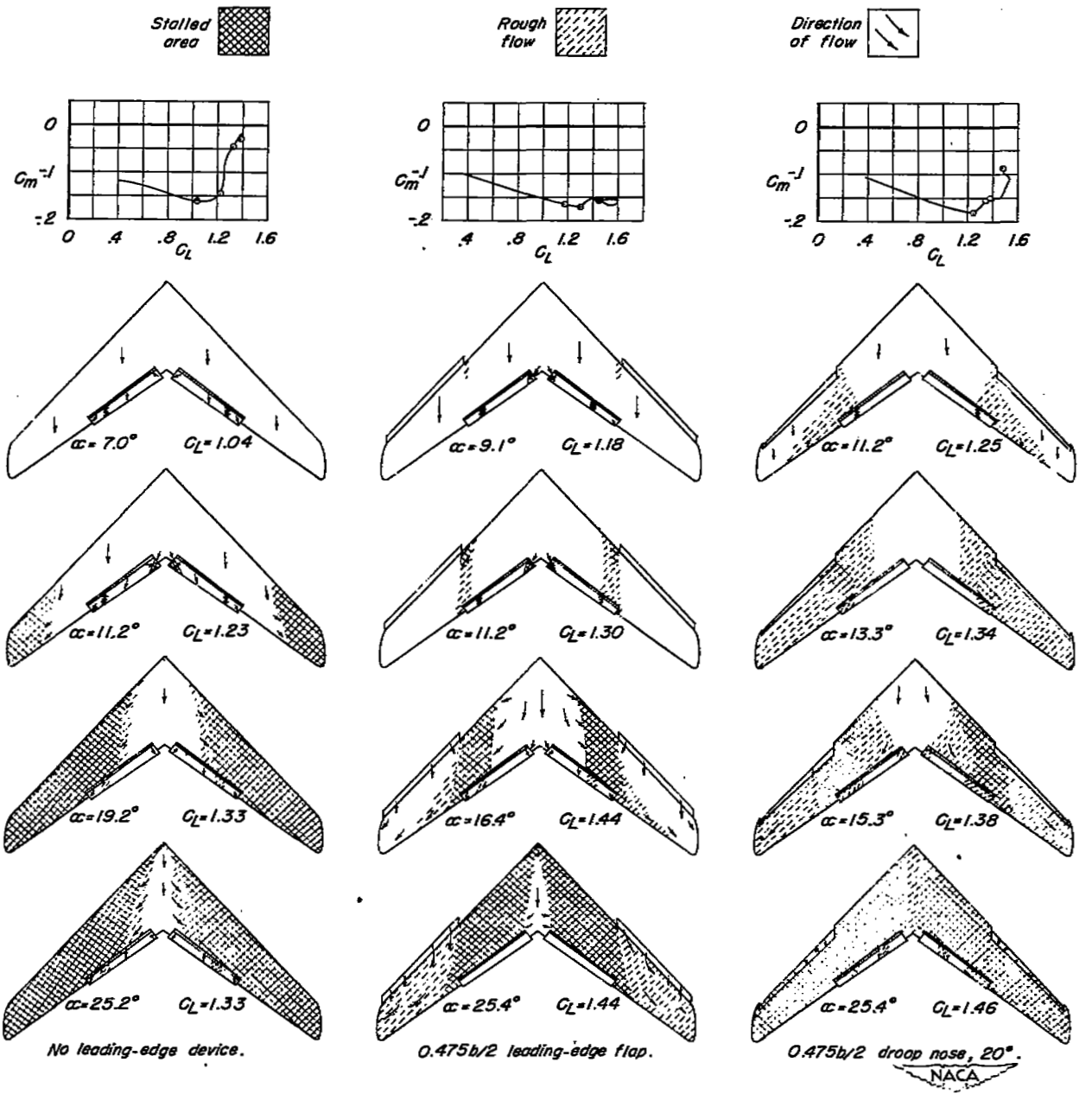


Figure 20.- Effects of various types of leading-edge devices on the stalling characteristics of a 47.7° sweptback wing of aspect ratio 5.1 with 0.516b/2 double slotted flaps. $R = 6.0 \times 10^6$.

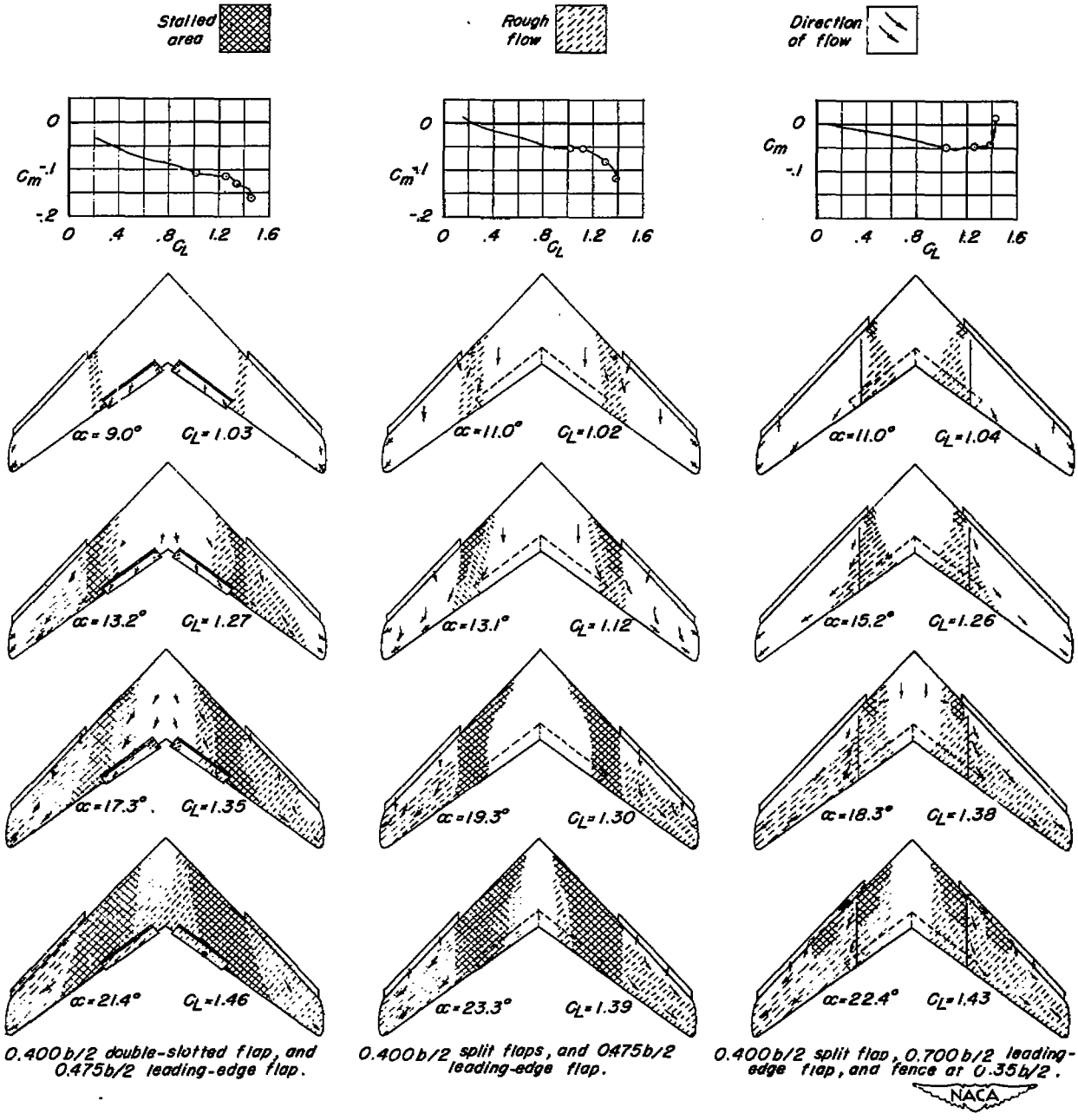


Figure 21.- Stall diagrams for various combinations of leading-edge flaps and trailing-edge flaps on a 47.7° sweptback wing of aspect ratio 5.1. $R = 6.0 \times 10^6$.

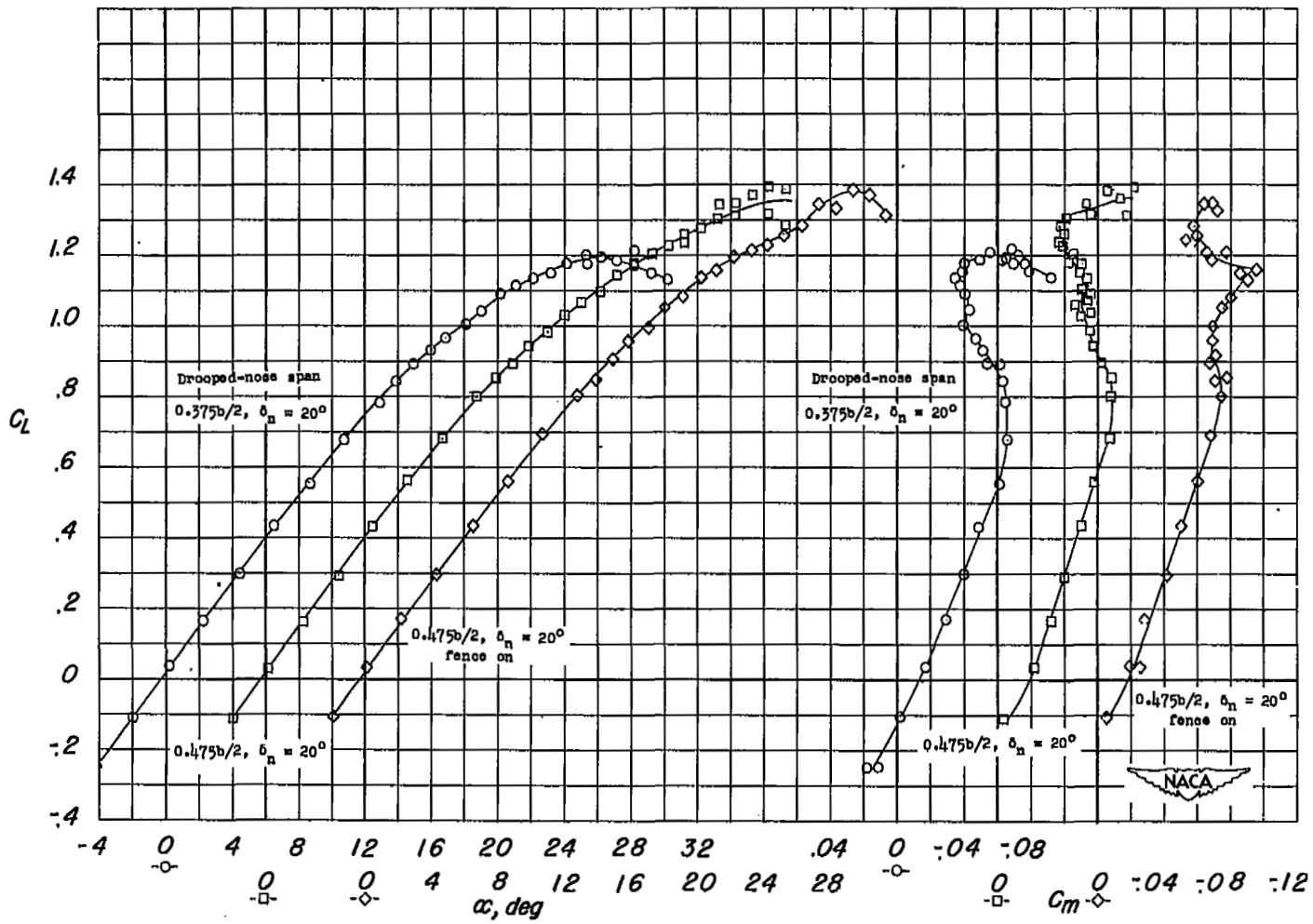


(a) $C_L$ against $\alpha$ and $C_m$.

Figure 22.- Effects of drooped-nose flaps on the aerodynamic characteristics of a 47.7° sweptback wing of aspect ratio 5.1. R = $6.0 \times 10^6$.

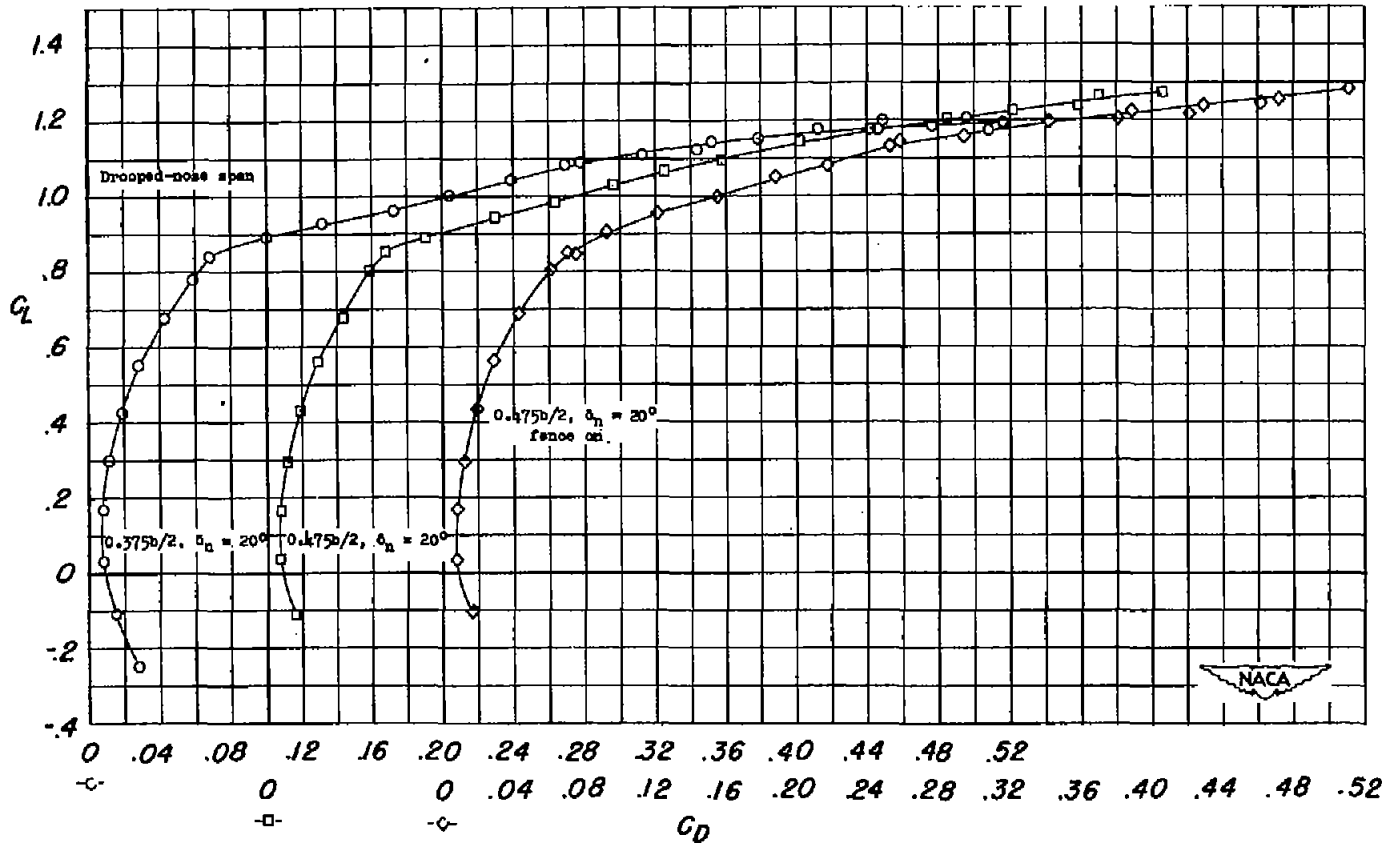


(b) $C_L$ against $C_D$.

Figure 22.- Concluded.

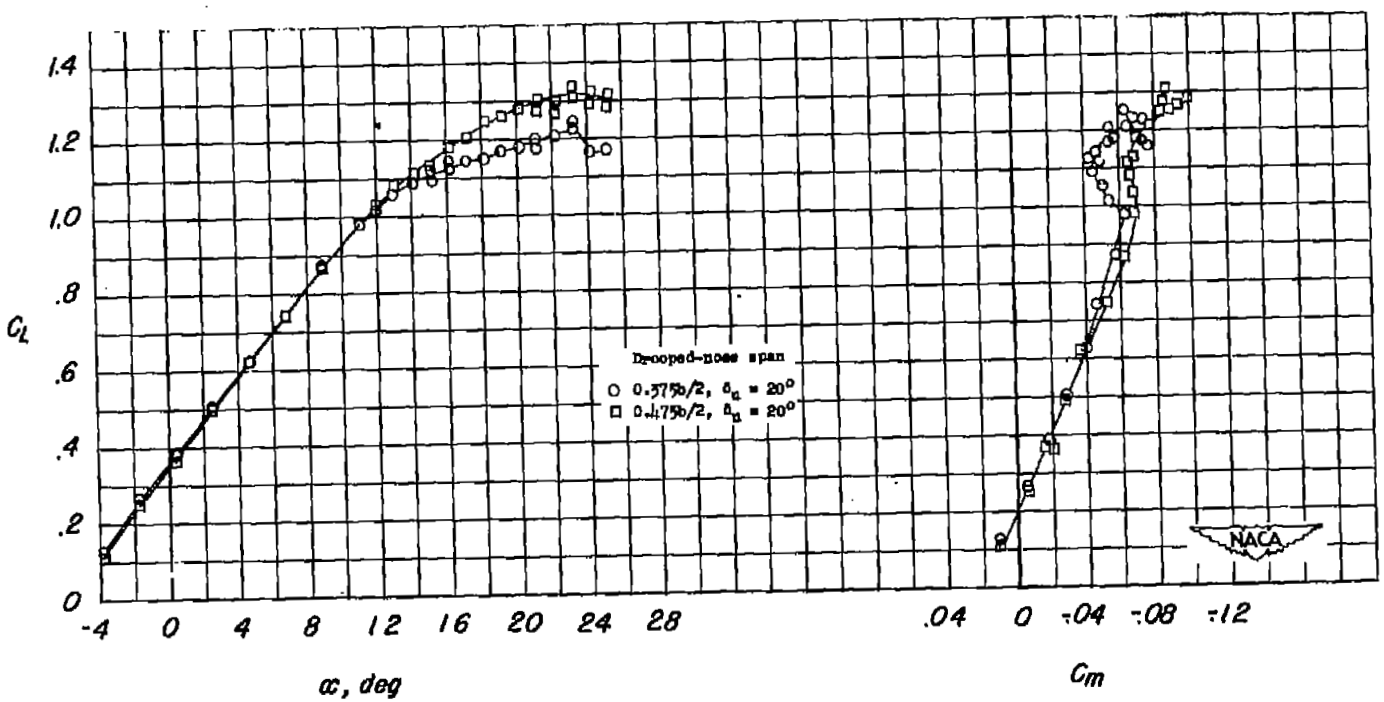


(a) $C_L$ against $\alpha$ and $C_m$.

Figure 23.- Effects of drooped-nose flaps on the aerodynamic characteristics of a 47.7° sweptback wing of aspect ratio 5.1 with 0.400b/2 trailing-edge split flaps. $R = 6.0 \times 10^6$.

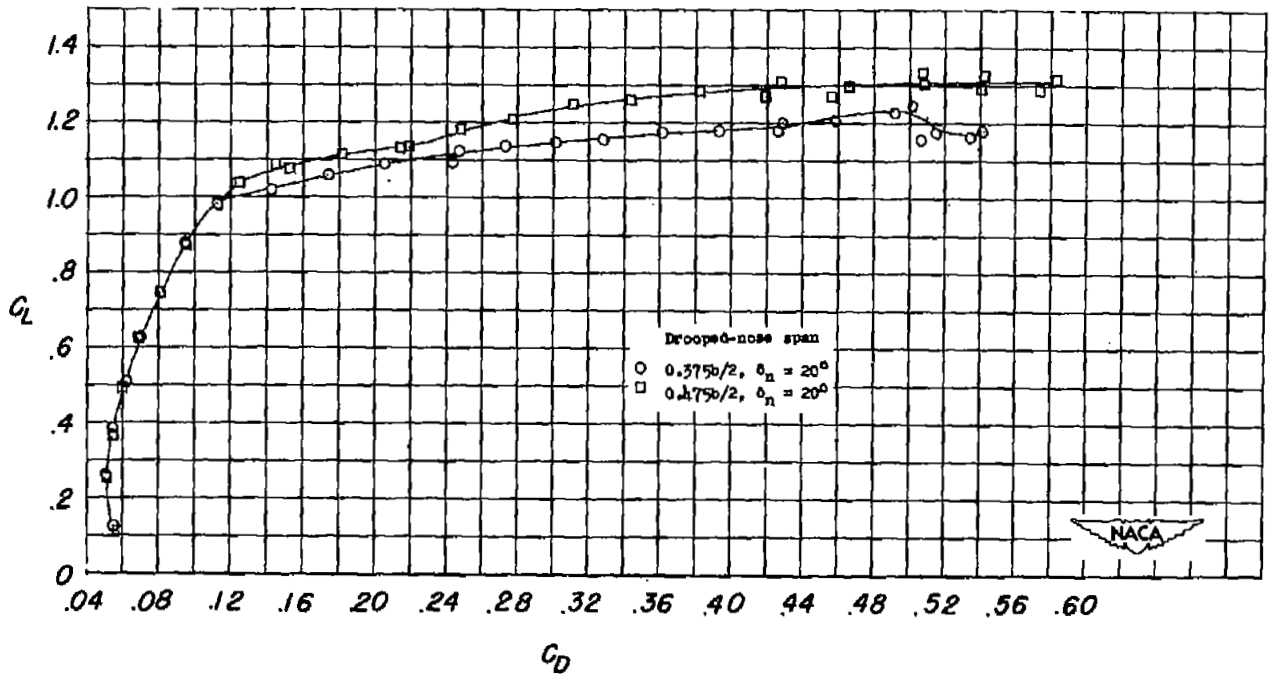


(b) $C_L$ against $C_D$.

Figure 23.- Concluded.

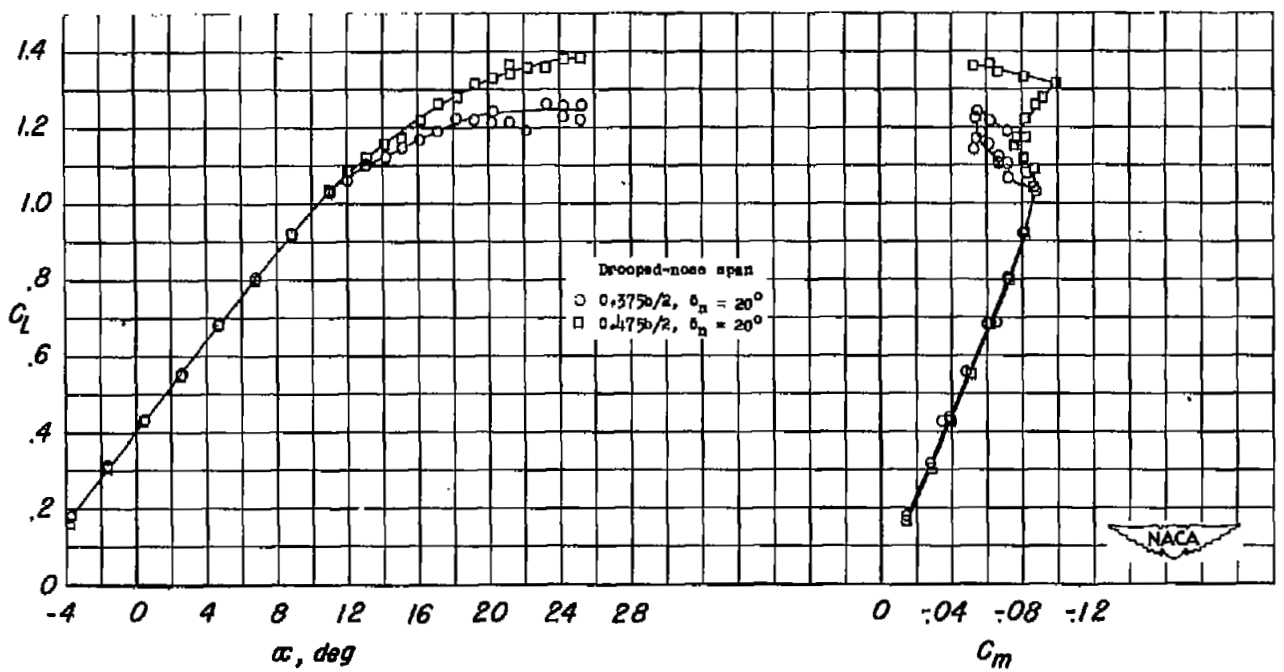


(a) $C_L$ against $\alpha$ and $C_m$.

Figure 24.- Effects of drooped-nose flaps on the aerodynamic characteristics of a 47.7° sweptback wing of aspect ratio 5.1 with 0.500b/2 trailing-edge split flaps. $R = 6.0 \times 10^6$.

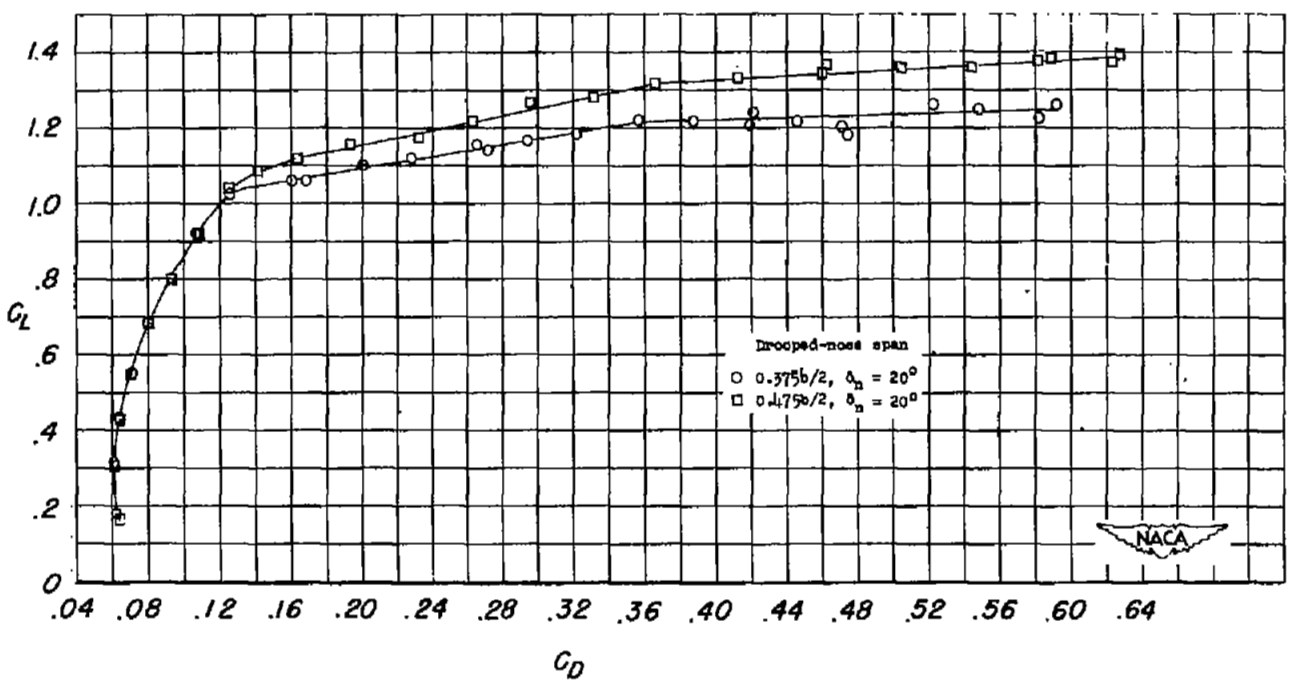


(b) $C_L$ against $C_D$.

Figure 24.- Concluded.

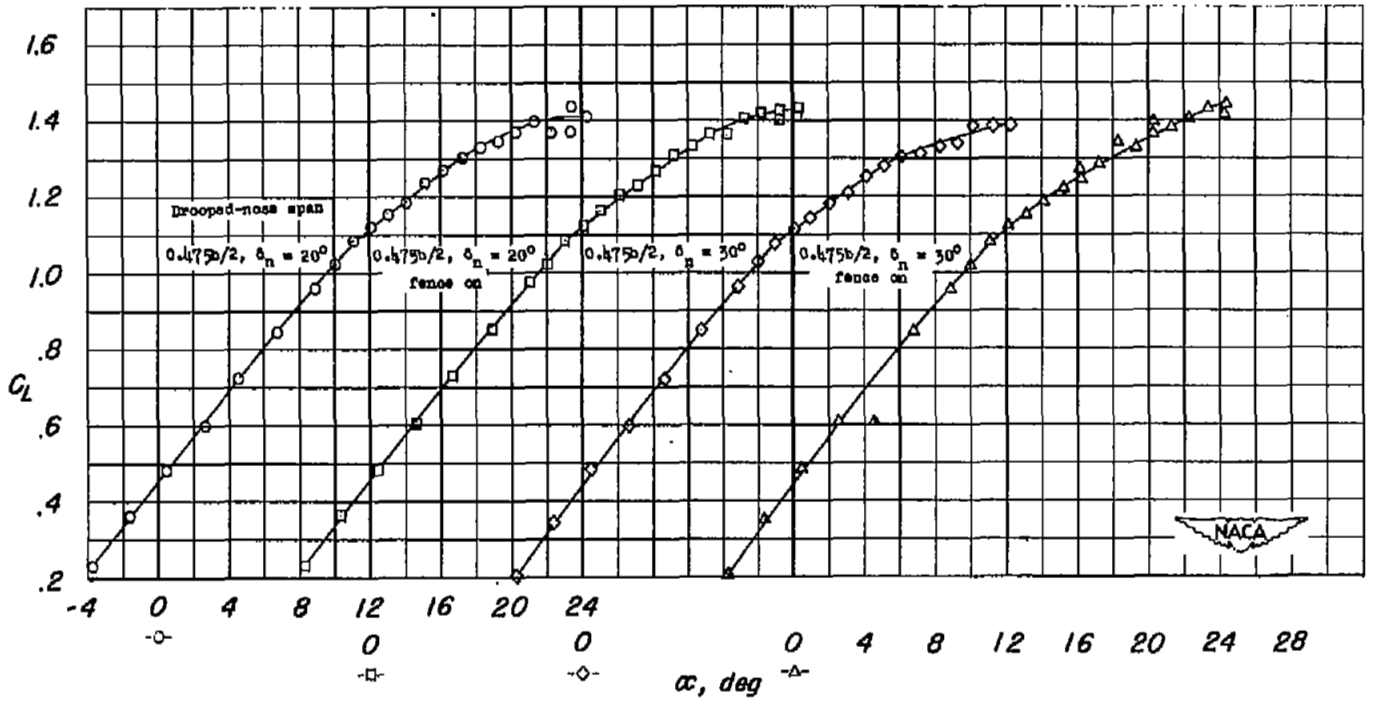


(a) $C_L$ against α.

Figure 25.- Effects of drooped-nose flaps on the aerodynamic characteristics of a 47.7° sweptback wing of aspect ratio 5.1 with 0.618b/2 split flaps deflected. R = $6.0 \times 10^6$.

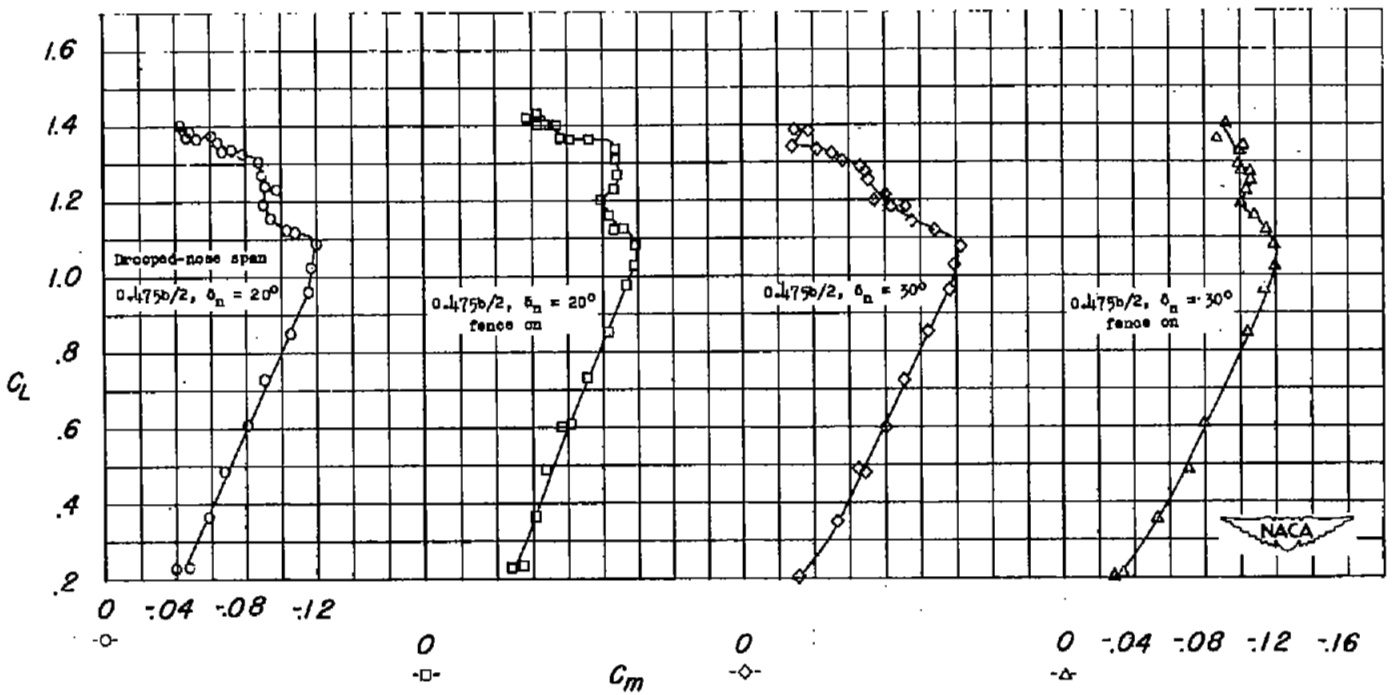


(b) $C_L$ against $C_m$.

Figure 25.- Continued.

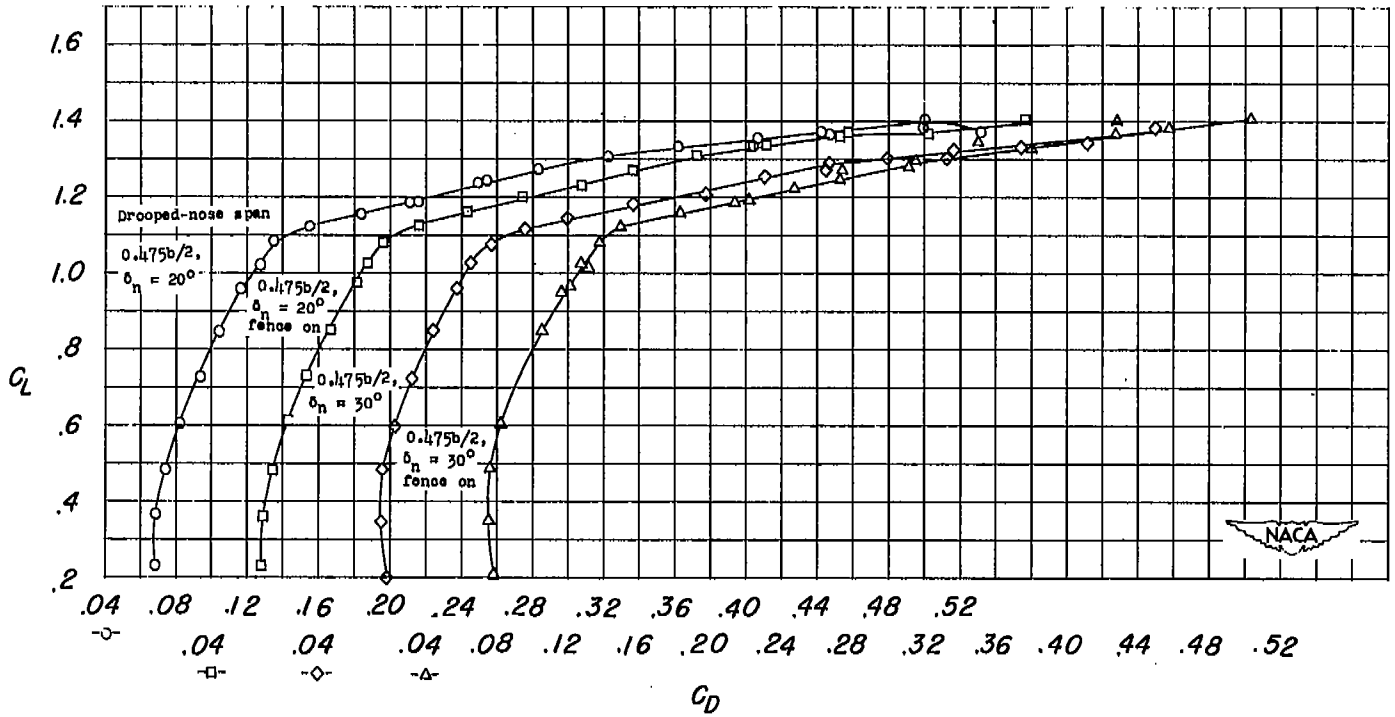


(c) $C_L$ against $C_D$.

Figure 25.- Concluded.

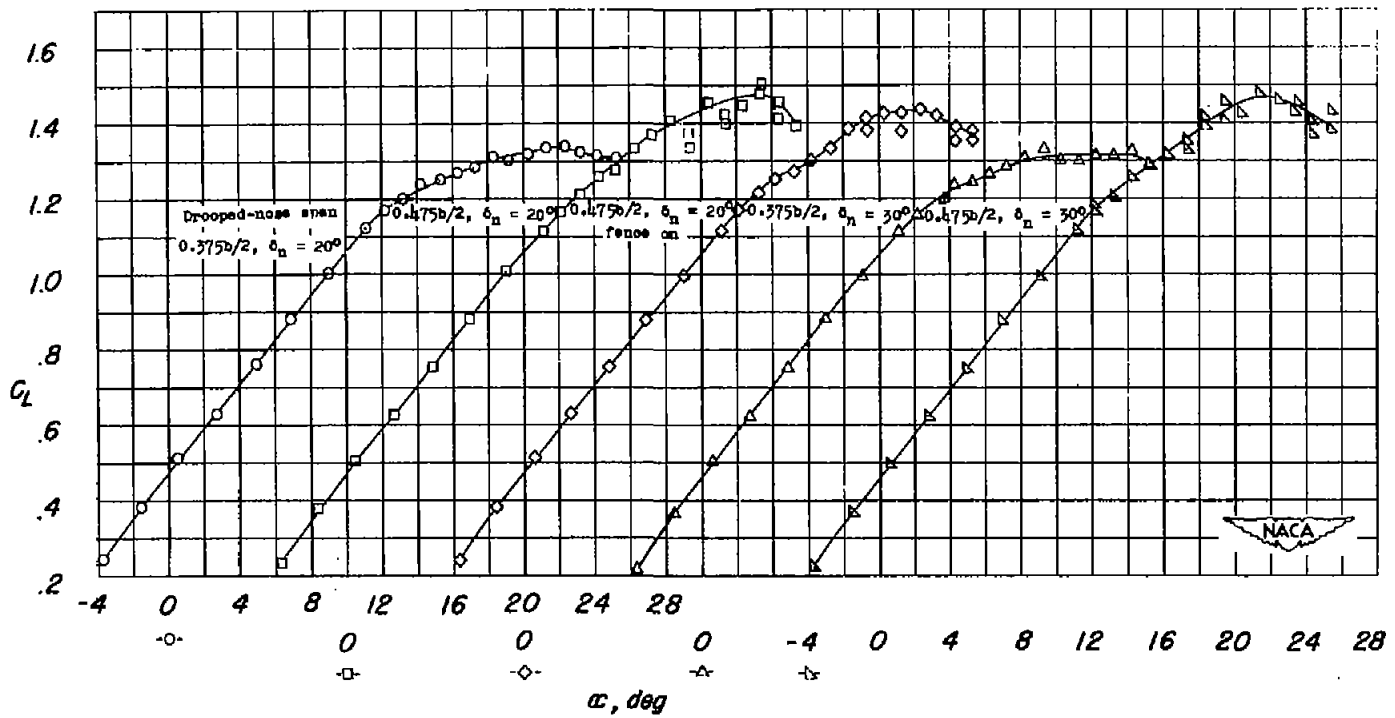


(a) $C_L$ against $\alpha$.

Figure 26.- Effects of drooped-nose flaps on the aerodynamic characteristics of a 47.7° sweptback wing of aspect ratio 5.1 with 0.400b/2 trailing-edge double slotted flaps. $R = 6.0 \times 10^6$.

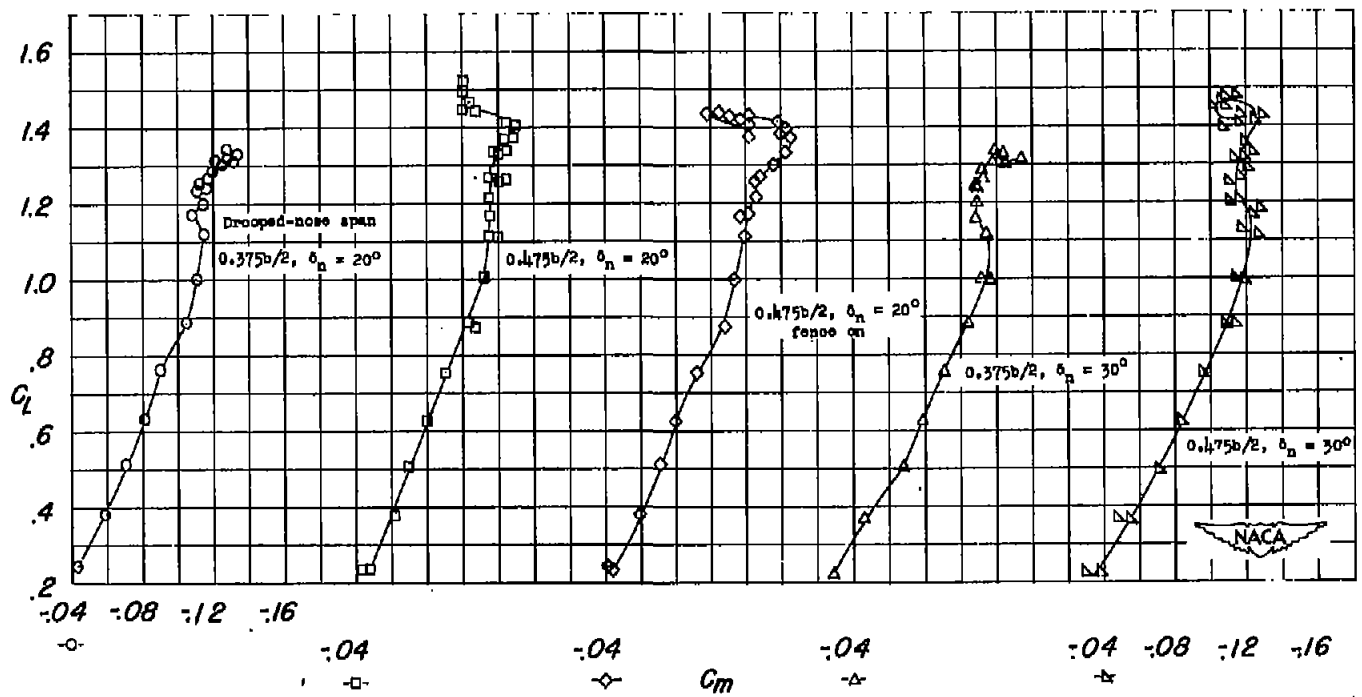


(b) $C_L$ against $C_m$.

Figure 26.- Continued.

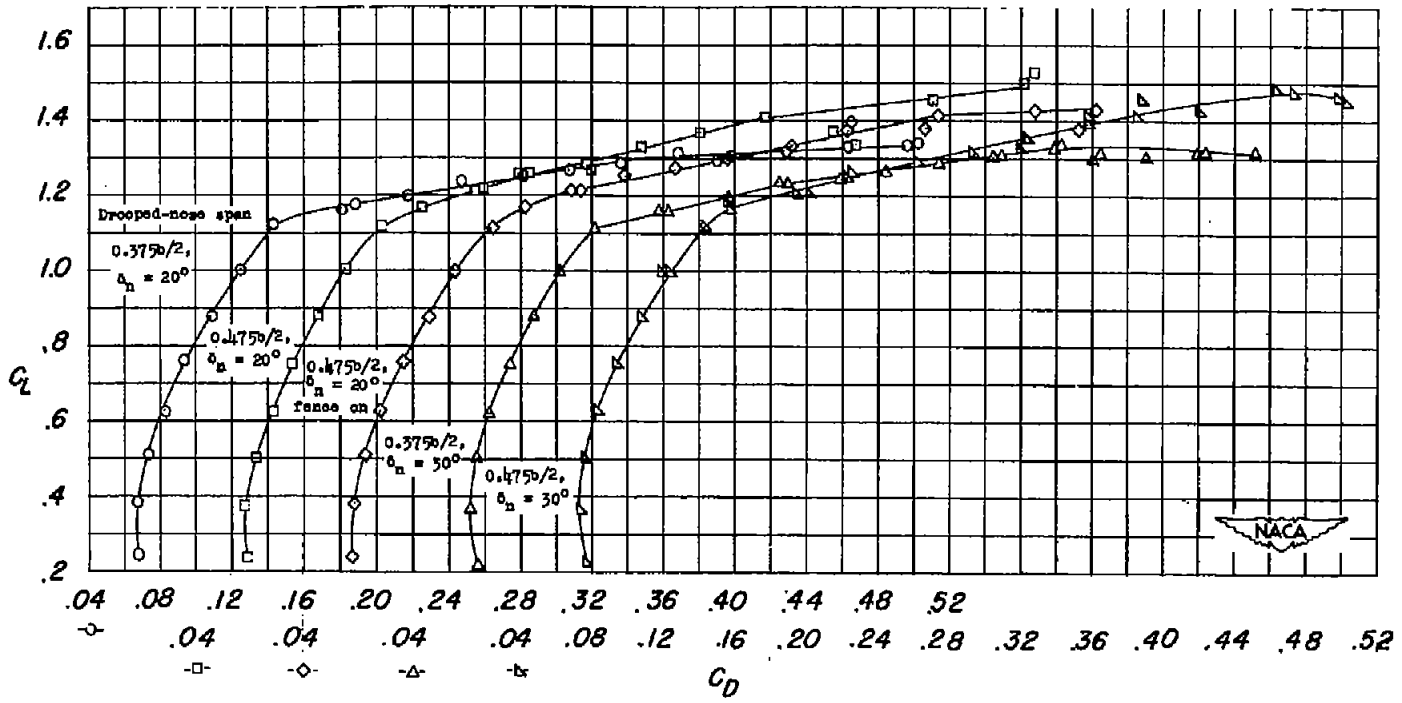


(c) $C_L$ against $C_D$.

Figure 26.- Concluded.

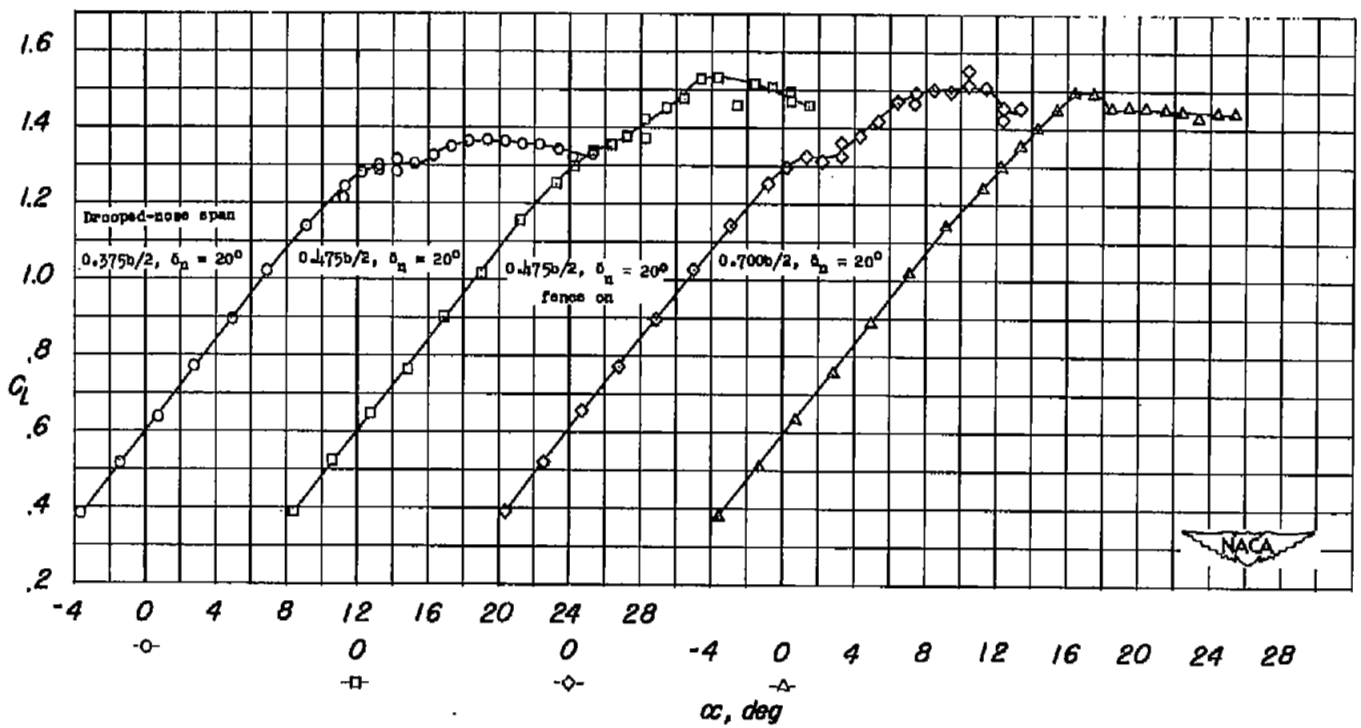


(a) $C_L$ against α.

Figure 27.- Effects of drooped-nose flaps on the aerodynamic characteristics of a 47.7° sweptback wing of aspect ratio 5.1 with 0.516b/2 trailing-edge double slotted flaps. $R = 6.0 \times 10^6$.

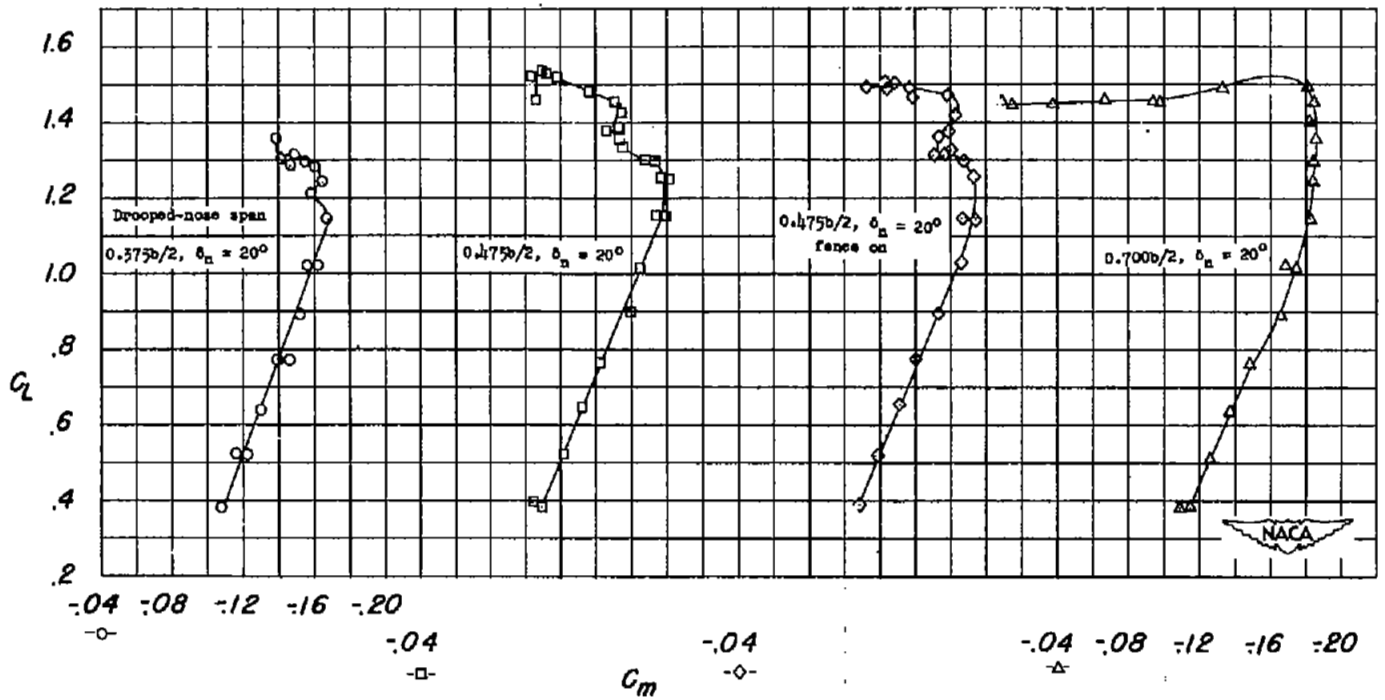


(b) $C_L$ against $C_m$.

Figure 27.- Continued.

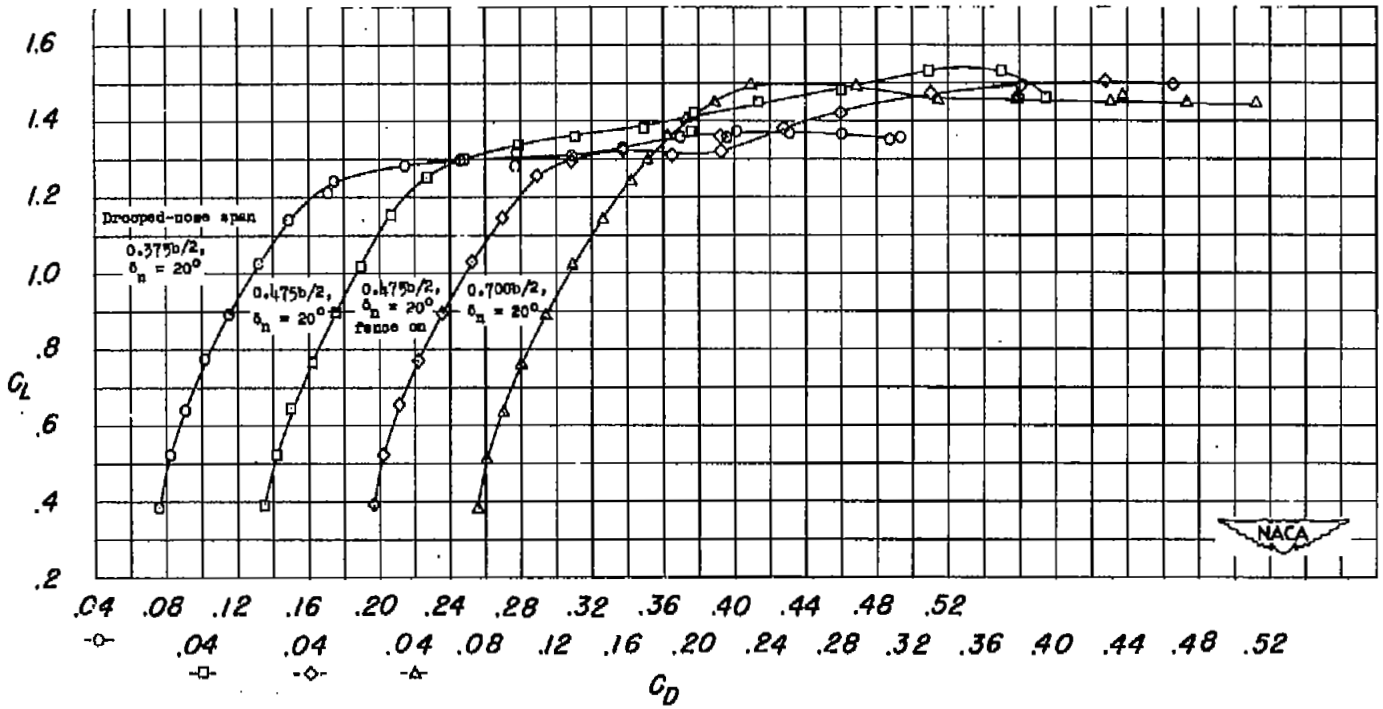


(c) $C_L$ against $C_D$.

Figure 27.- Concluded.

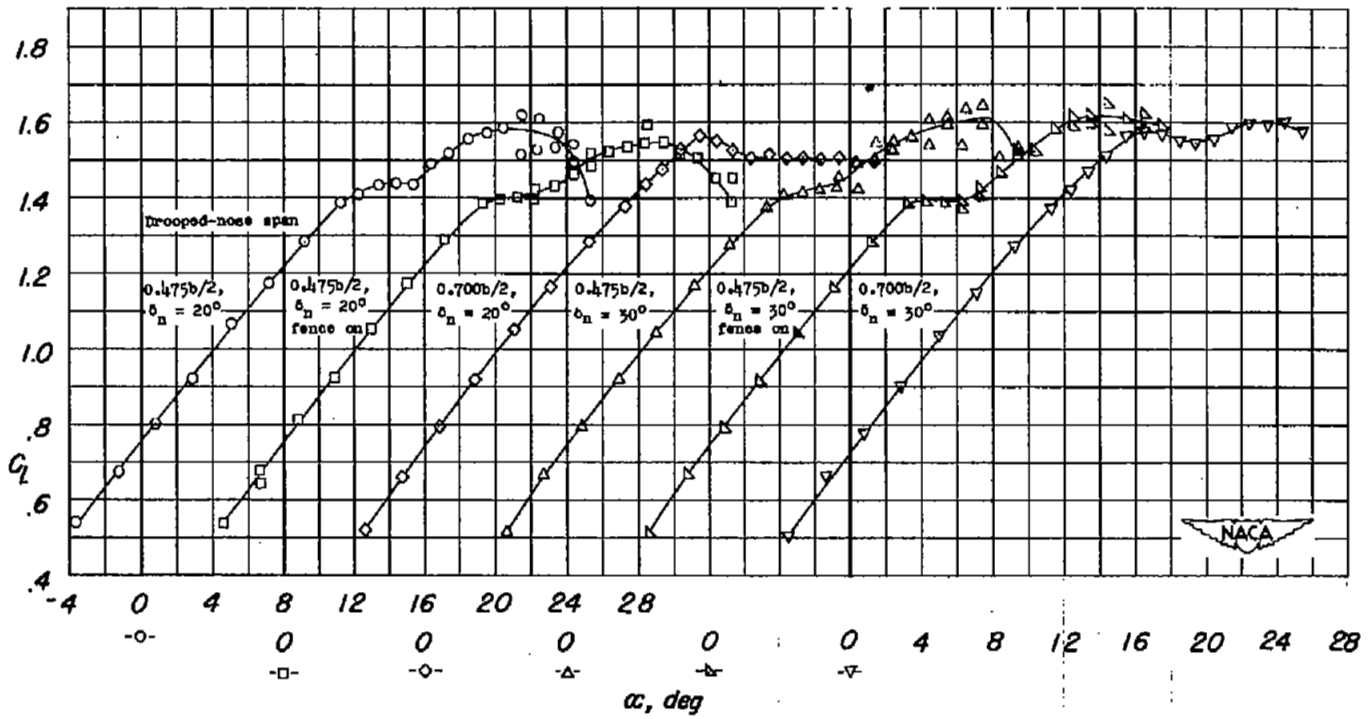


(a) $C_L$ against α.

Figure 28.- Effects of drooped-nose flaps on the aerodynamic characteristics of a 47.7° sweptback wing of aspect ratio 5.1 with 0.626b/2 trailing-edge double slotted flaps. $R = 6.0 \times 10^6$.

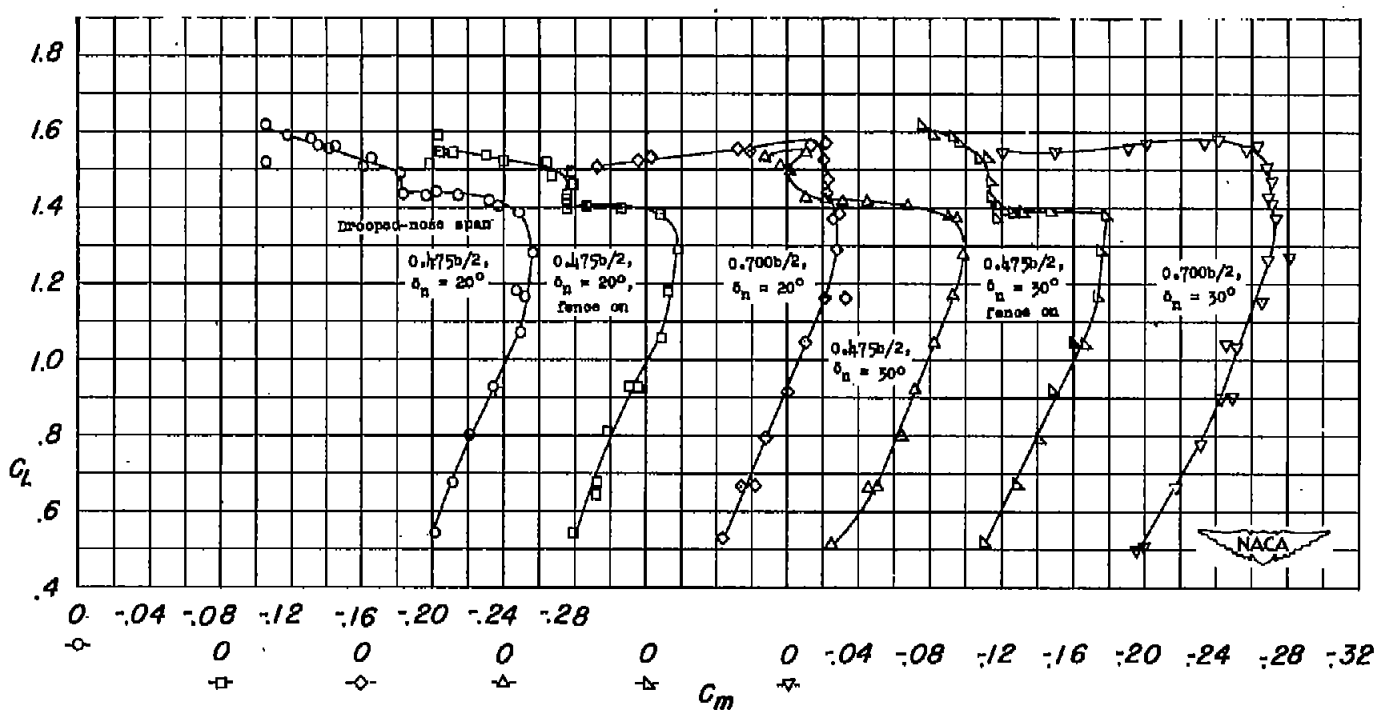


(b) $C_L$ against $C_m$.

Figure 28.- Continued.

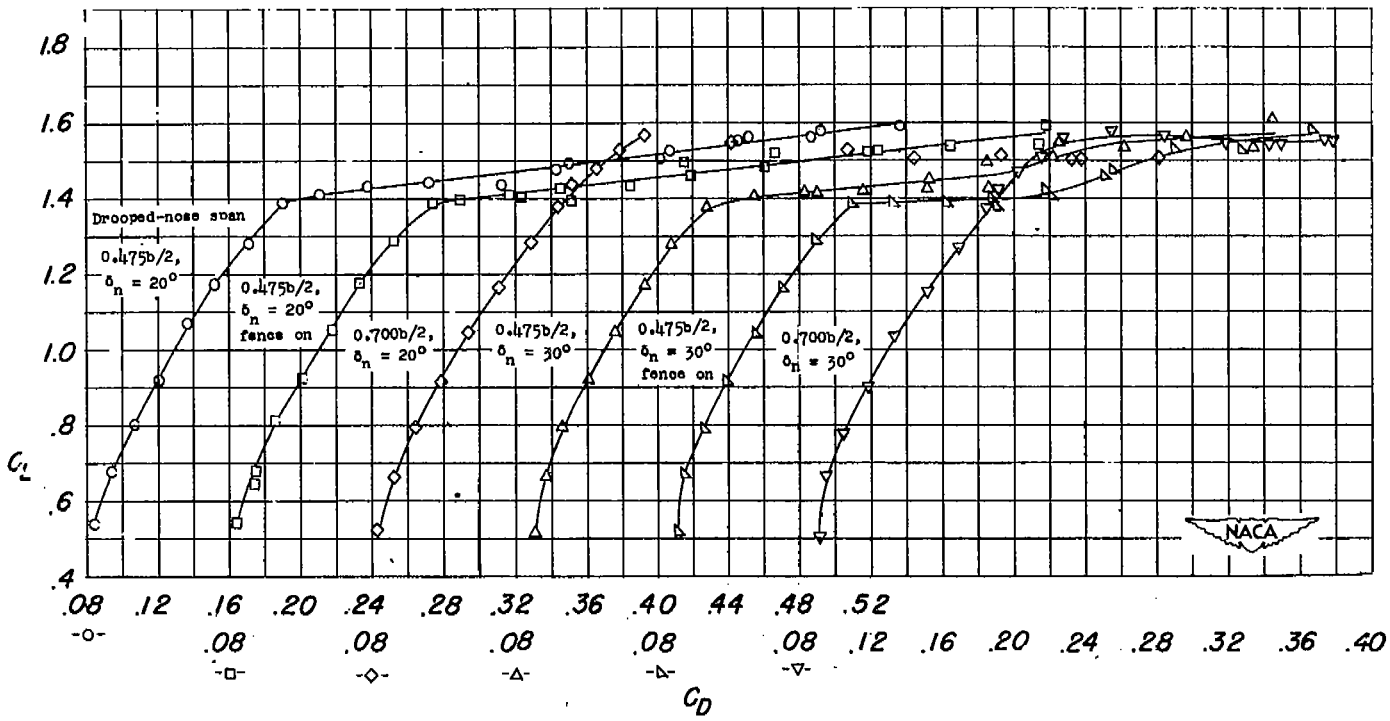


(c) $C_L$ against $C_D$.

Figure 28.- Concluded.

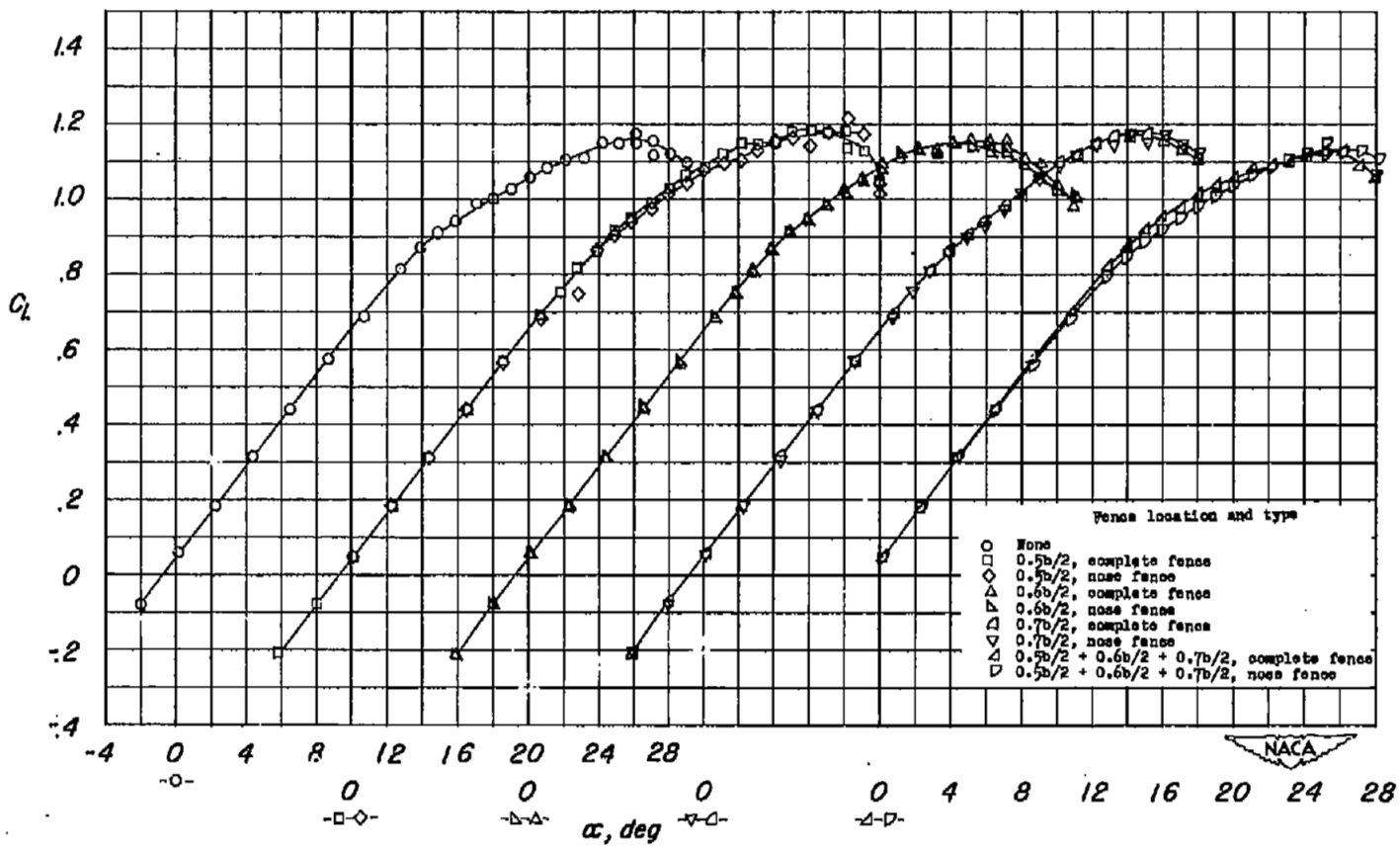


(a) $C_L$ against $\alpha$.

Figure 29.- Effects of wing fences on the aerodynamic characteristics of a 47.7° sweptback wing of aspect ratio 5.1. $R = 6.0 \times 10^6$.

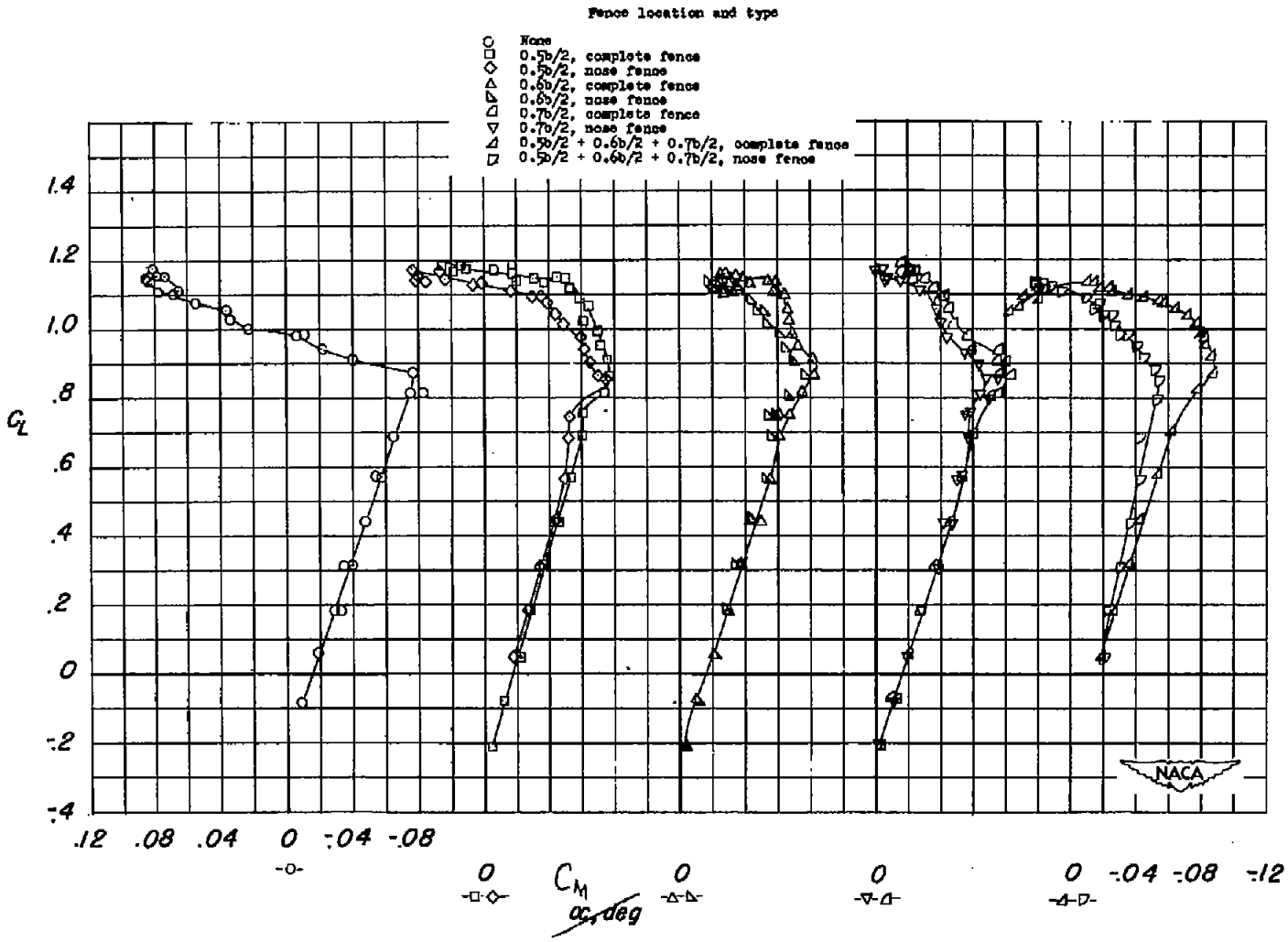


(b) $C_L$ against $C_m$.

Figure 29.- Continued.

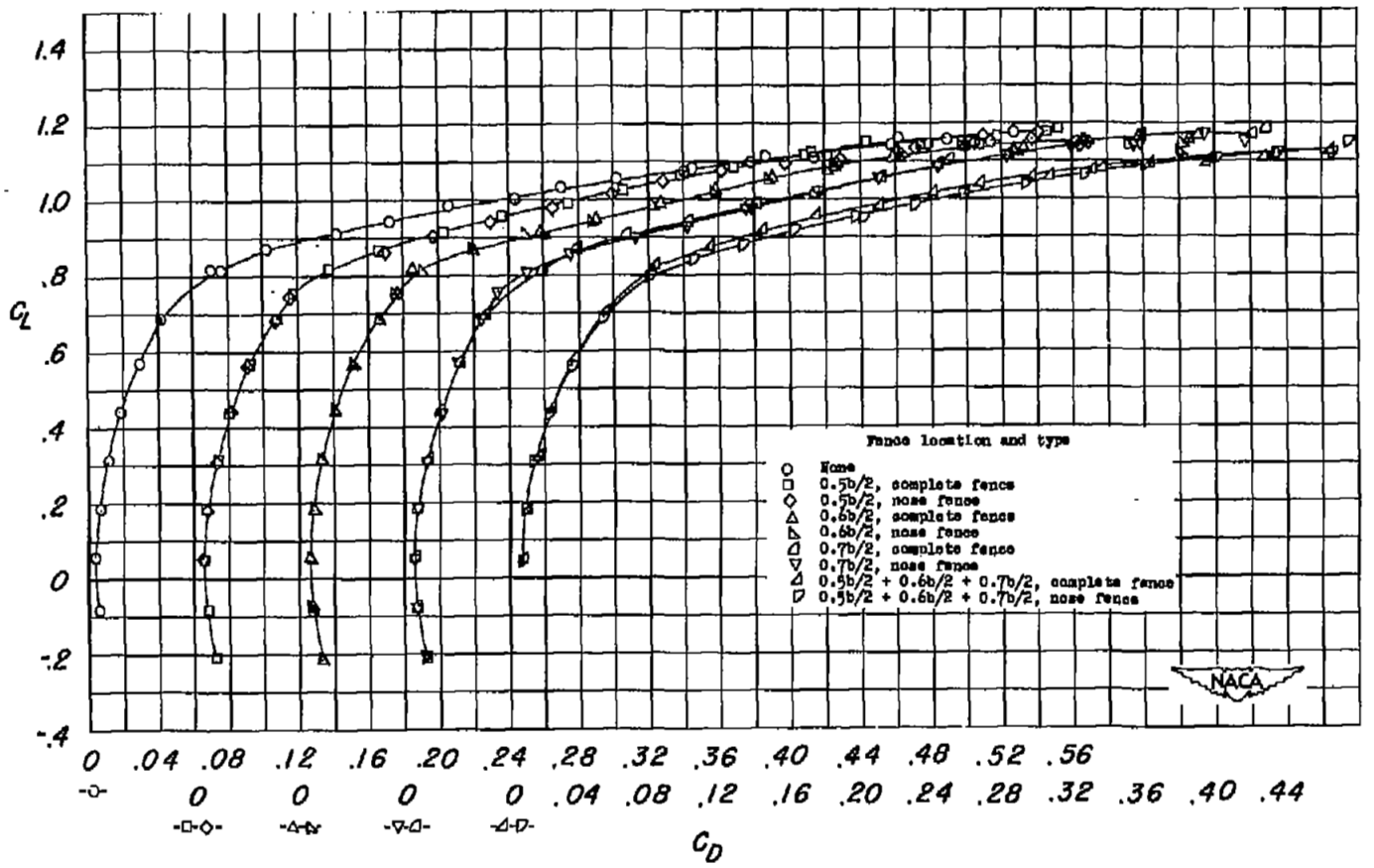


(c) $C_L$ against $C_D$.

Figure 29.- Concluded.

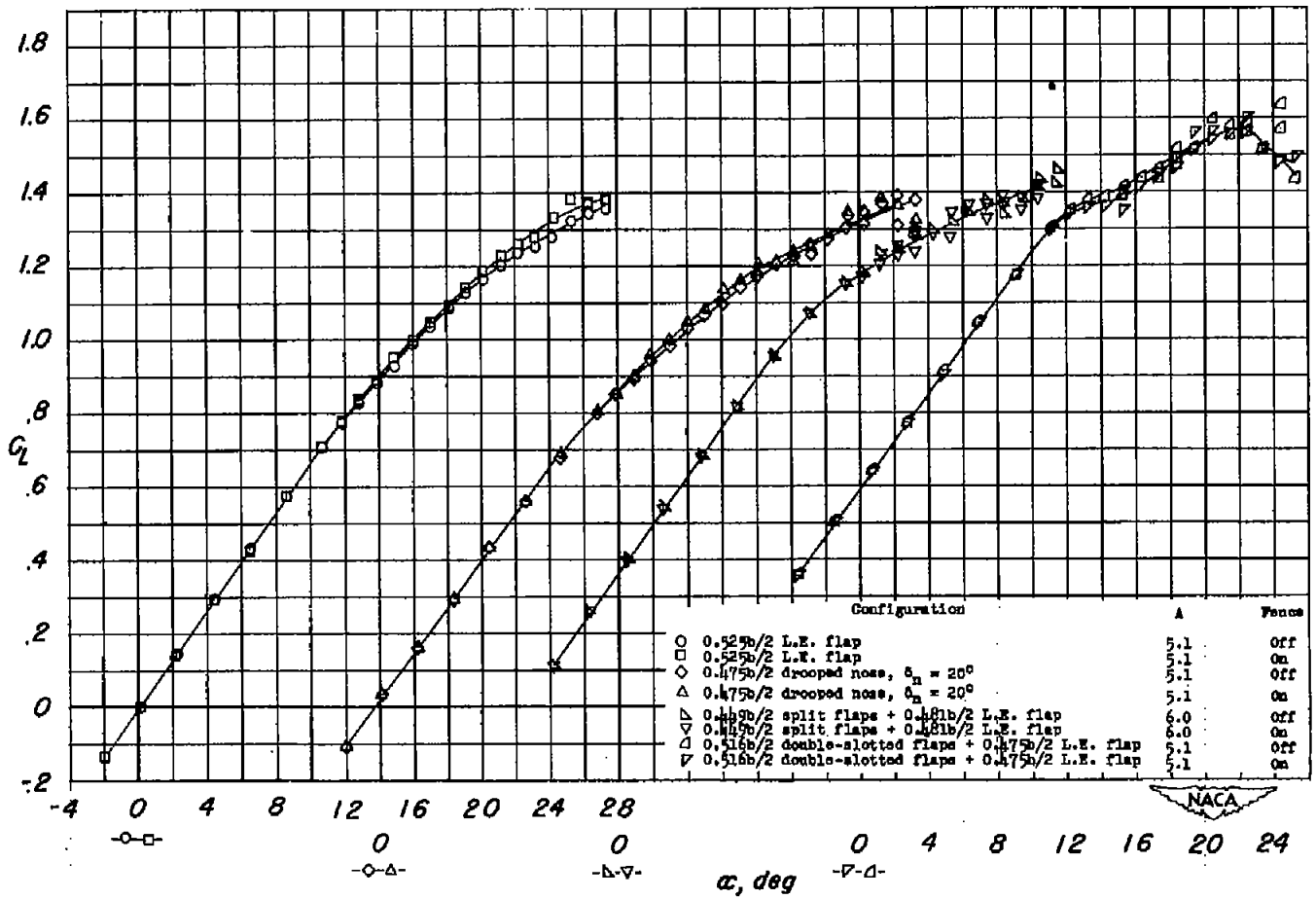


(a) $C_L$ against α.

Figure 30.- Effects of wing fences on the aerodynamic characteristics of two 47.7° sweptback wings of aspect ratios 5.1 and 6.0 with various combinations of trailing-edge and leading-edge devices. R = $6.0 \times 10^6$.

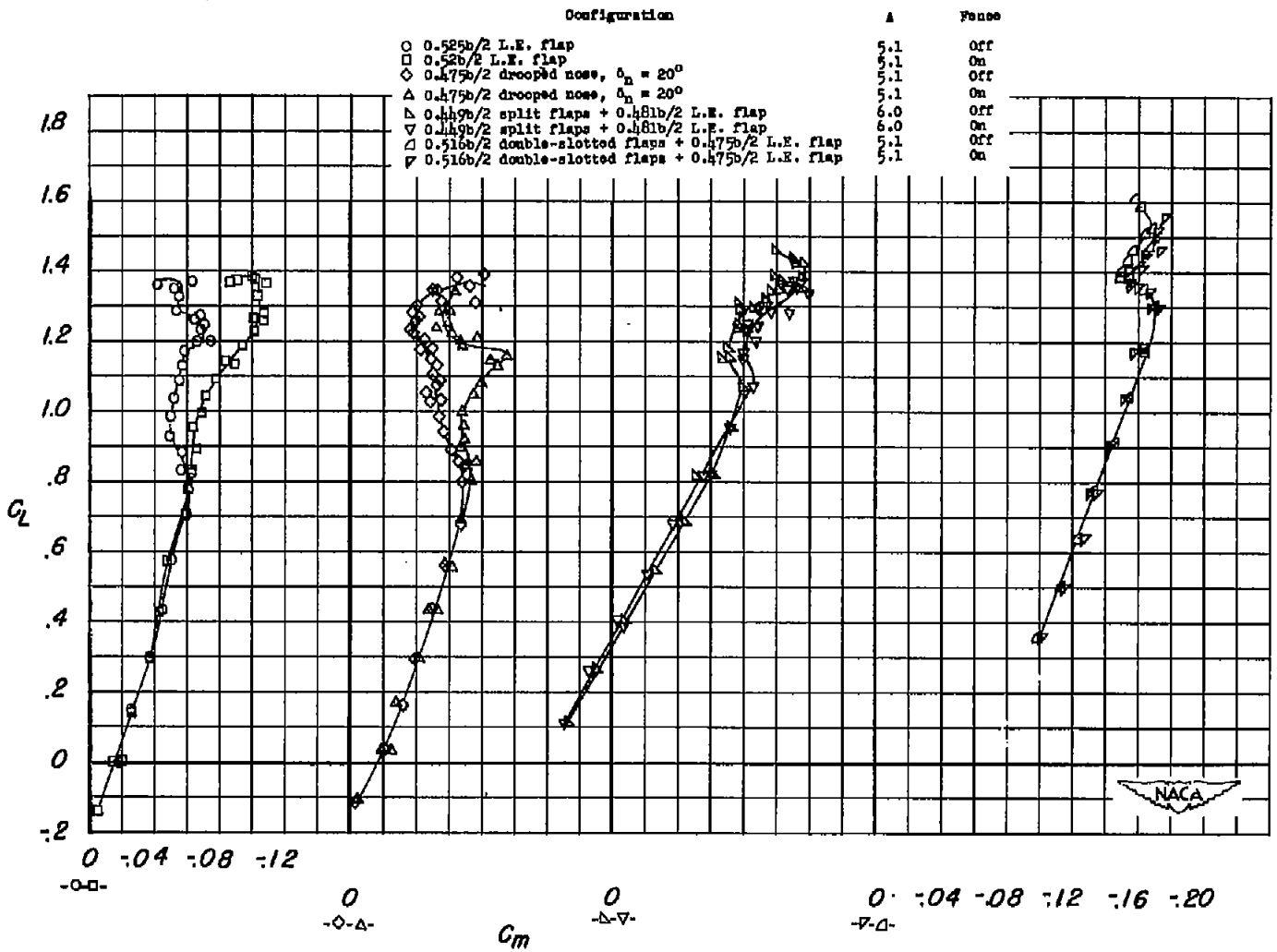


(b) $C_L$ against $C_m$.

Figure 30.- Continued.

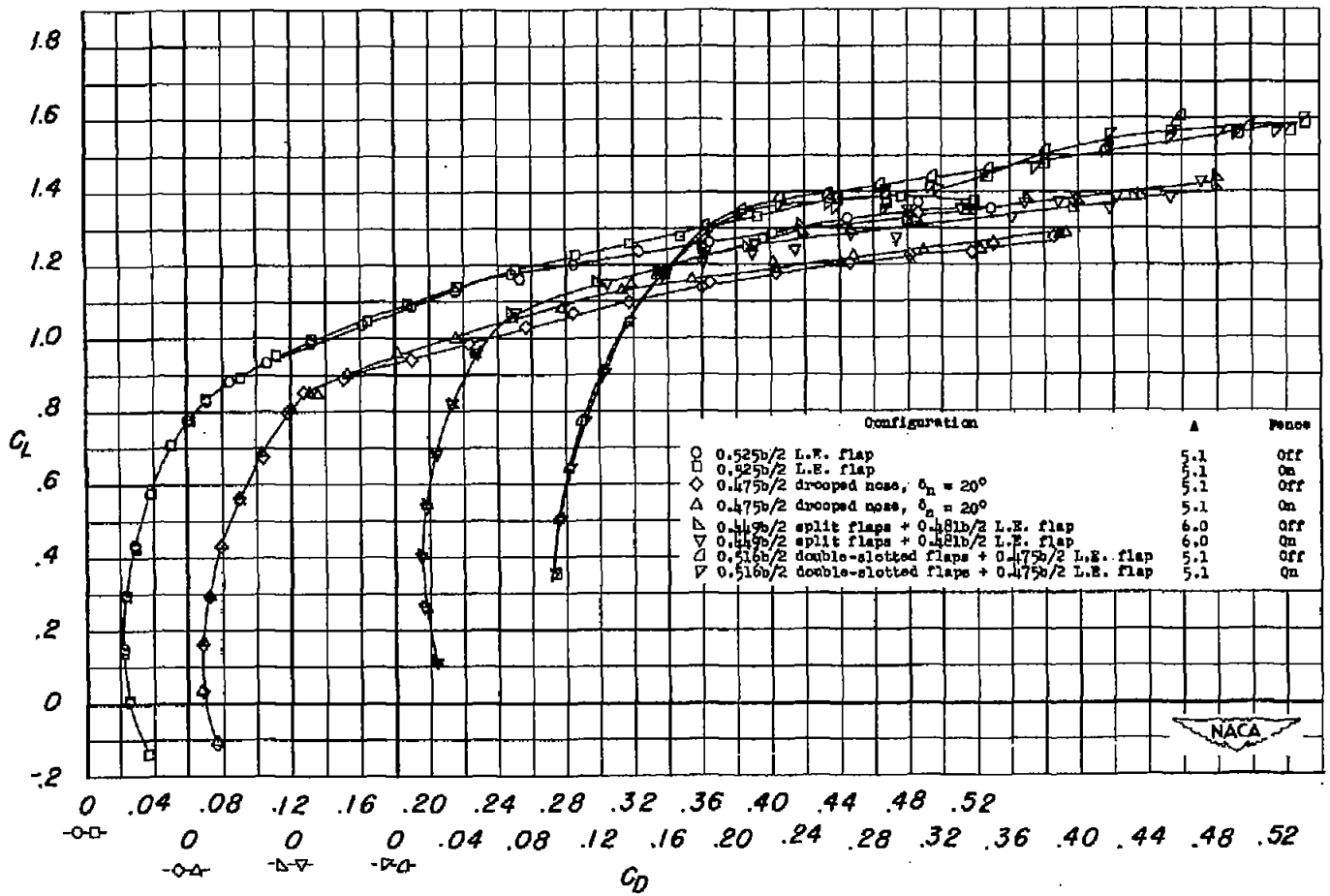


(c) $C_L$ against $C_D$.

Figure 30.- Concluded.

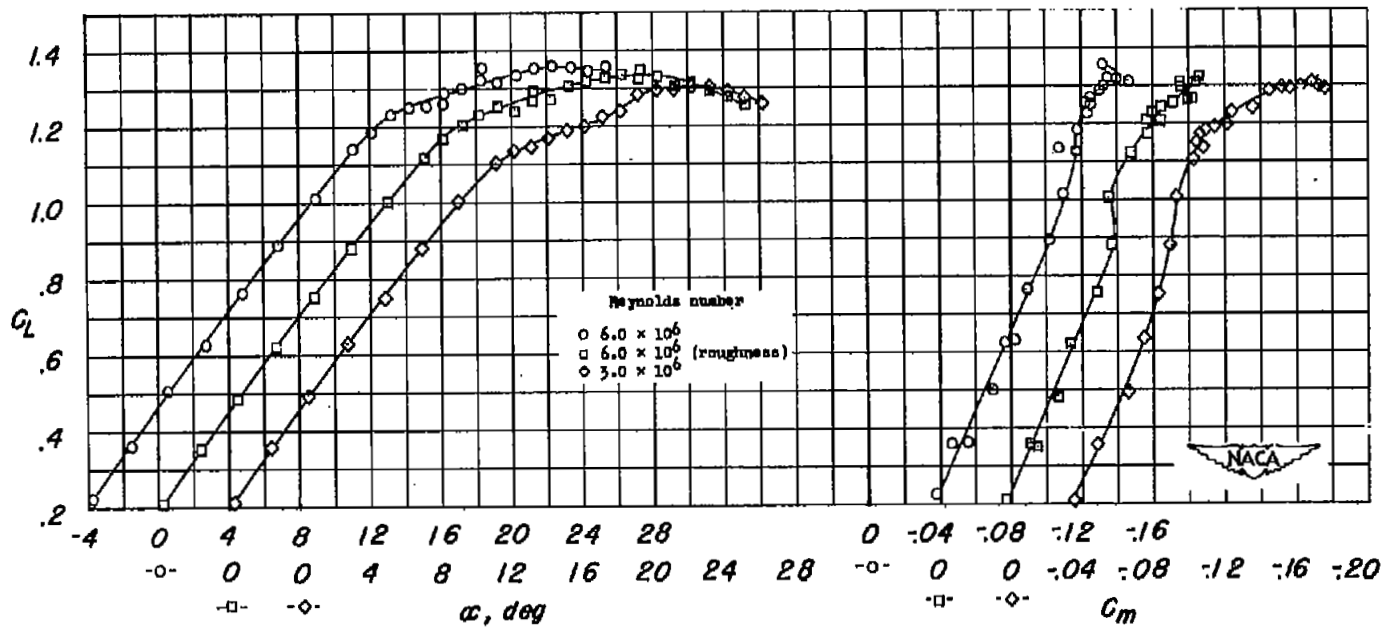


(a) $C_L$ against $\alpha$ and $C_m$.

Figure 31.- Effects of wing roughness and Reynolds number on the aerodynamic characteristics of a 47.7° sweptback wing of aspect ratio 5.1 with 0.400b/2 trailing-edge double slotted flaps and 0.375b/2 leading-edge flaps. $R = 6.0 \times 10^6$.

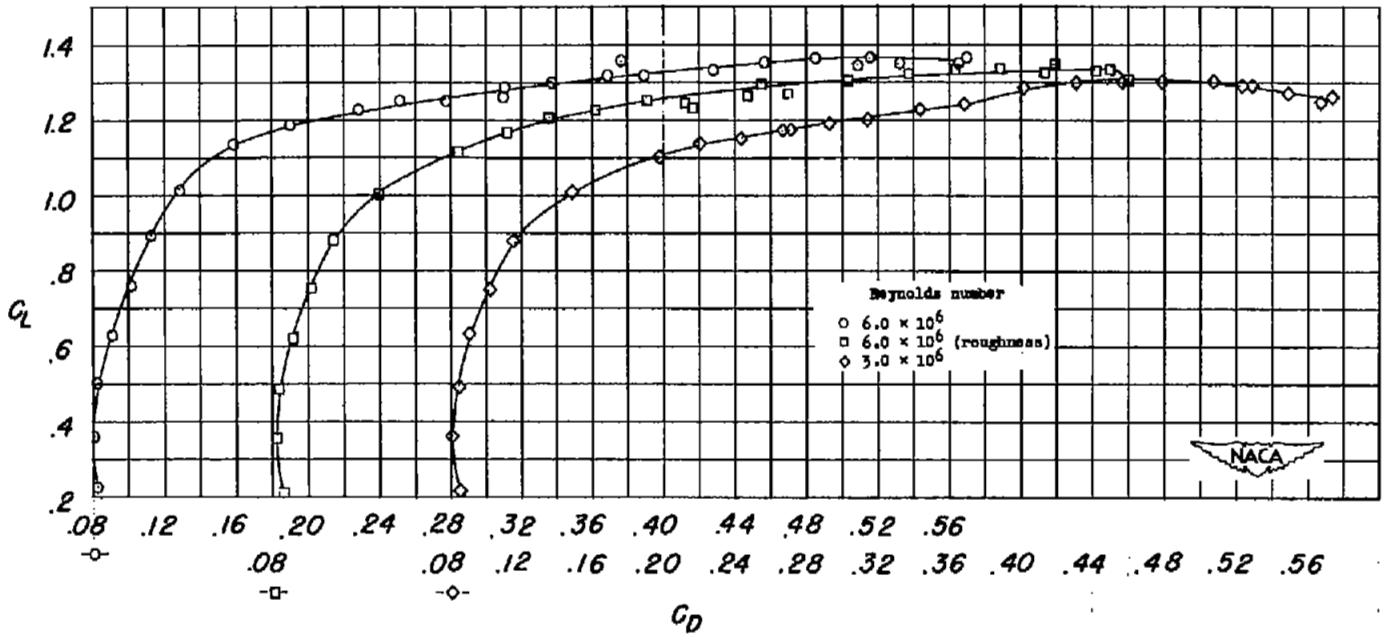


(b) $C_L$ against $C_D$.

Figure 31.- Concluded.

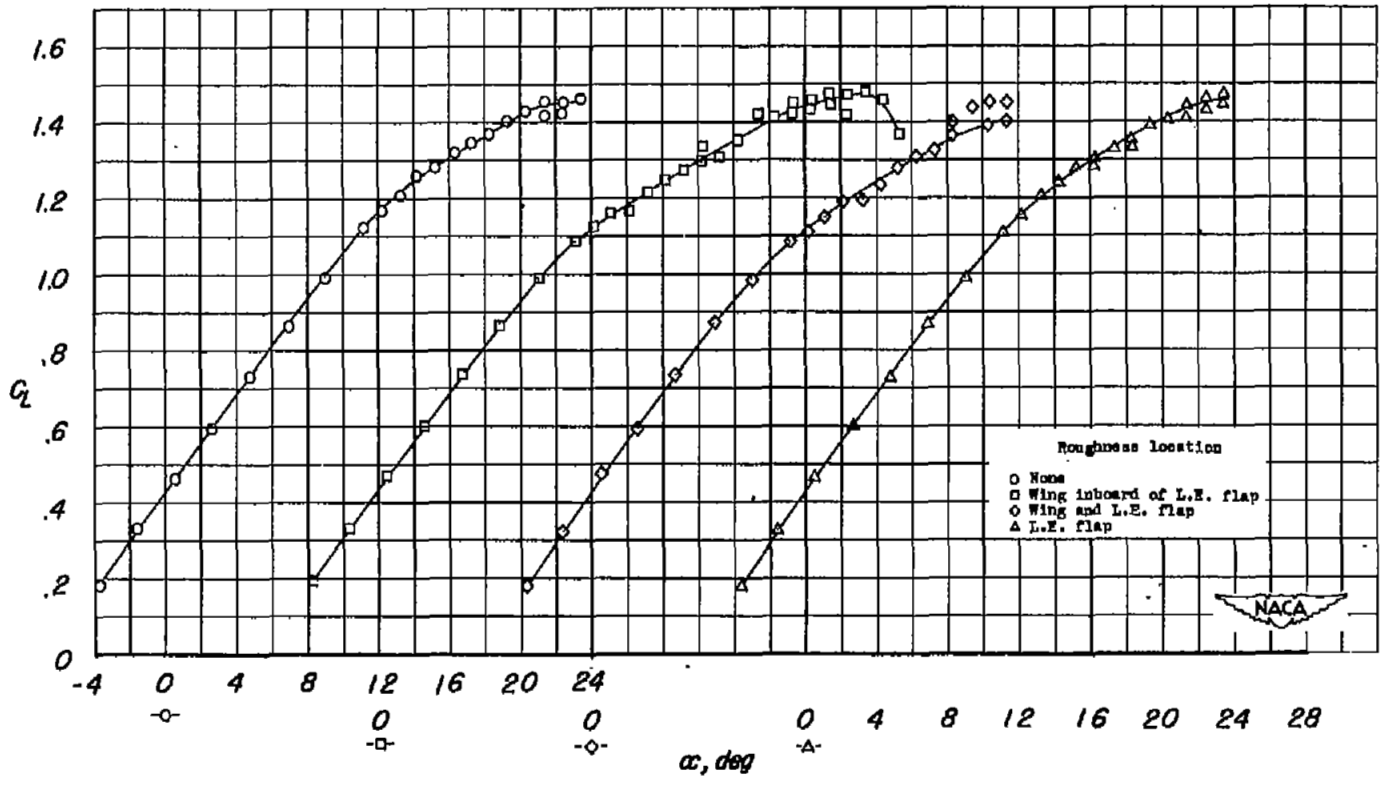


(a) $C_L$ against α.

Figure 32.- Effects of wing roughness at various locations along the leading edge on the aerodynamic characteristics of a 47.7° sweptback wing of aspect ratio 5.1 with 0.618b/2 trailing-edge split flaps and 0.475b/2 leading-edge flaps. $R = 6.0 \times 10^6$.

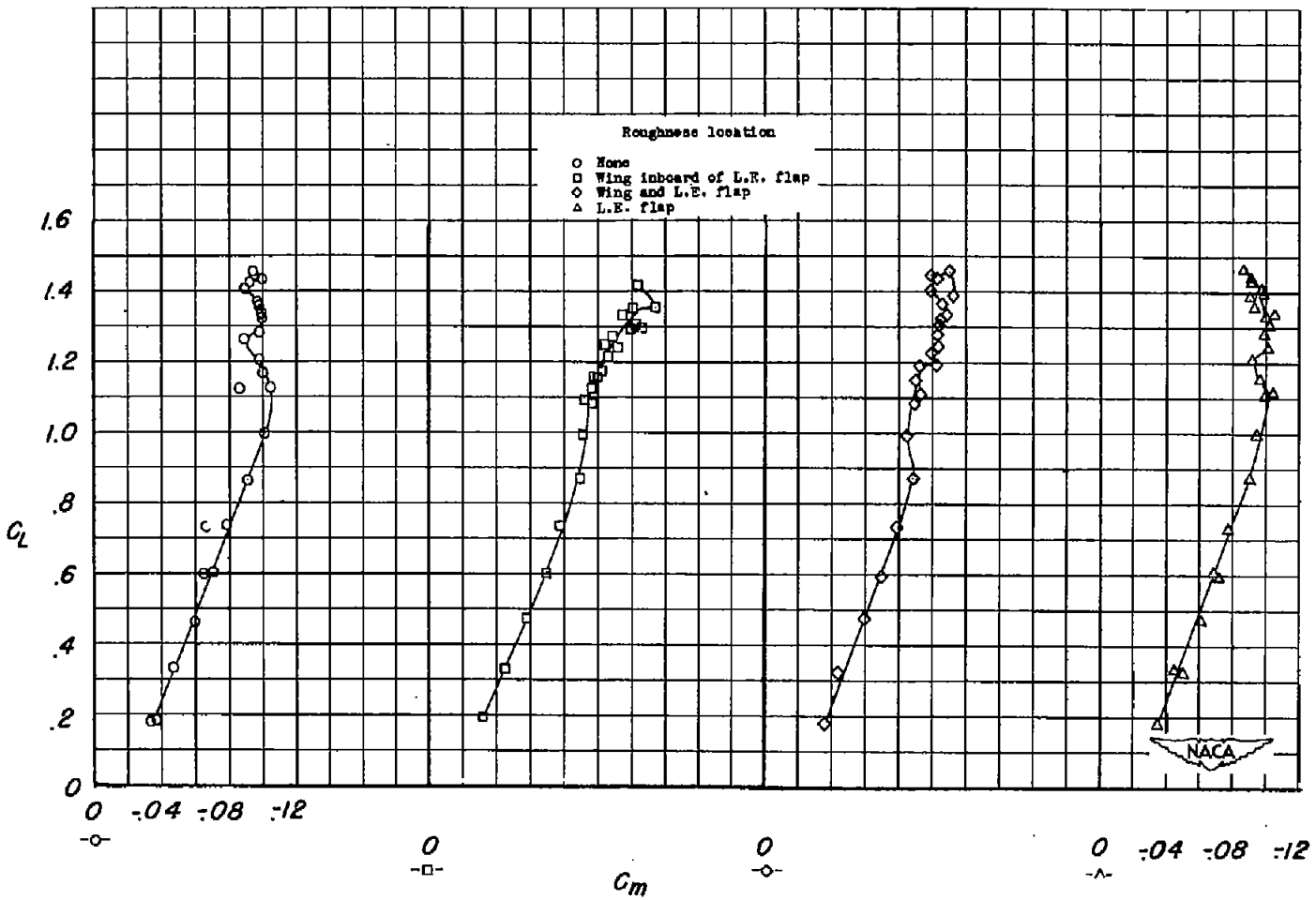


(b) $C_L$ against $C_m$.

Figure 32.- Continued.

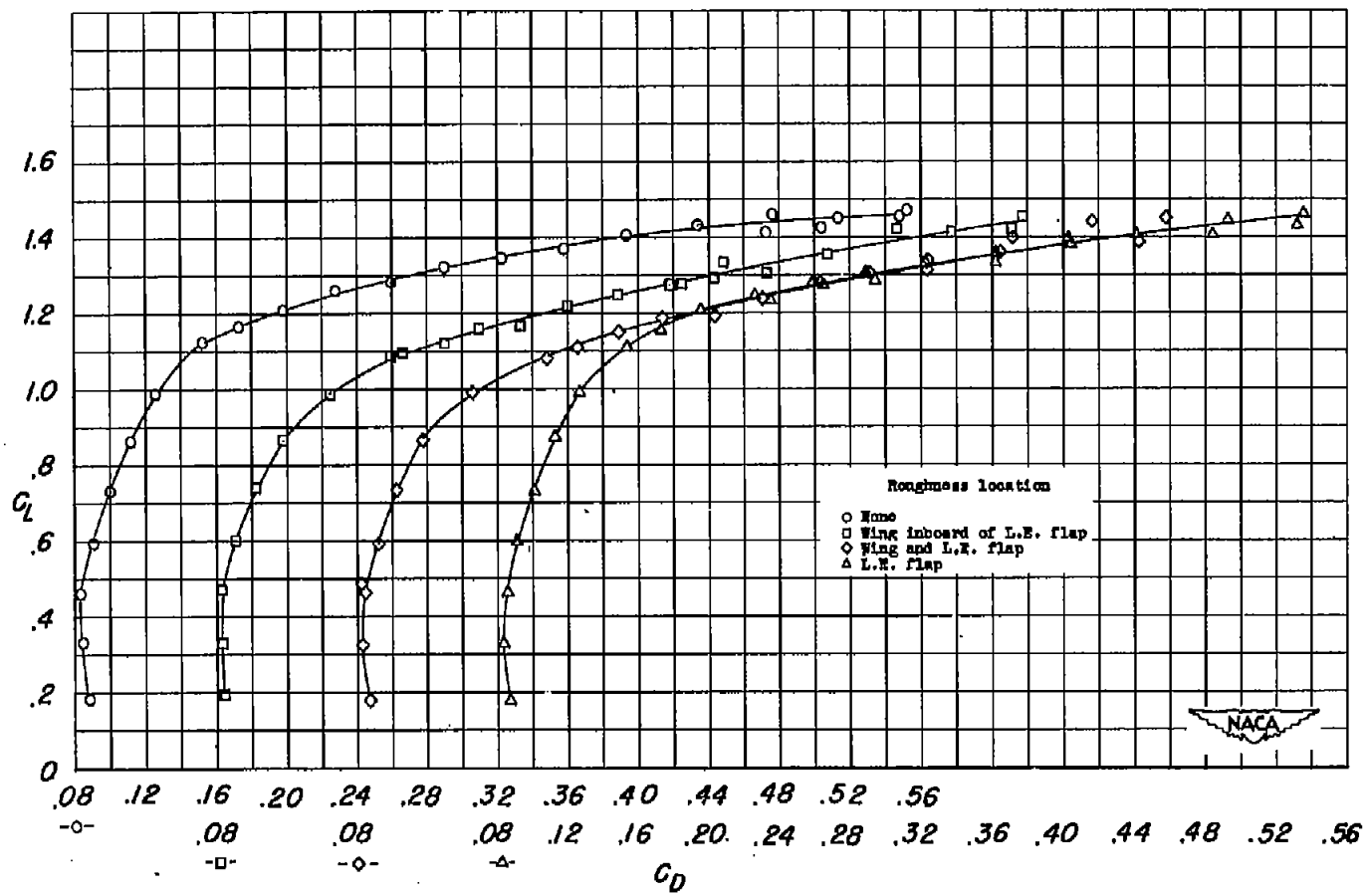


(c) $C_L$ against $C_D$.

Figure 32.- Concluded.

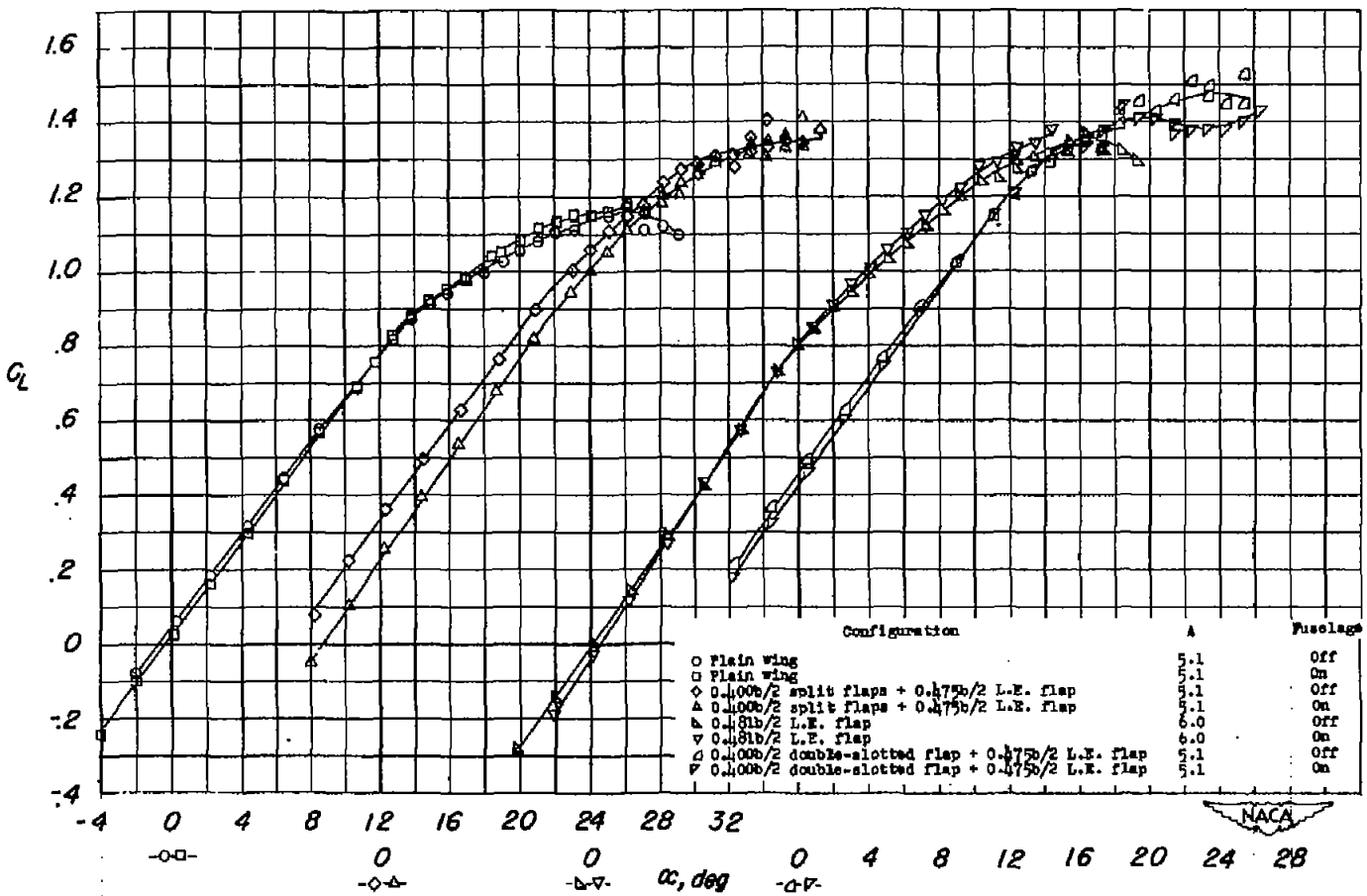


(a) $C_L$ against α.

Figure 33.- Effects of a fuselage on the aerodynamic characteristics of two 47.7° sweptback wings of aspect ratios 5.1 and 6.0 with various trailing-edge and leading-edge devices. $R = 6.0 \times 10^6$.

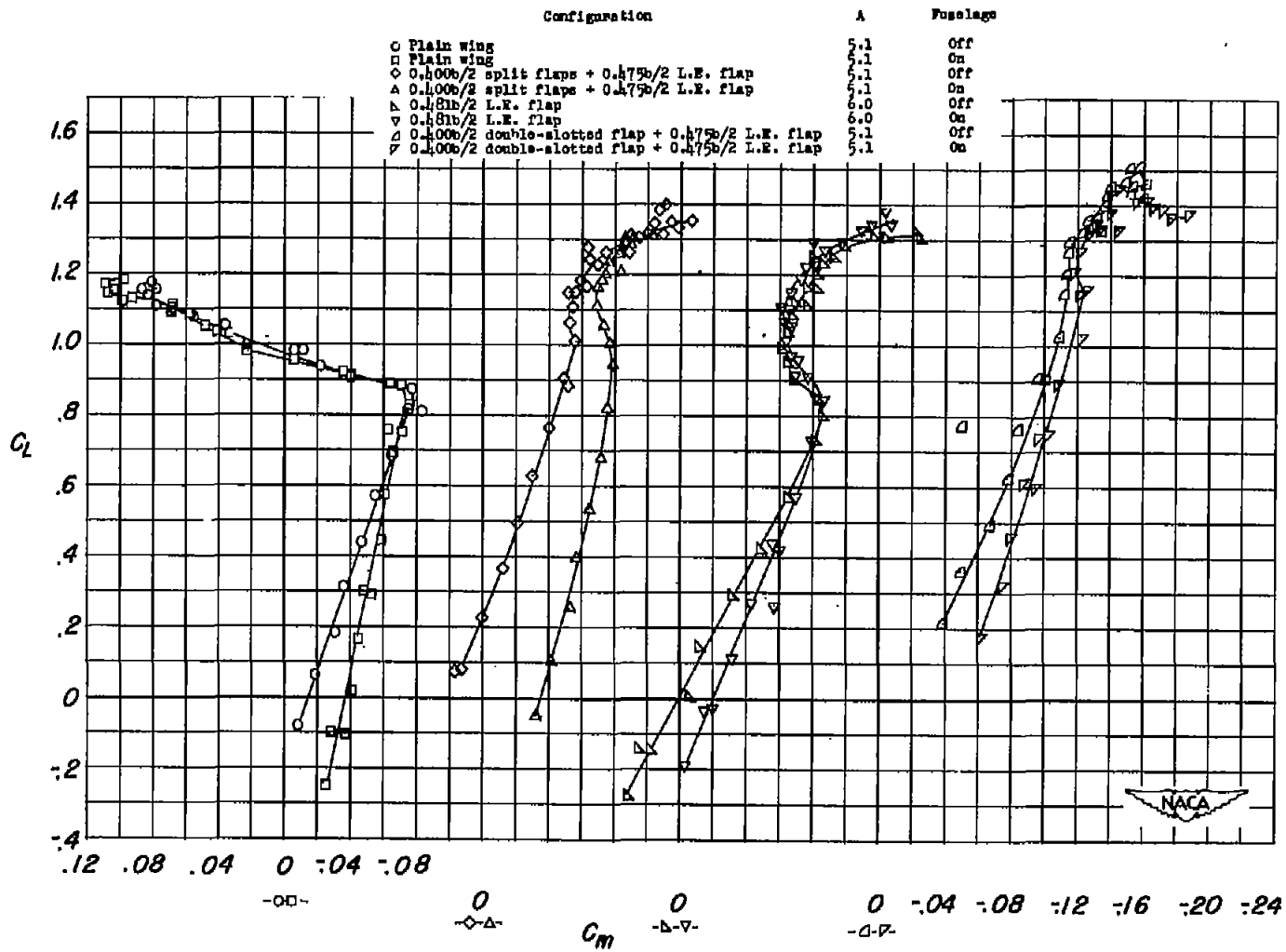


(b) $C_L$ against $C_m$.

Figure 33.- Continued.

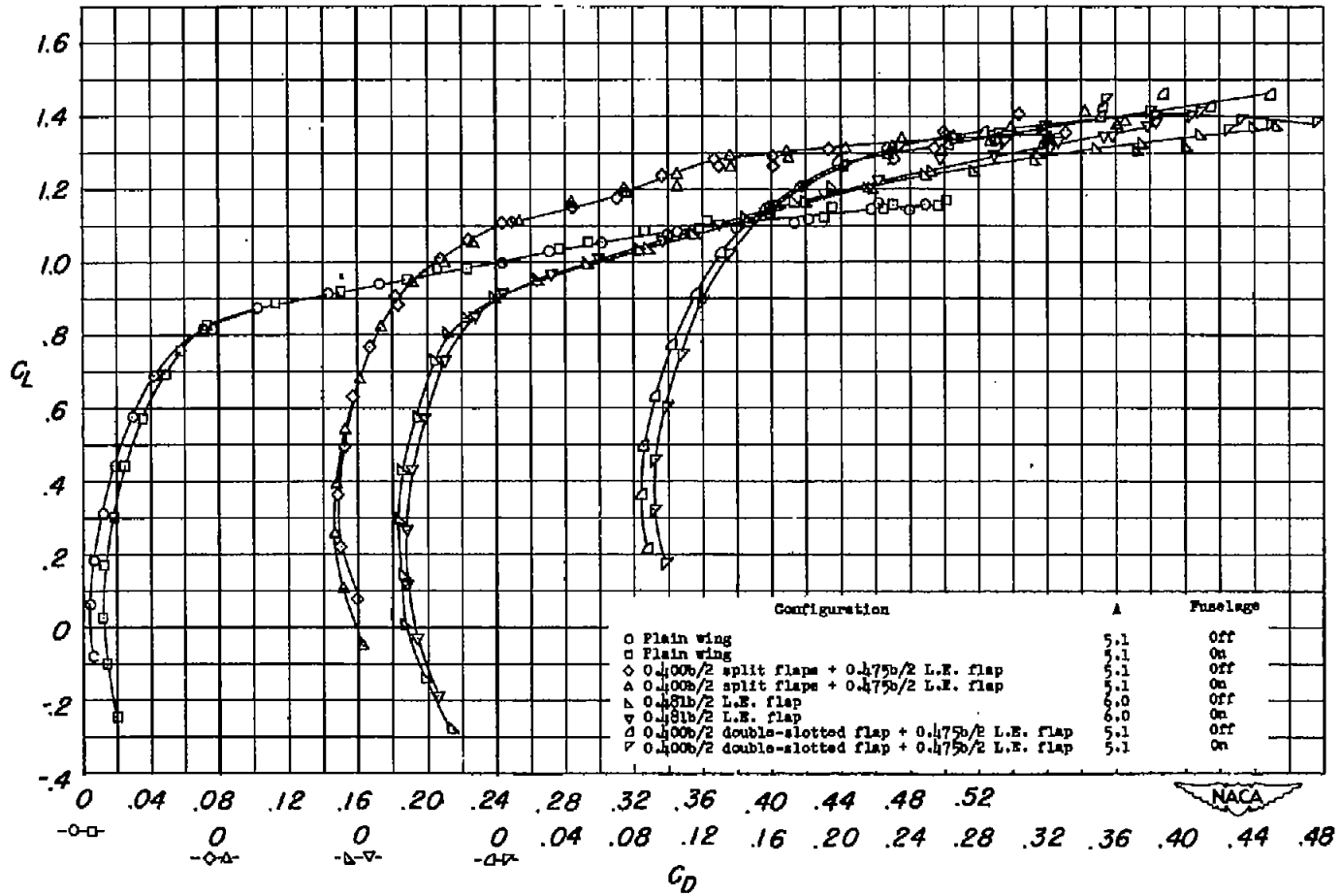


(c) $C_L$ against $C_D$.

Figure 33.- Concluded.

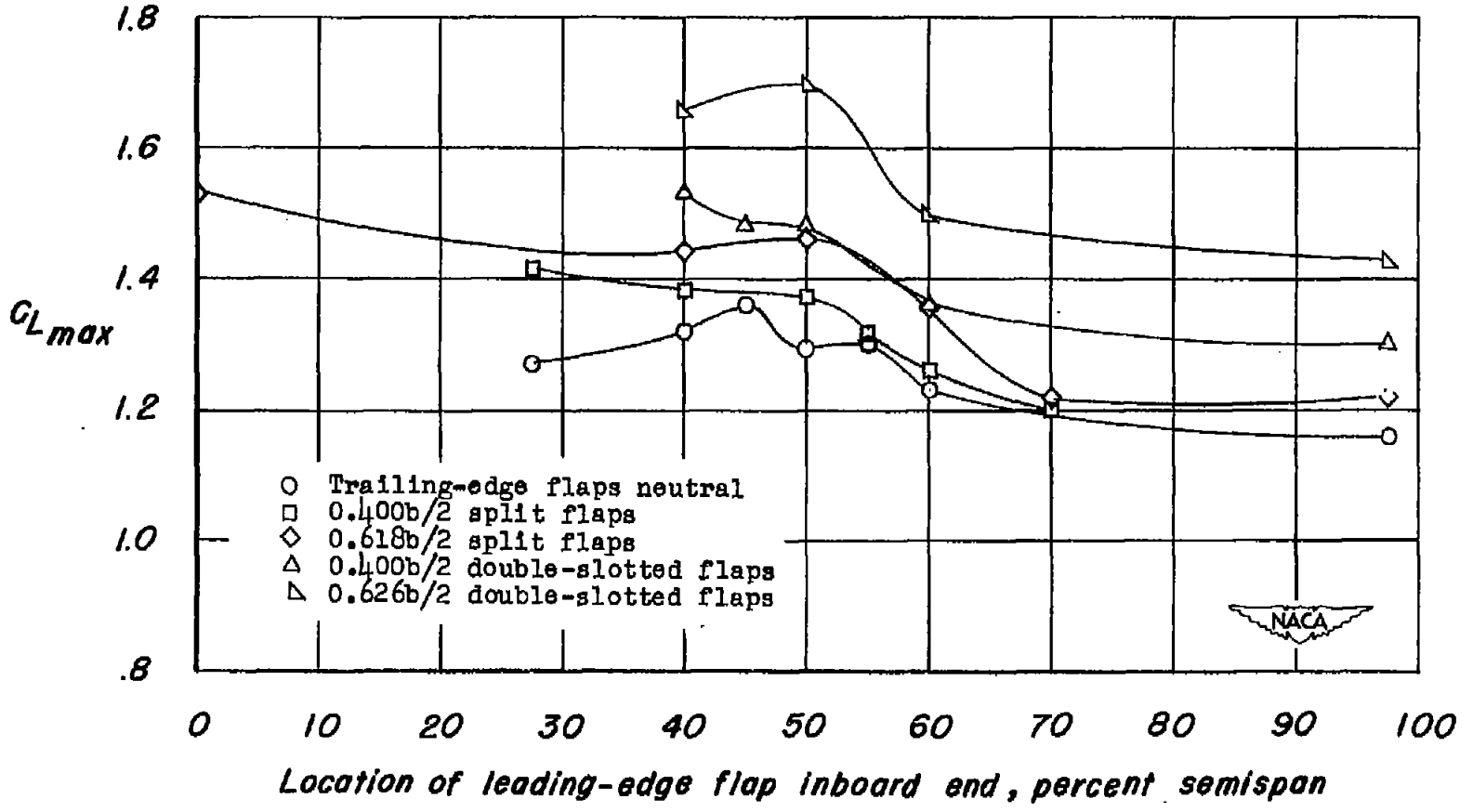


Figure 34.- Variation of the maximum lift coefficient with leading-edge flap span for a 47.7° sweptback wing of aspect ratio 5.1 with various trailing-edge flaps. $R = 6.0 \times 10^6$.

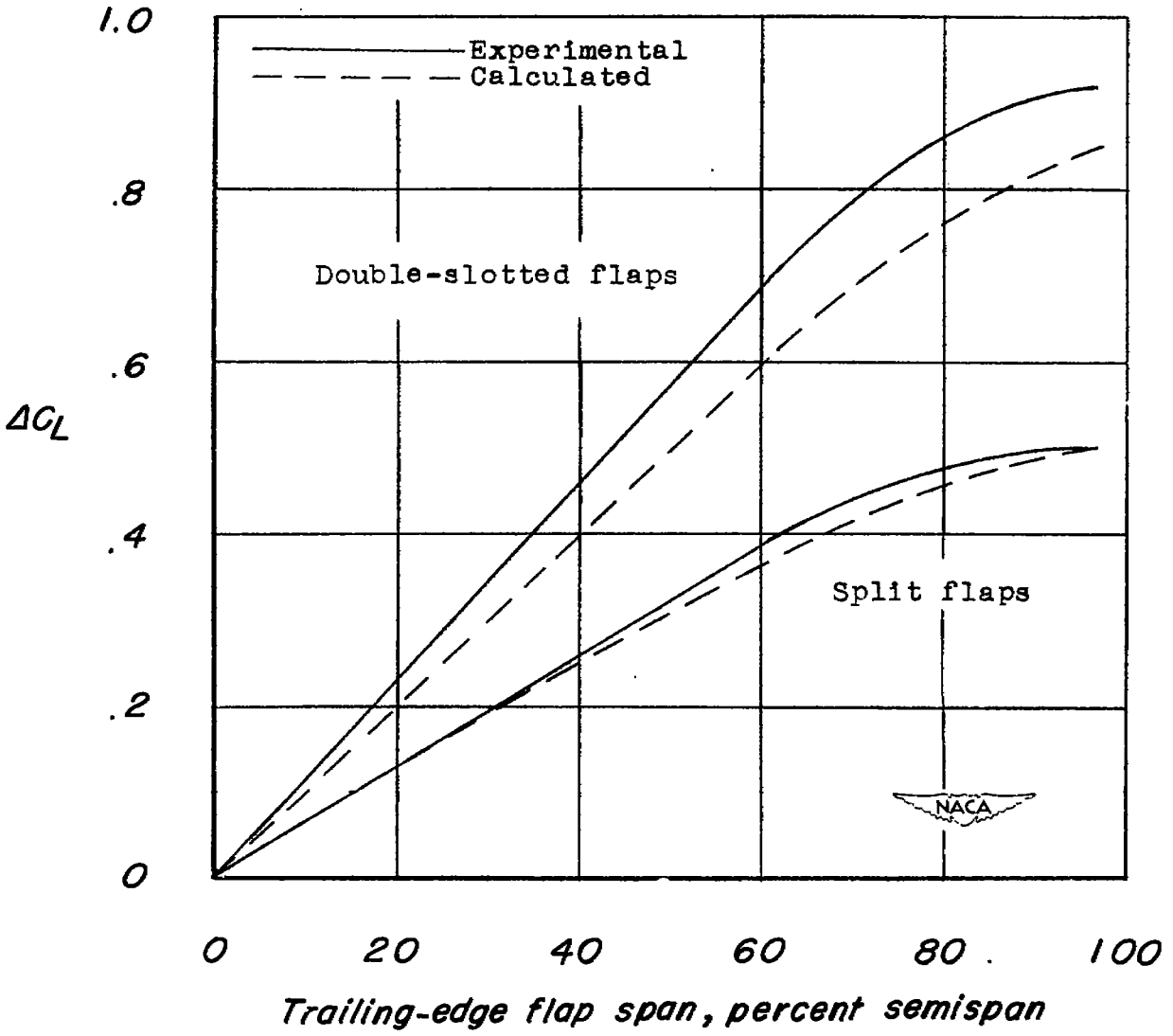


Figure 35.- Comparison of measured and calculated trailing-edge flap effectiveness at zero angle of attack for a 47.7° sweptback wing of aspect ratio 5.1.

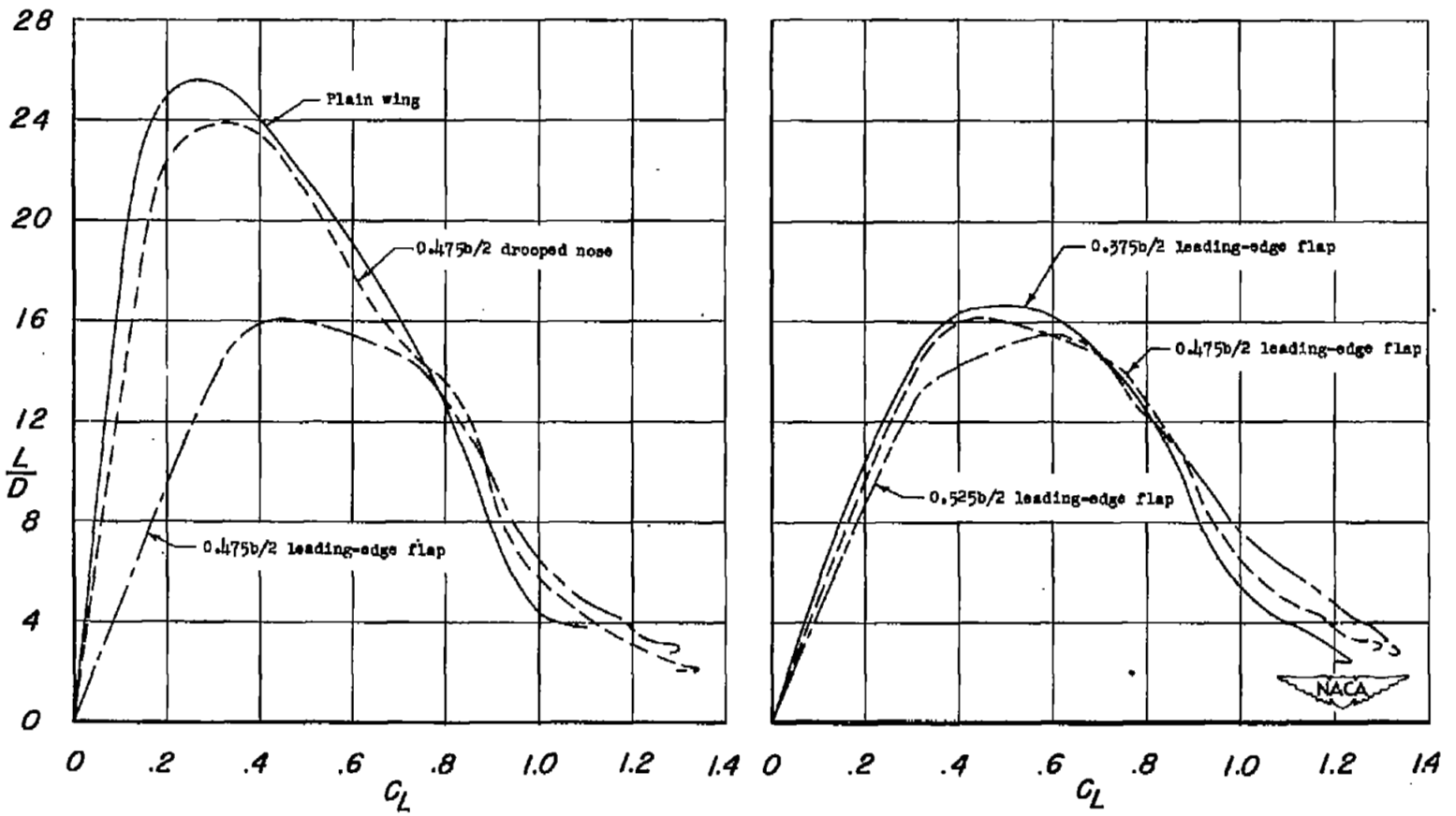


Figure 36.- Effects of various leading-edge devices on the lift-drag ratio of the aspect ratio 5.1 wing. $R = 6.0 \times 10^6$.

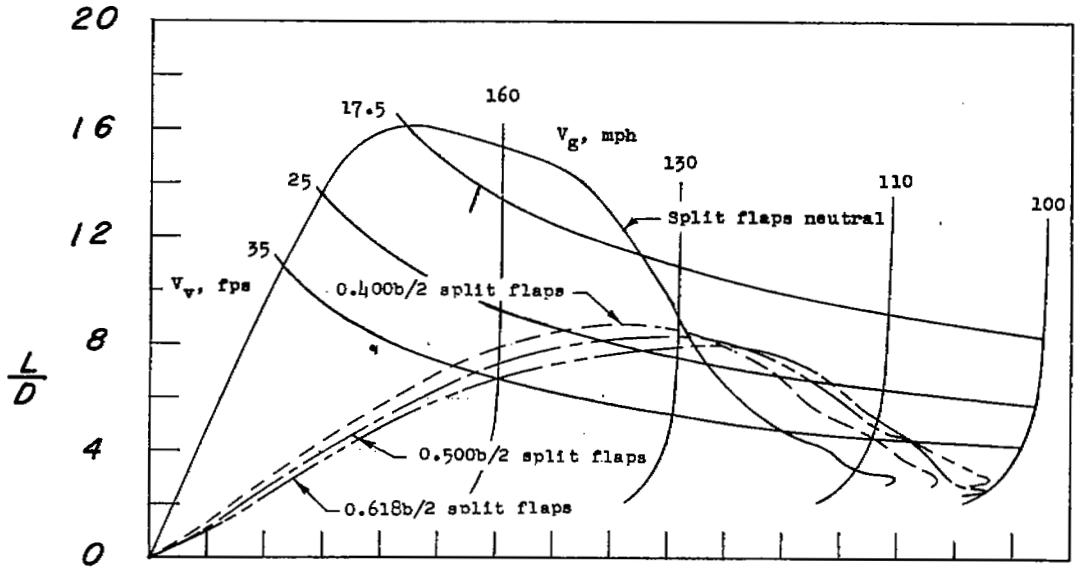


(a) Split flaps.

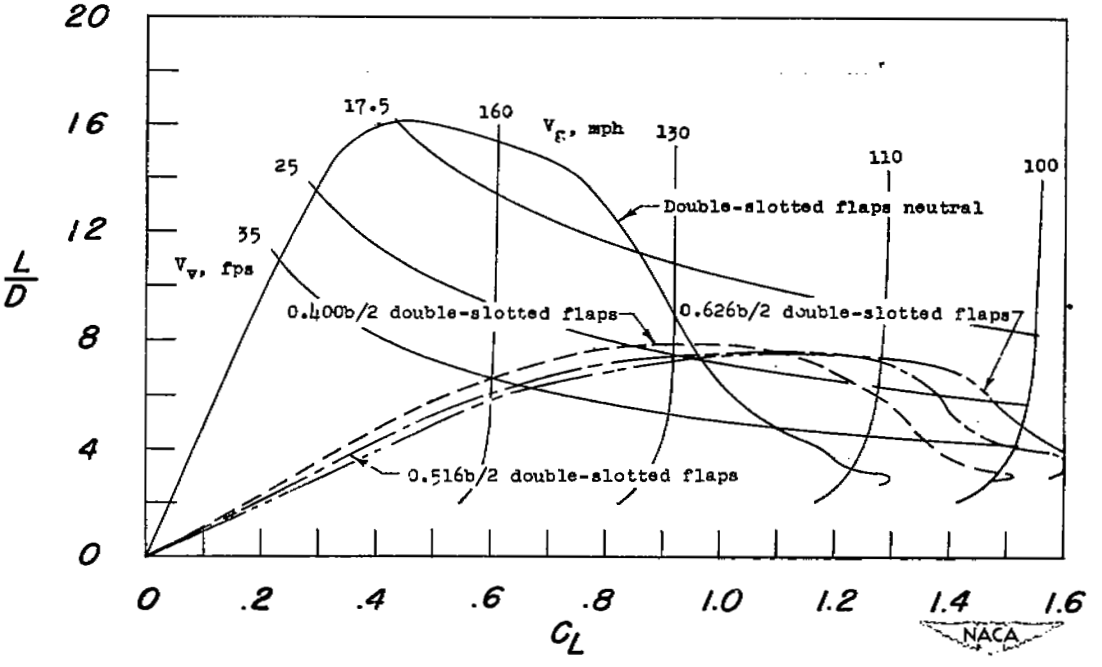


(b) Double slotted flaps.

Figure 37.- Effects of trailing-edge flap span on the lift-drag ratio of the aspect ratio 5.1 wing with 0.475b/2 leading-edge flaps. $R = 6.0 \times 10^6$. Assumed wing loading of 40 pounds per square foot.

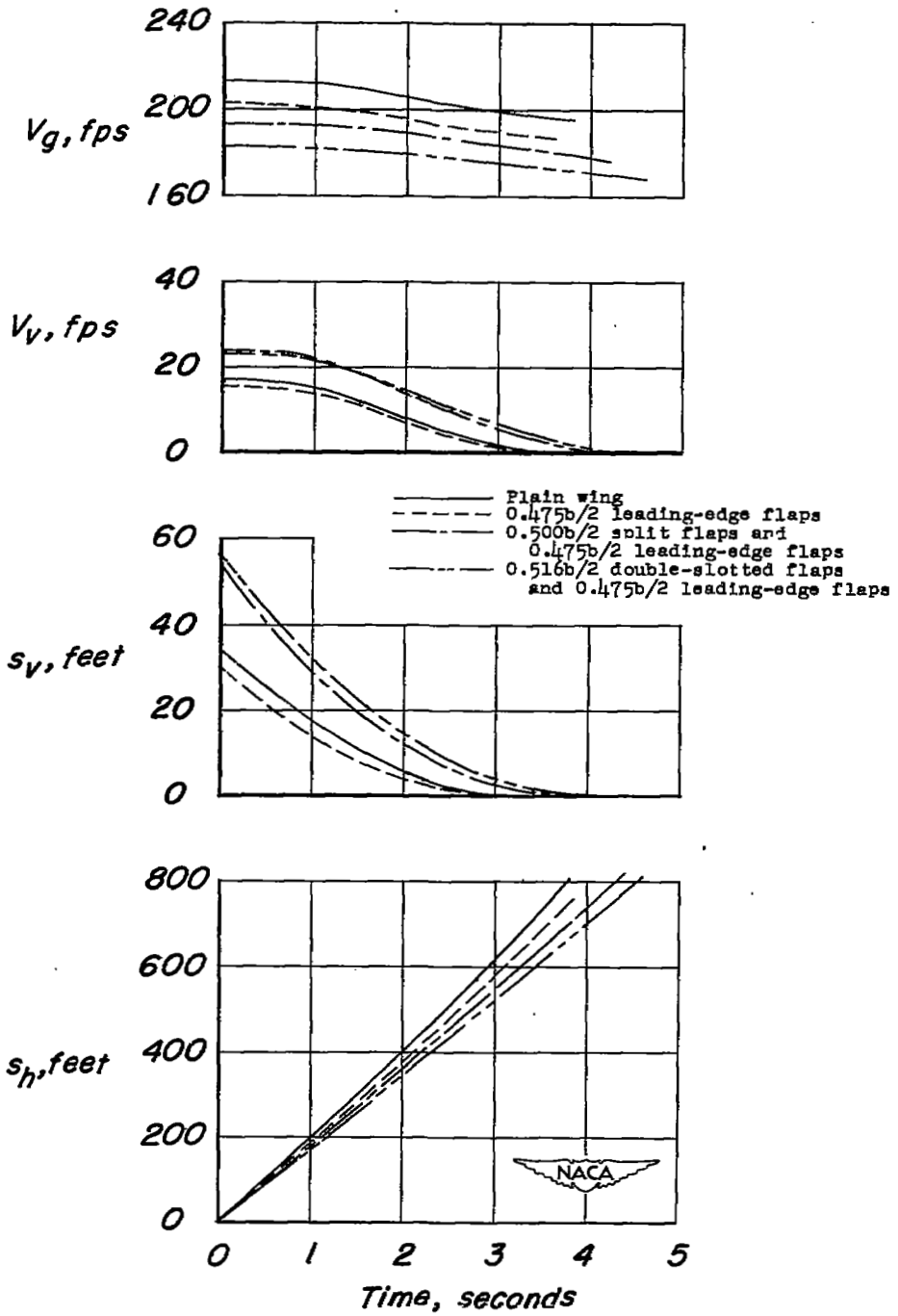


Figure 38.- Power-off landing-flare characteristics of a 47.7° sweptback wing of aspect ratio 5.1 with various combinations of leading-edge flaps and trailing-edge flaps. $R = 6.0 \times 10^6$. Assumed wing loading of 40 pounds per square foot.